Macromolecules
PERSPECTIVE

Macromolecules **2011**, *44*, 1073–1109 **1073**
DOI: 10.1021/ma102360t

Polyhedral Phenylsilsesquioxanes

Richard M. Laine*,†,‡ and Mark F. Roll‡

†*Department of Materials Science and Engineering,* ‡*Macromolecular Science and Engineering Center, University of Michigan, Ann Arbor, Michigan 48109-2136, United States*

Received October 15, 2010; Revised Manuscript Received January 11, 2011

ABSTRACT: Our objectives are to provide a comprehensive review solely concerning the synthesis and chemistries of polyhedral phenylsilsesquioxanes. The review covers the basic efforts to synthesize and characterize the compounds $[PhSiO_{1.5}]_8$, $[PhSiO_{1.5}]_{10}$, and $[PhSiO_{1.5}]_{12}$. Thereafter, we discuss general methods of functionalizing these compounds with emphasis on electrophilic substitution to produce, for example, $[NO_2PhSiO_{1.5}]_8$, $[NO_2PhSiO_{1.5}]_{12}$, $[p\text{-}IPhSiO_{1.5}]_8$, $[p\text{-}IPhSiO_{1.5}]_{10}$, $[p\text{-}IPhSiO_{1.5}]_{12}$, $[o\text{-}BrPhSiO_{1.5}]_8$, $[2,5Br_2PhSiO_{1.5}]_8$, and $[Br_3PhSiO_{1.5}]_8$ as well as Friedel−Crafts alkylation products. Second-generation compounds and nanocomposite materials derived from these intermediates are also discussed in detail. The review ends with a discussion of the apparent 3-D photophysical properties of third-generation functionalized phenylsilsesquioxanes.

Introduction

In principle, control of a material's global properties through nanometer-by-nanometer (nm × nm) assembly of structure-precise nanobuilding blocks (NBs) offers an optimal mechanism for tailoring and refining such properties.[1−7] Here global properties encompass mechanical, photonic, and/or electronic properties, to name just a few.[8,9] In practice, multiple problems must be overcome for such an assembly process to be successful. NBs themselves must be carefully tailored to enable the desired assembly. In particular, NBs will require

1. High symmetry to minimize the number of $T\Delta S$ induced defects and facilitate removal of misalignment defects in assembly by annealing
2. Functionality that can be introduced or altered
   a. To direct assembly
   b. To change the spacing between NBs to control for example micro (nano)porosity
   c. To vary the degree and mechanical character of the connectivity
   d. To provide electronic conjugation or insulation
   e. To alter optical activities and absorption or emission properties for photonic applications
3. High thermal and chemical stability
4. Easy syntheses with high yields and simple purification

On a first principles basis, one would like NBs that fill space to minimize incurring defects during assembly. Given that the seven Bravais lattices are all spacing filling, it seems reasonable to expect that NBs that have structures similar to Bravais lattice unit cells would satisfy this requirement. Furthermore, among the seven crystal systems, cubic symmetry should offer the best opportunity to fulfill the minimum defect requirement. The rationale is that misaligned cubic NBs would require the least energy to realign (maximum 45° movement) based simply on their high symmetry.[10] One can envision NB derived 3-D nanostructures as suggested in Figure 1a,b.

The Escher-like image on the left (a) offers an excellent perspective of what a nanostructured material might look like at the smallest length scales. Realistically, bonding constraints limit the types of cubic bonding structures one might generate to Eaton's idealized (b) polycubane structure.[10−12] Eaton notes in his review,

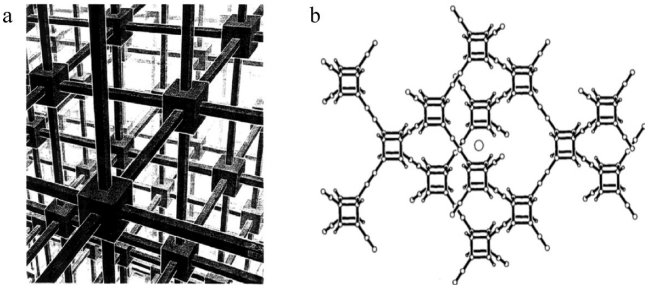

Figure 1. Cubic nanostructure models: (a) NBs connected through faces; (b) connected at corners (ref 12).

"Fortunately, any good student, having gone through the procedure once to become familiar with its details, can easily make 10 grams of (cubane) in a month or so." It appears, for practical purposes, that 3-D materials assembly using cubane NBs is limited by the time-consuming syntheses.

In contrast, silsesquioxanes (SQs, Scheme 1) with cubic symmetry are easily synthesized using several well-defined methods in kilogram quantities with good-to-excellent yields in days.[13−24] They are easy to make and (after functionalization) often quite soluble, making them easy to purify.

Furthermore, a wide variety of functional groups can be introduced.[13−26] The SQ cores $[SiO_{1.5}]_8$ for the T_8 (three Si−O bonds) and the $[OSiO_{1.5}]_8$ Q_8 systems (four Si−O bonds) represent the smallest single crystal of silica (cristobalite).[21] As such, most SQs offer thermal stabilities up to 100 °C higher than carbon analogues because of the heat capacity of the silica core.

SQs have been used successfully to model catalytic surfaces,[27] develop new catalysts,[22,28] prepare novel porous media,[29] serve as NMR standards,[30] and act as encapsulants[31] and as building blocks for nanocomposite materials.[32−43] This interest has generated 14 full reviews covering many aspects concerning the synthesis, chemistry, and properties of silsesquioxanes.[13−26] With some exceptions, these reviews tend to be relatively broad.

Given the exceptional recent interest in silsesquioxanes in general and polyhedral silsesquioxanes (SQs) in particular, it is now pertinent to review one specific class of these polyhedral silsesquioxanes, the phenyl derivatives. Readers interested in the other families of silsesquioxane materials including those used as nanobuilding blocks are directed to the many excellent reviews cited

*Corresponding author. E-mail: talsdad@umich.edu.

Published on Web 03/01/2011

above.[13−26] These SQs, although of great interest because of their high thermal stabilities (> 400 °C/air), have not received the attention related SQs have, mostly because the most common phenylSQ, $[PhSiO_{1.5}]_8$, exhibits very poor solubility;[44−50] only ≈200 mg of $[PhSiO_{1.5}]_8$ dissolves in 1 L of boiling CH_2Cl_2. The THF solvate of $[PhSiO_{1.5}]_{12}$ has a solubility of 600 mg/L of THF at 28 °C.[48] Little is known about $[PhSiO_{1.5}]_{10}$, but it appears to be more soluble than the other two.[48] It is therefore difficult to isolate and has only been produced in hundred milligram quantities.[50]

Richard (Rick) M. Laine has undergraduate and graduate degrees in Chemistry, receiving his Ph.D. under the Supervision of Professor Robert Bau at USC. He then did postdoctoral studies with Richard F. Heck (University of Delaware) and Peter C. Ford (UCSB) followed by 11 years at Stanford Research Institute, last as Associate Director of Inorganic and Organometllic Programs. He moved to the Materials Science and Engineering Department at the University of Washington in 1987 as a full research professor and director of the polymeric materials laboratory in the Washington Technology Center. In 1990, he moved to the Materials Science and Engineering Department at the University of Michigan where he is now a full professor and Director of the Macromolecular Science and Engineering Center.

Mark F. Roll received his B.E. in Mechanical Engineering from The Cooper Union for the Advancement of Science and Art. He earned his Ph.D in Macromolecular Science and Engineering with Prof. R.M. Laine at The University of Michigan at Ann Arbor. He is presently a National Research Council postdoctoral fellow at the National Institute of Standards and Technology with Dr. Vivek Prabhu in Polymers Division of the Materials Measurement Laboratory. His postdoctoral work focuses on the evaluation of functional polymer thin films using a simultaneous light reflectance/quartz-crystal microbalance technique.

In the following sections we first discuss the synthesis of the three phenylSQs, $[PhSiO_{1.5}]_n$ where $n = 8$, 10, and 12, and several related compounds. Thereafter, we discuss the synthesis of functionalized phenylSQs primarily via electrophilic substitution. These discussions are followed by studies on efforts to further functionalize the electrophilically functionalized phenylSQs.

Synthesis of PhenylSQ Polyhedra

The various $[PhSiO_{1.5}]_n$ polyhedra have been synthesized from a variety of starting materials using both acid and base catalysis. Base-catalyzed syntheses usually offer better yields.[44−50]

The earliest studies on the synthesis of $[PhSiO_{1.5}]_n$ were reported by Barry et al. in 1955.[43] This group used base-catalyzed rearrangement of polySQs to isolate the $n = 6$ product, later reformulated as the $n = 8$ compound. Thereafter, Sprung and Guenther described the synthesis of $[PhSiO_{1.5}]_8$ from a high $[PhSiO_{1.5}]_n$ polymer produced from a mixture of phenyltriethoxysilane, water, tetraethylammonium hydroxide, and methyl isobutyl ketone.[45] Olsson et al.[46,47] and Brown et al. prepared $[PhSiO_{1.5}]_{8-12}$ by base-catalyzed equilibration of polyphenylsilsesquioxane at reflux.[48−50]

Brown and co-workers were the first to explore hydrolysis of $PhSiCl_3$ to produce $PhSi(OH)_3$ as an intermediate in the acid-catalyzed synthesis of phenylSQs, as generally illustrated in Scheme 2.[48−50] Initial efforts focused on developing soluble, processable "T" resin systems; however, cage compounds were found to form simultaneously.

Coincidentally, Brown characterized one set of isolated materials as the ladder compounds suggested in Scheme 2, going so far as to publish a detailed paper on the theory and expected properties of silsesquioxane ladder polymers.[50] A follow on paper by Frye and Koslowski disputed the existence of silsesquioxane ladder polymers.[51] To date there are no detailed reports supporting the existence of high molecular weight ladder silsesquioxanes, although several groups have successfully made and isolated oligomeric SQ ladders, suggesting that these materials would be difficult to make as long chain, high molecular weight polymers.[21,52−54]

The acid-catalyzed synthesis of $[phenylSiO_{1.5}]_{8,10,12}$ proceeds from initial hydrolysis of the trichlorosilane monomer to form the triol, $PhSi(OH)_3$, which must first condense to form dimer. The dimer in turn preferentially forms the all cis-isomer of reaction 1 possibly via a linear tetramer.[55] Several groups have isolated the all-cis-tetramer,[56−58] with Feher et al. reporting the crystal structure shown in Figure 2.[56] The half-cage slowly transforms in the solid state into $[phenylSiO_{1.5}]_8$ most likely driven by the cofacial hydrogen bonds.

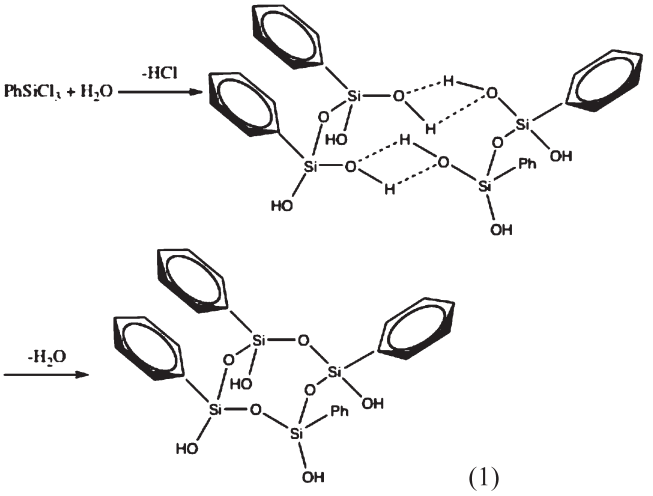

(1)

Although numerous groups have now studied the synthesis of $[PhSiO_{1.5}]_8$, we found it necessary to develop a reliable scaled reaction

Scheme 1. (a, b) Cubic T_8[13,19] and (c) Q_8 SQ[21] NBs with Multiple Types of Functionality

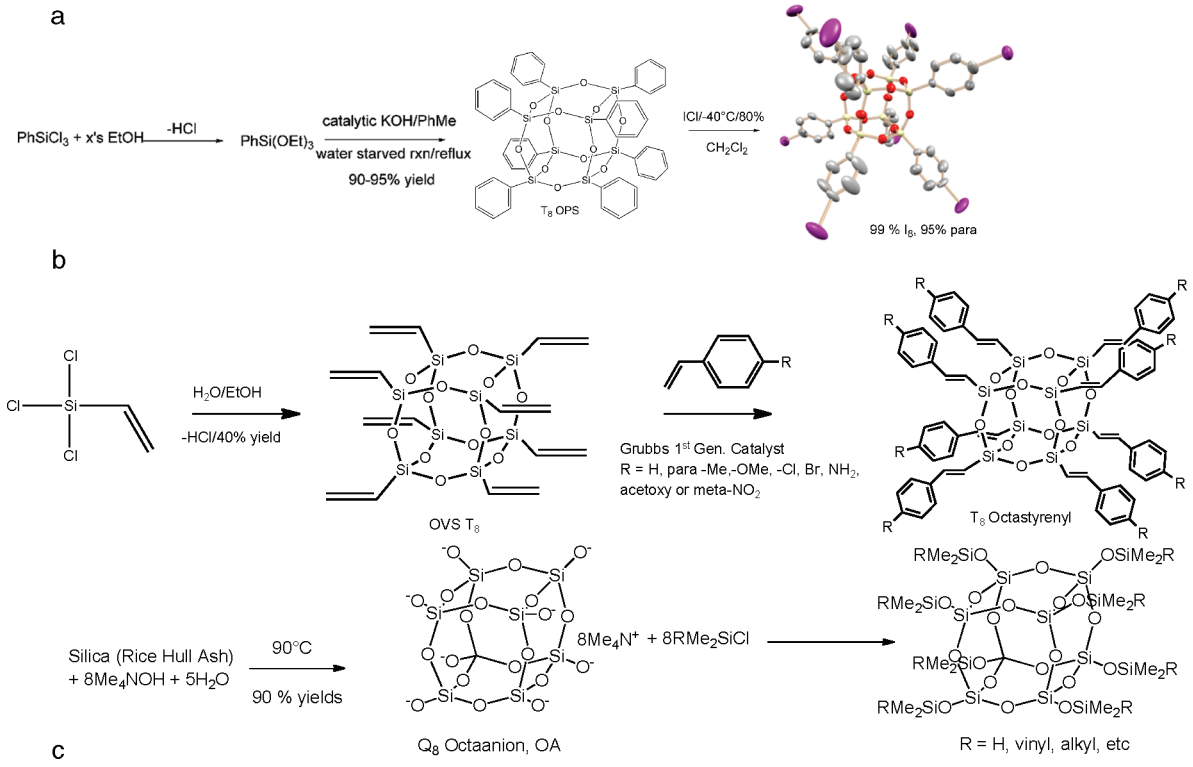

Scheme 2. General Pathway for the Hydrolysis and Condensation of $RSiX_3$ Where X = Cl, Br, OR, OAc, etc.

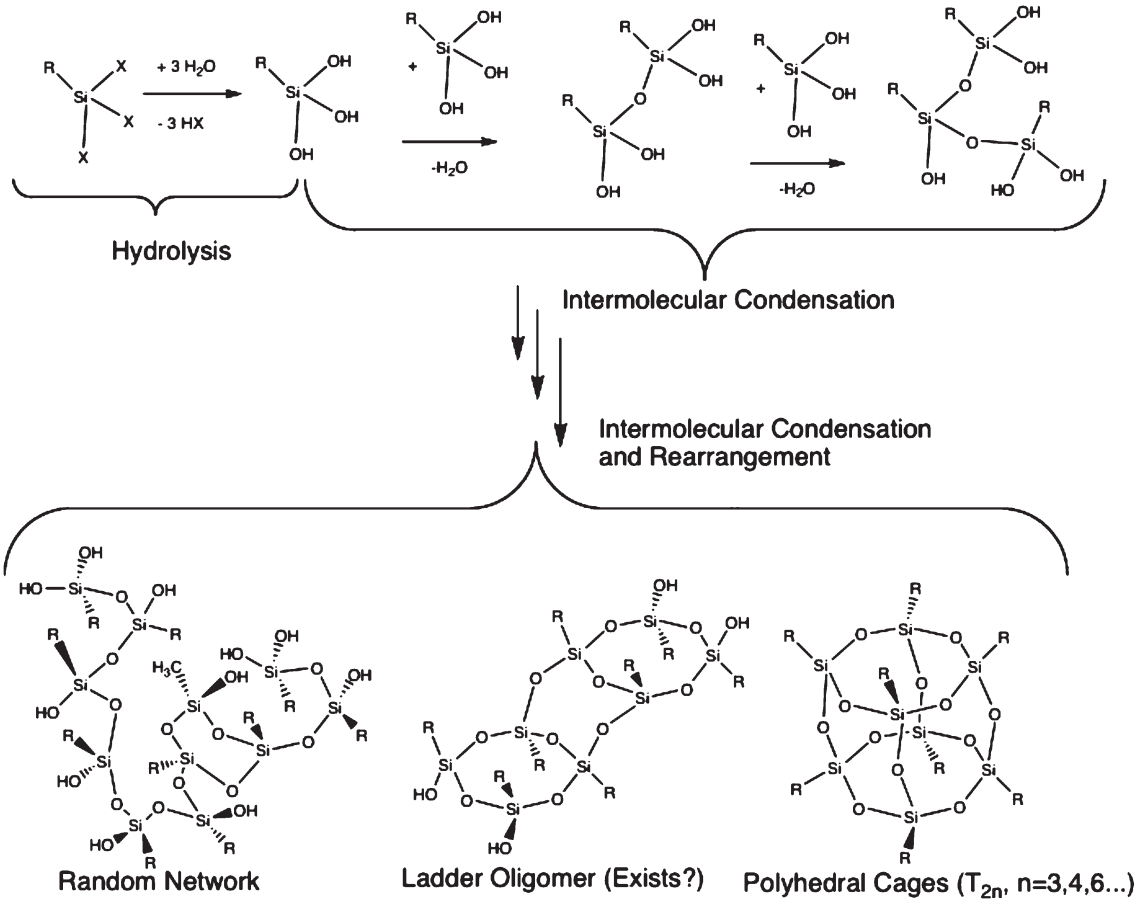

to reproducibly prepare this compound from $PhSiCl_3$. We have identified two general paths to $[PhSiO_{1.5}]_8$ as seen in Scheme 3.

As noted just above, multiple methods of forming $[PhSiO_{1.5}]_8$ have been described. In our experience these are typically complex,

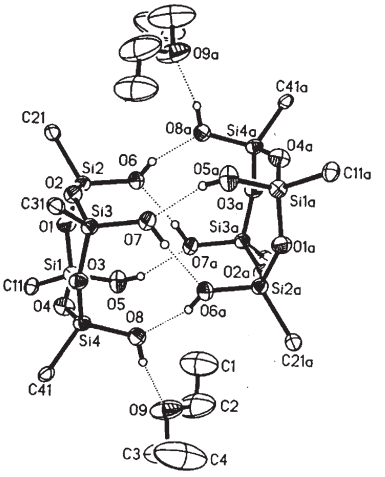

Figure 2. Single crystal X-ray diffraction study of the all-cis-half-cage.[56]

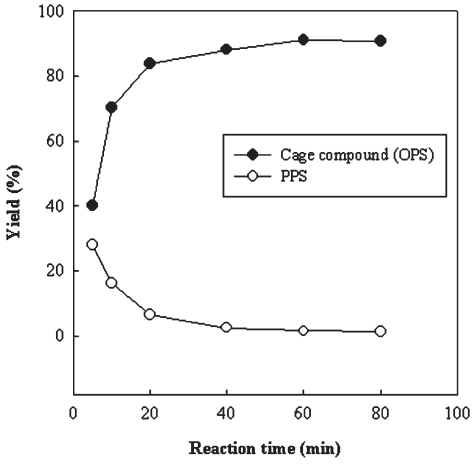

Figure 3. Yield of $[PhSiO_{1.5}]_8$ (OPS) and $[PhSiO_{1.5}]_n$ (PPS) formed by reflux with polymeric PTES under water scarce conditions: 7 g, 29.1 mmol of PTES, water (0.5 mL, 10 wt %), and KOH (0.5 g, 7.5 wt %) in 50 mL of toluene.[58]

multistep, and often low yield. Scheme 3 illustrates the two pathways we have explored.[58] The process begins with the conversion of $PhSiCl_3$ into phenyltriethoxysilane (PTES) by reaction in ethanol. Surprisingly, depending on the reaction conditions (reflux for 2 h vs 4−6 h), the product is either the liquid monomer PTES or a polymeric version (polymeric PTES), both of which provide $[PhSiO_{1.5}]_8$ with some polymeric material $[PhSiO_{1.5}]_n$ by reaction with catalytic amounts of KOH and minimal amounts of water, as specified below. Both products are easily separated and purified.

$[PhSiO_{1.5}]_8$ produced by hydrolysis of $PhSiCl_3$ forms more readily in benzene, nitrobenzene, benzyl alcohol, pyridine, and ethylene glycol dimethyl ether, whereas the dodecamer, $[PhSiO_{1.5}]_{12}$, forms preferentially in tetrahydrofuran.[48] Hydrolysis of $PhSiCl_3$ in acetonitrile, diglyme, acetone, and methyl isobutyl ketone gives high-MW $[PhSiO_{1.5}]_n$.[48] Many $[PhSiO_{1.5}]_8$ syntheses use benzene as a solvent which is now known to be carcinogenic; thus, toluene is now often used as a substitute.[44,47,48]

Key to the synthesis of $[PhSiO_{1.5}]_8$ in high yields is the use of scarce water conditions. Water must be added dropwise over about 30 min in our standard reaction. Thus, 0.125−1.5 mL (6.9−83.3 mmol) is added slowly to solutions containing 7 g of PTES (29.1 mmol) and 50 mL of solvent. The amount of water to be added must be calculated exactly to ensure optimal yield, 27.8 mmol (29.1 theory), of $[PhSiO_{1.5}]_8$. *The water concentration should be just slightly less than the equivalents of PTES or polymeric PTES used.* Optimal water concentration for Figure 3 reaction is 0.5 mL. Some adventitious water, present in the reaction system, makes up the difference. Polymeric PTES always gives better yields of $[PhSiO_{1.5}]_8$ than PTES probably because some of the cage structure is preformed in the polymer (Scheme 3).

The yields of $[PhSiO_{1.5}]_8$ and PPS are also affected by concentrations of KOH, water, reaction time, and solvents. Figure 3 illustrates the rate of formation of $[PhSiO_{1.5}]_8$, as a function of reaction time under a standard set of conditions.[58] It appears that an equilibrium is reached after 4−50 min of reaction time. As can be seen, the equilibrium yields appear to be 90:10 in favor of $[PhSiO_{1.5}]_8$, recalling that it is mostly insoluble in the reaction solution.[58]

The synthesis of dodecaphenylsilsesquioxane, $[PhSiO_{1.5}]_{12}$, in our experience is relatively facile using a simple modification of Brown et al.'s original procedure[48,49,59] that begins with the synthesis and isolation of an oligomer of $PhSi(OH)_3$ produced by hydrolysis of $PhSiCl_3$ in ethyl acetate at 0 °C with the addition of excess water. This oligomer is then carefully heated with Me_4NOH in a 3:1 THF:ethanol to reflux for 7 days. After ≈24 h, white powder begins to precipitate. Following filtration and purification, the $[PhSiO_{1.5}]_{12}$ can be isolated in 60% yields.

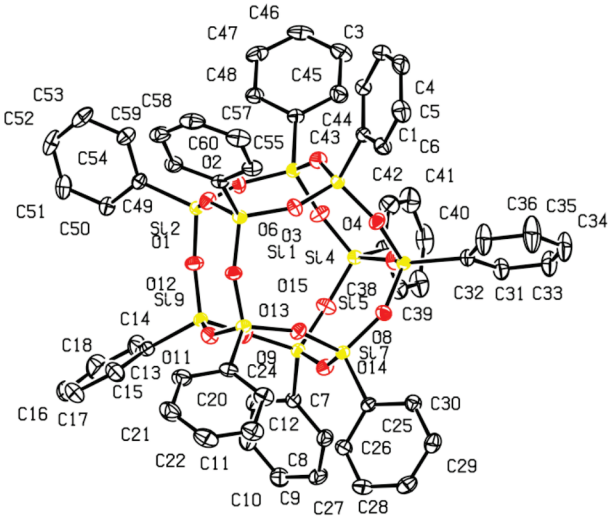

Figure 4. 50% thermal ellipsoid plots of decaphenylsilsesquioxane·toluene. H atoms and toluene solvate are omitted for clarity.[60]

In contrast, there are no concise methods of preparing the decameric $[PhSiO_{1.5}]_{10}$ despite its isolation by Brown et al. almost 50 years ago. We have now learned to prepare it in isolable yields using a set of unusual conditions.[60] We find that anhydrous base-catalyzed (BaO/18-crown-6) equilibration of $[PhSiO_{1.5}]_{12}$ in *m*-xylene at high dilution (3 g $[PhSiO_{1.5}]_{12}$/100 mL *m*-xylene) permits isolation of $[PhSiO_{1.5}]_{10}$ albeit in 15% yield, after repeated recrystallization.[60]

Crystals grown from toluene permit a single crystal X-ray analysis as seen in Figure 4. This very unusual molecule has 5-fold symmetry, and consequently it or uniform derivatives such as the para-iodo derivative discussed below may offer some unusual packing properties as well as novel electronic properties.

The base-catalyzed route most likely passes through multiple species similar to those suggested in Scheme 2. Indeed, by using stoichiometric concentrations of base, it is possible to isolate species that may be intermediates involved in the formation of the complete polyhedral species. For example, Shchegolikhina et al. report a second route to the half-cage of reaction 1 using stoichiometric amounts of NaOH in nBuOH, reaction 2.[61−63] This approach can be used to make full cages with mixed functional groups by silylating *cis*-$[PhSi(ONa)O]_4$.[61−63]

Scheme 3. General Pathways for Formation of $[PhSiO_{1.5}]_8$ and $[PhSiO_{1.5}]_n$[58,59]

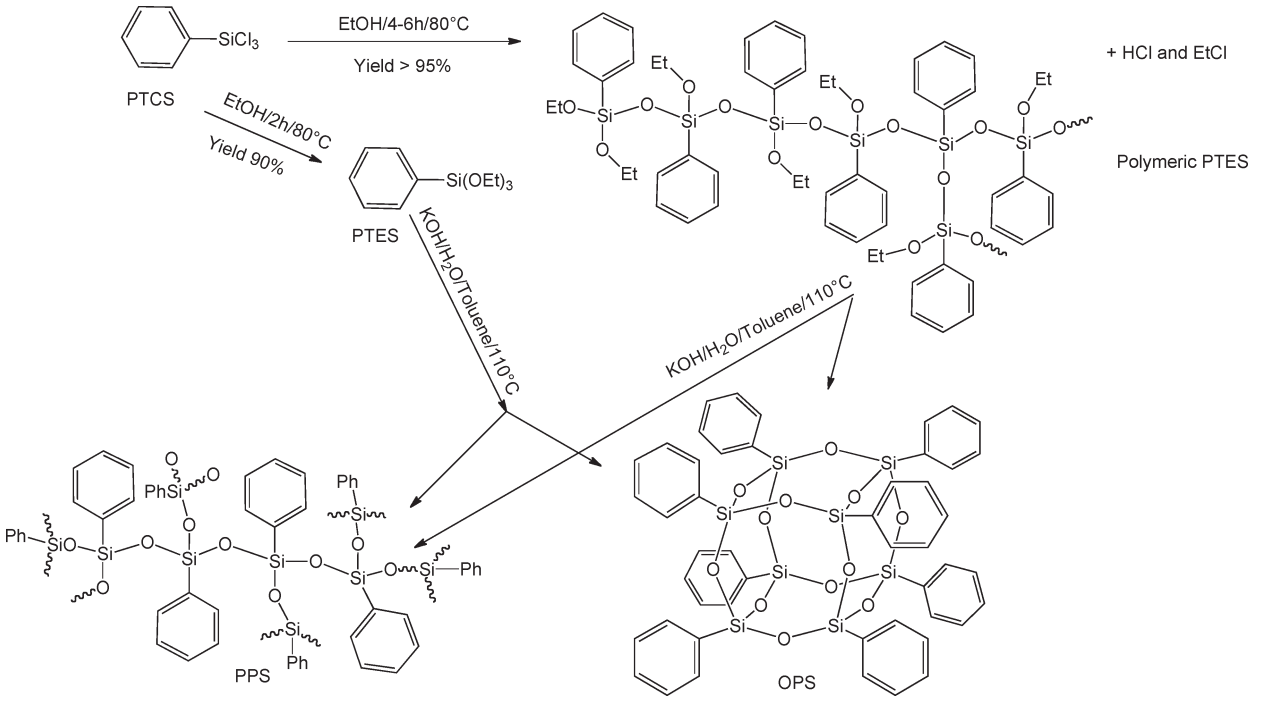

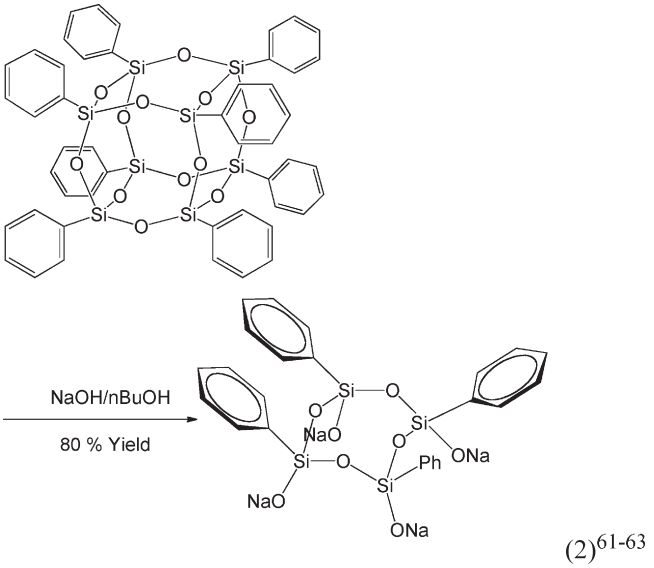

(2)[61-63]

Double-Decker and Other Ring-Opened SQs

Different products are obtained by varying the ratio of base to ($PhSiO_{1.5}$) units. Thus, several Japanese groups have synthesized sets of open cage compounds per reactions 3 and 4.[64−68]

Reaction 3 provides one example of a set of corner open partial cages that permit introduction of a single functional group providing a whole range compounds that allow incorporation[60−64] of SQs as terminal or pendant groups in polymers or as nanoreinforcing materials in composites as reviewed earlier.[17,19,22] In addition, this same type of compound permits the introduction of a variety of metal species wherein the partial cage serves as a stabilizing ligand.[20] In these compounds, the cage acts to mimic silica surfaces, and the resulting compounds offer properties akin to heterogeneous catalysts but in a soluble form. Their utility as silica emulating homogeneous catalysts was recently reviewed by Duchateau.[20]

In contrast, the reaction 4 products are quite unique, and their potential properties are just now being investigated.[63−68] To date, R= isobutyl, glycidoxy, vinyl, methacrylate, chloropropyl, norbornene anhydride, and cyanomethyl derivatives have been made. As suggested in reaction 4, the R group substituted products consist of the *cis* and *trans* isomers. Reaction of isobutyl-$SiCl_3$ with the double-decker product allowed isolation of the *cis* and *trans* dihydroxy compounds, which were be separated by careful chromatography coupled with selective recrystallization. Subsequent dehydrocoupling, reaction 5,[67] provides polymers with the cage in the chain. The polydispersities are 1.5−1.8, relatively low for a step growth polymerization, where a PDI > 2 would be expected. T_gs average just over 30 °C and $T_m \approx 300$ °C

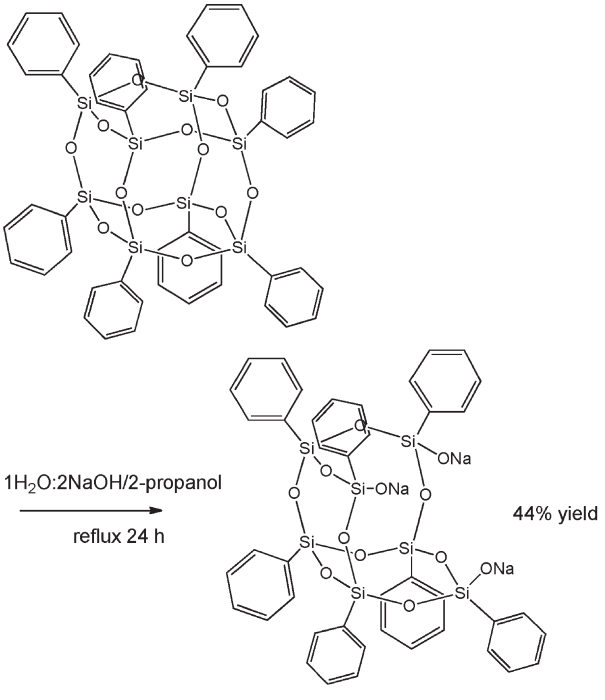

(3)

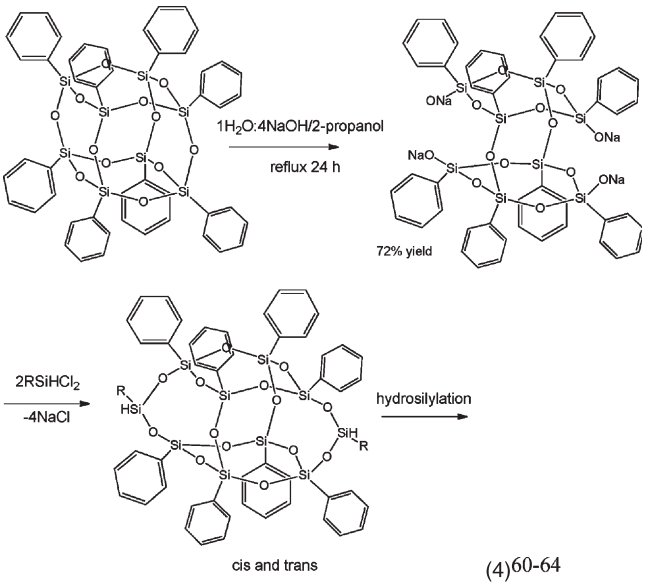

(4)[60-64]

for the *cis* compound and 360 °C for the *trans* compound. Reported M_n values range from 5K to 50K Da.

Most important, films of these compounds are air stable to > 450 °C and transparent in the visible range.[67] These values are superior to those of simple polydimethylsiloxane polymers offering the potential to make new types of reinforced polysiloxane materials. Kakimoto et al. made related polymers by hydrosilylating the methyl vinyl derivative with the same Si−H capped tetramer with essentially identical results.[66]

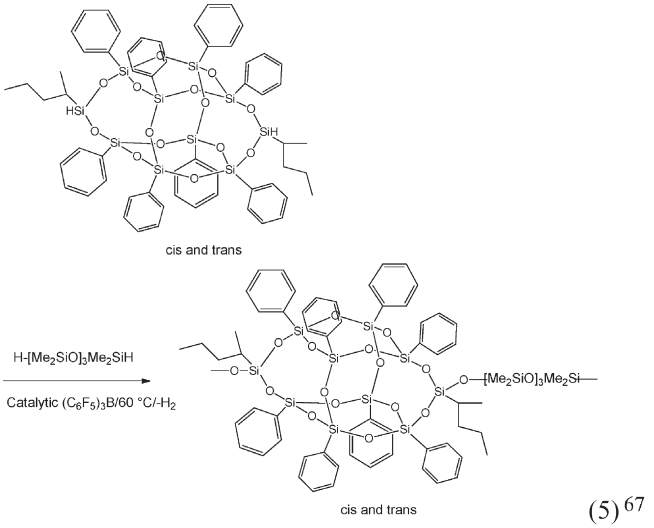

(5)[67]

Kakimoto et al. also prepared the methylsilyl analogue and hydrosilylated alkynes and dialkynes to produce linear polymers.[65,67,68] Thus, using 1,4-diphenylethynylbenzene in reaction 6 produces a polymer with $M_n \approx 29$K Da, a polydispersity of 4, a $T_g \approx 150$ °C, and a $T_d > 500$ °C in N_2.

No evidence was found for hydrosilylation of the internal double bonds most probably because of the large steric interactions involved. Unfortunately, no further characterization of the resulting polymers for example their photonic properties is reported. Imides made from the norbornene anhydride, reaction 7, offer processability and high temperature stability, but only selected derivatives (with meta substituents) are processable.[68]

Given the simplicity of the syntheses, they appear to be easy to scale; we anticipate that many new materials will arise based on these well-defined double-decker materials in the future. As discussed below, such polymer materials may show electron delocalization through the cage.

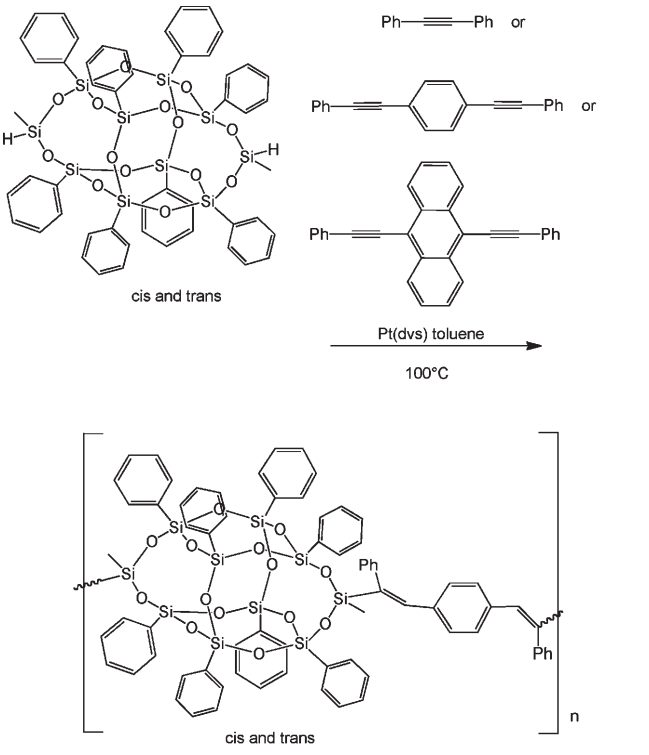

(6)[65]

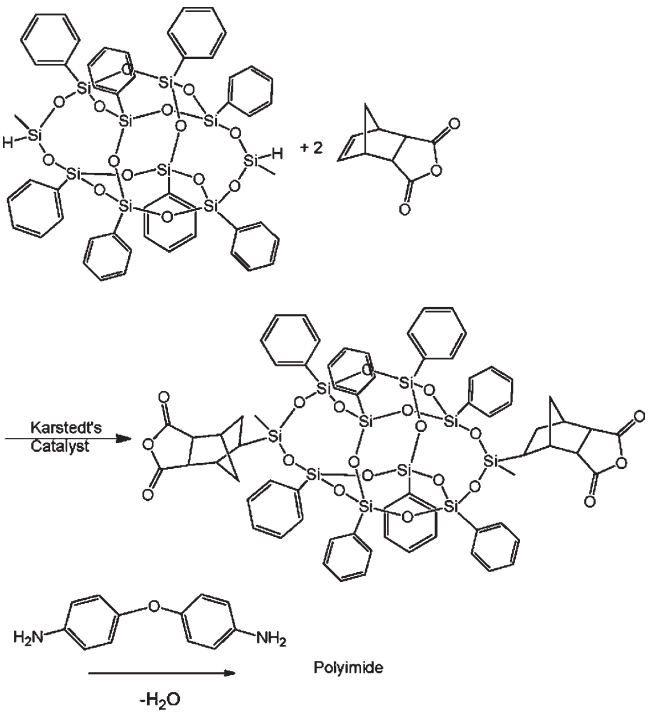

(7)[68]

One remaining example of a cage opened derivative has been described following the synthetic route shown in reactions 8 and 9.[69] The ring-opened triflate intermediate undergoes nucleophilic displacement, providing difunctionality along one edge of the original cage.

The resulting dianilino material of reaction 9 can be used to produce polyimides with good processability, high-temperature stability, and also good resistance to atomic oxygen. The latter studies were run emulating conditions experienced by satellites in low-Earth orbit.[69]

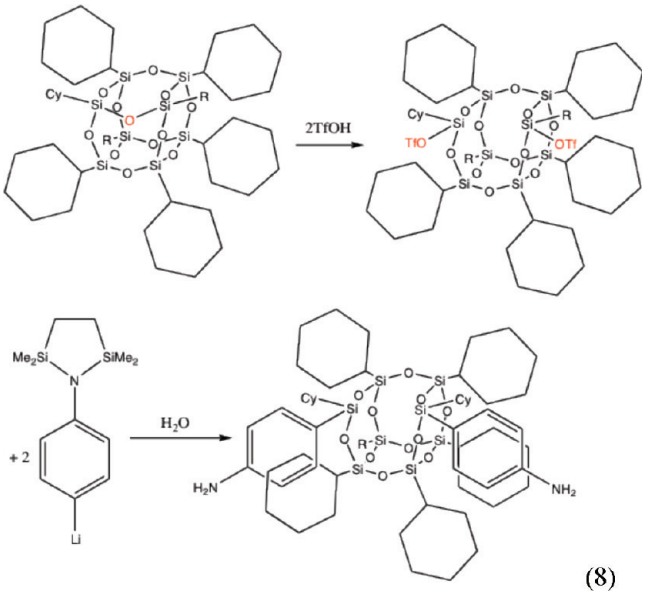

(8)

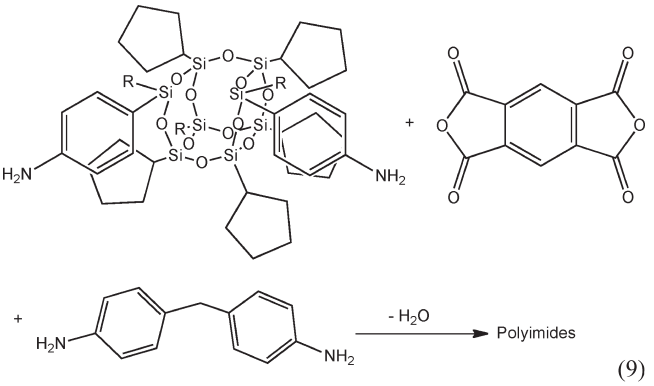

(9)

The above reactions summarize efforts to produce functionalized cages and partial cages through manipulations of the core. The next sections cover efforts to functionalize complete cages starting with the electrophilic functionalization of the aromatic rings themselves.

Nitration and Reduction to AminophenylSQs

The first example of electrophilic substitution was nitration of $[PhSiO_{1.5}]_8$, reported by Olssen and Gronwall in 1961 in Arkiv fur Chemie.[47] These researchers found that $[PhSiO_{1.5}]_8$ (OPS) dissolves completely in fuming nitric acid at 0 °C, leading to nitration of each phenyl ring just once over a very short reaction period to give $[(NO_2)PhSiO_{1.5}]_8$.[47] The product is isolated in 80$^+$% yield by precipitation into ice water. Given the ease with which trimethylsilyl aromatics undergo protodesilylation,[70] this observation seems quite surprising. Of note is that the authors reported that efforts to reduce the nitro groups to amines were unsuccessful,

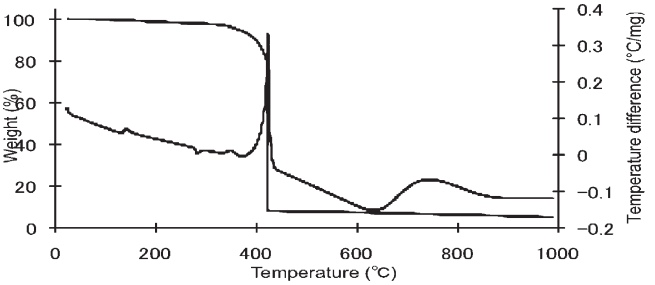

Figure 5. TGA/DTA data of $[(NO_2)_2PhSiO_{1.5}]_8$.

describing the nitro groups as "inert".[47] This paper went unnoticed for some 38 years.

Given that nitro groups are rarely inert, we revisited this reaction and discovered that they are easily reduced using formic acid/Et_3N as the reducing agent with Pd/C as catalyst. This reduction method works effectively providing $[NH_2PhSiO_{1.5}]_8$ or octaaminophenylsilsesquioxane (OAPS). The nitration pattern and hence the amine substitution pattern indicate that nitration occurs at both the *meta* and *para* positions in the approximate ratio of 65:25 *m:p*; which can be inferred from the substitution pattern of $[(NO_2)_2PhSiO_{1.5}]_8$ (see Table 1).[74] This ratio can vary depending on reaction conditions.

It is also possible to dinitrate $[PhSiO_{1.5}]_8$ (OPS) to produce the $[(NO_2)_2PhSiO_{1.5}]_8$ heating the initial reaction mixture to temperatures ≈50 °C (reaction 10).[72] It is also possible to dinitrate the dodecamer, $[PhSiO_{1.5}]_{12}$.[72] One of the more interesting results of dinitration is the observation that HDNPS decomposes explosively (Figure 5) at 400 °C, suggesting that it is an unusually stable, albeit explosive, material.[72]

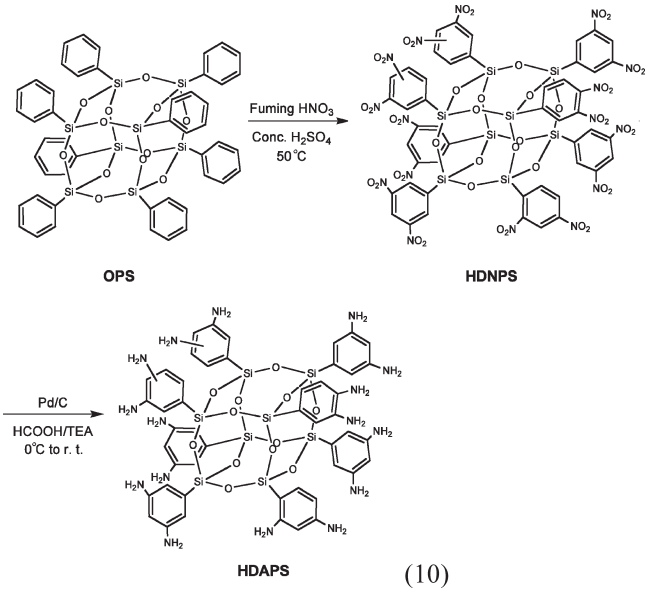

(10)

Table 1. NH_4F Cleavage of $[(NO_2)_2PhSiO_{1.5}]_8$ ^{1}H NMR Data (^{A}±2%)

^{1}H-NMR	Assignment	Mol %^{A}	Isomer on HDNPS
8.92	1,3-dinitrobenzene	90%	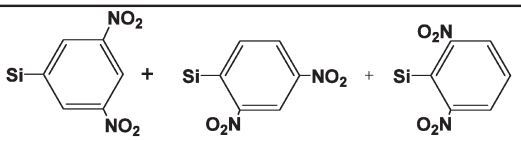
8.38	1,2-dinitrobenzene	10%	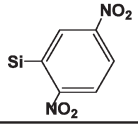

Since our original report on the reduction of the $[(NO_2)PhSiO_{1.5}]_8$ to OAPS,[71] and more recently the $[(NO_2)PhSiO_{1.5}]_{12}$ to dodecaaminophenylsilsesquioxane (DDAPS),[72] a number of groups have followed up on this reaction using the resulting OAPS as a synthetic building block to make a wide number of hybrid nanocomopposite materials.[73−82] All of these researchers produced OAPS using the formic acid/Et_3N method except for Zhang et al.,[78] who report the use of $FeCl_3$/active carbon and hydrazine hydrate at 60 °C. The advantage of this method is that Pd/C is an expensive catalyst. The disadvantage may be that hydrazine hydrate can be quite reactive and caution should be employed if one chooses to use it.

The OAPS and the dodecamer analogue DDAPS offer the potential to synthesize a wide variety of derivatives for numerous potential applications as suggested by Scheme 5. Among the more interesting compounds are OMIPS, the OLED compounds, and the luminescent chelates.

OMIPS is an octamaleimide that could be used with other maleimides (see ref 78) to produce stable, high-temperature imide materials without the need to process the imide component coincidentally with the formation of the composite. This has the advantage of avoiding the need for high-temperature curing often required to force complete imidization. It also avoids the elimination of water during this step, which can degrade imide properties. Zhang et al.[78] describe what appears to be a very simple method of producing these materials compared to the original preparation with the highest reported synthesis temperature being 60 °C.

The condensation of 2-pyridinecarboxyaldehyde with OAPS, Scheme 4vi, provides a novel imine, solutions of which emit green under UV light.[83] This compound was synthesized with the idea of providing sites for binding metals for trace metal analyses because of its novel luminescent properties and for a wide variety of display applications.[83] To date, this compound has not been studied for such applications.

As noted in the Introduction, the 3-D nature of SQs coupled with the fact that they offer multiple functional sites and exceptional thermal stability has prompted numerous efforts to use OAPS and DDAPS as replacements for aromatic amines in epoxy resins, polyimides, and related materials.[34−43,68−82] In the following sections, we provide a brief overview of epoxy resin materials and polyimides. Some aspects of Q_8 silsesquioxane epoxy

Scheme 4. Reactions of OAPS[a]

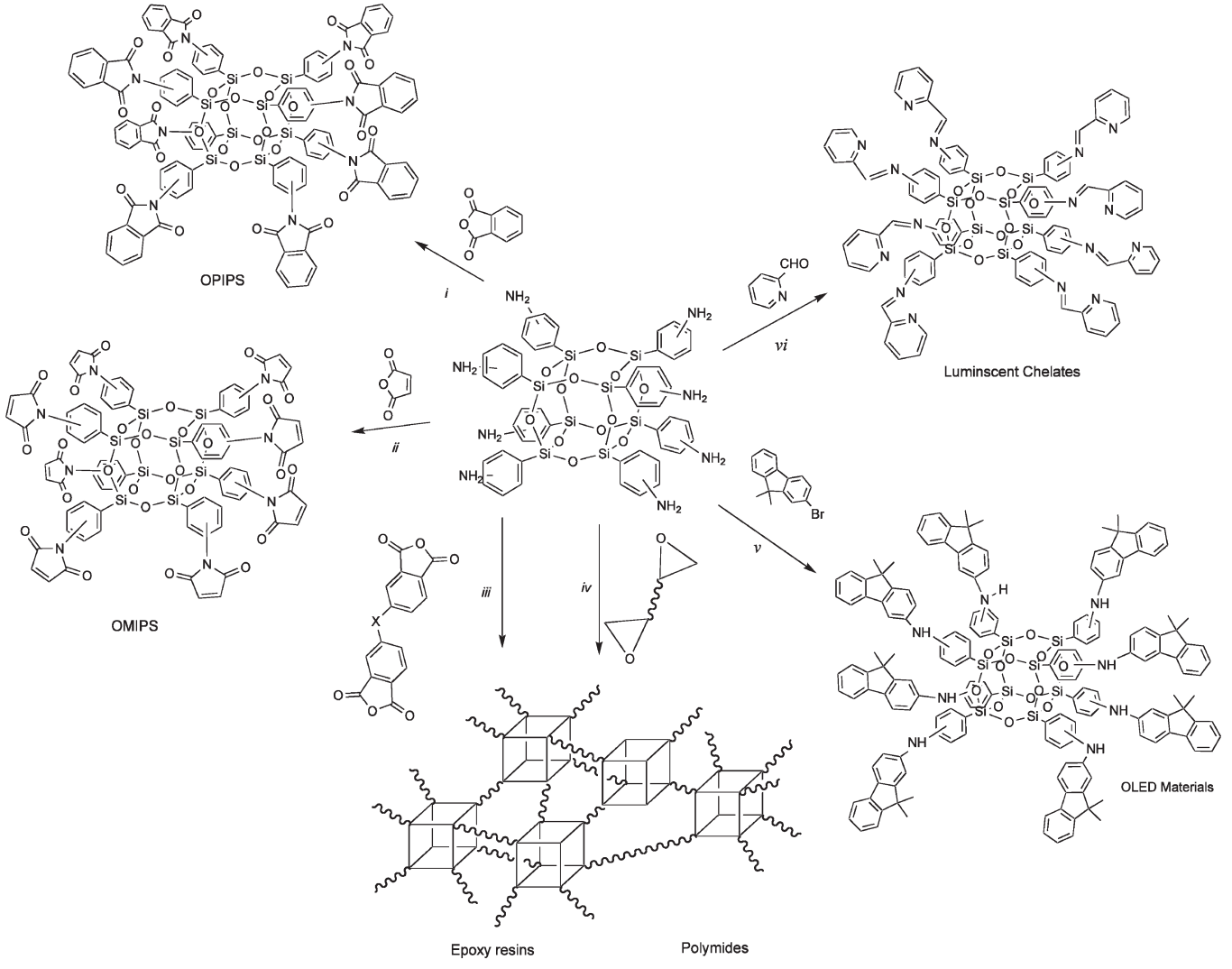

[a] Reactants and conditions: (i) 1:8.4 OAPS:phthalic anhydride in NMP 350 °C/N_2/4 h; (ii) 1:8 OAPS:maleic anhydride in DMA 60 °C/N_2/3 h with acetic anhydride and Et_3N; (iii) 1:8 OAPS:pyromellitic anhydride in NMP 350 °C/N_2/3 h; (iv) 1:8 OAPS:epoxy neat at 200 °C/6 h/N_2; (v) 1:8.8 OAPS:2-bromo-9,9-dimethylfluorene, $Pd_2(dba)_3$, (dcbp)P, glyme 100 °C/N_2/5.5 h; (vi) 1:8 OAPS:2-pyridinecarboxaldehyde Na_2SO_4/THF/RT/N_2/22 h.

Scheme 5. Epoxy Curing Reactions as a Function of Amine:Epoxy Ratios

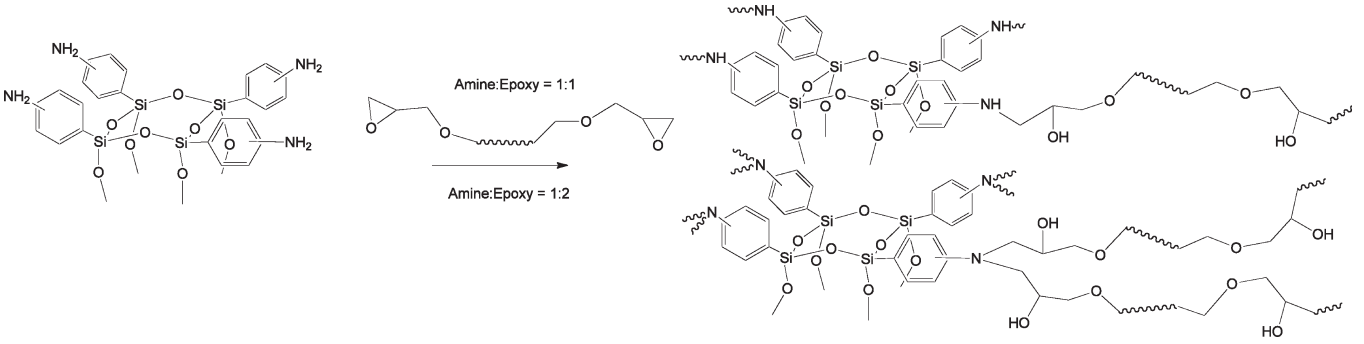

resin synthesis, processing, and properties were covered in an earlier review.[23]

Amino-SQ Epoxy Resins

Traditional epoxy resin chemistry involves the reaction of NH_2 groups with epoxy groups to form aminols of the type shown in Scheme 5 and reaction 11. The aminol functional groups form hydrogen bonds easily; hence, epoxy resins exhibit a great propensity to imbibe moisture, swell, and degrade, reducing their utility in humid environments. In addition, the aminols decompose easily limiting their thermal stability. The 1:2 ratio materials of Scheme 5 will exhibit much higher cross-link densities than the 1:1 ratio materials.

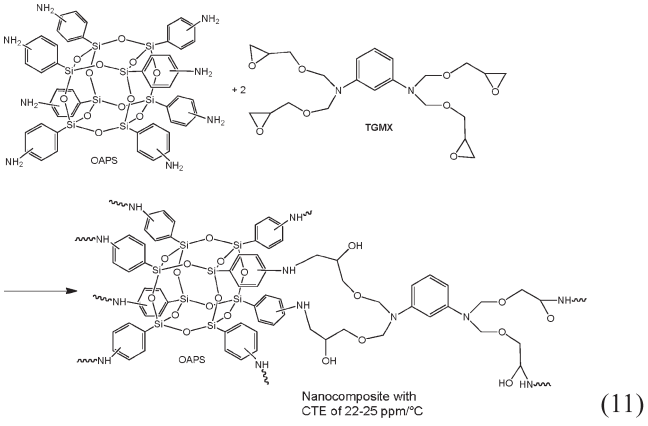

(11)

The type of product obtained depends on both the initial ratio used and also the steric congestion at either the epoxy or the amine; thus, some epoxy systems may not cure fully even with stoichiometrically correct ratios.[33,36] Furthermore, as curing with polyfunctional amines will always lead to cross-linking, as the reaction proceeds, the viscosity of the reaction mixture increases to the point (gel point) where further cross-linking is greatly hindered even with increases in reaction temperature. This leads to defects in the epoxy resin system that can greatly influence mechanical properties.[36]

Traditional epoxy resins with at most four epoxy units per molecule and common aromatic amine curing agents with two amines per molecule, 1:2 ratios, are practiced commercially. The resulting cured resins are commonly brittle but offer good tensile strengths and hardnesses. Furthermore, by tailoring the linkages between the epoxy groups, one can introduce toughness and control curing temperatures and also T_gs. However, with the use of OAPS, with eight amine groups one can achieve very high cross-link densities using amine:epoxy ratios of 1:1 or 1:2. The latter systems can be expected to be extremely brittle.

Thus, it is possible by both changing the stoichiometry and the type of epoxy resin to tailor the coefficients of thermal expansion,

Table 2. CTEs of OAPS Cured at 200 °C with Selected Amine:Epoxy Molar Ratios of 1:1 (1) or 1:2 (0.5)[82]

epoxy	molar ratio	CTE (ppm/°C) ± 3 ppm
TGMX[a]	0.5	55
TGMX	1	25
TGMX	1 wt % Al_2O_3	22
ECHX[b]	0.5	91
ECHX	1	55
diglycidyl ether bisphenol A (DGEBA)	0.5	80
DGEBA	1	72
$[glycidylSiMe_2SiO_{1.5}]_8$	0.5	196
$[glycidylSiMe_2SiO_{1.5}]_8$	1	141
$[cyclohexenylepoxyethylSiMe_2SiO_{1.5}]_8$	0.5	185
$[cyclohexenylepoxyethylSiMe_2SiO_{1.5}]_8$	1	217

[a] TGMX = tetraglycidyl ether *m*-xylene diamine. [b] ECHX = 3,4-epoxycyclohexylmethyl-3,4-epoxycyclohexanecarboxylate.

the mechanical properties, and also the barrier properties of OAPS epoxy resin systems. Table 5 taken from ref 82 (Table 2 in that work) shows that it is possible to produce epoxy resins with CTEs that vary over an order of magnitude from 25 to 220 ppm/°C. An important point is that these systems can offer relatively low processing viscosities (e.g., 1000 mPa·s).

CTEs in the range of 22−25 ppm/°C are very desirable in "flip-chip" applications where integrated circuits (CTE ∼ 4−6 ppm/°C) and printed circuit boards (CTE ≥ 40 ppm/°C) are bonded together. Otherwise, the addition of silica filler is necessary, which can raise processing viscosities to 10K mPa·s and interfere with solder bumps contacting the PCB prior to soldering.[82]

Note that in Table 2 the best properties are exhibited for the 1:1 amine:epoxy ratios rather than the traditional 1:2 ratios. There are several possible explanations for this. First, the total volume fraction of OAPS is higher in the 1:1 case, limiting the amount of the flexible TGMX component. Alternately, this results in a higher concentration of the rigid OAPS cage, thereby limiting the potential for thermal expansion. The other explanation might be that at a 1:2 ratio curing is incomplete, for the reasons noted above, leading to unreacted chain ends that allow defects in the resin system that cannot resist thermal expansion. Both explanations are likely operative. This same set of explanations may be used to justify observations concerning the barrier properties of these materials.

Whereas siloxane-based polymer membranes often exhibit high oxygen permeabilities, OAPS epoxy and polyimide membranes can be tailored to offer oxygen permeabilities comparable to commercial oxygen barrier membranes.[43] Table 3 compares oxygen transport properties of a set of solvent-cast OAPS epoxy and imide membranes cured under various conditions.

In contrast to the CTE values given in Table 2, the best barrier properties are obtained at 1:2 molar ratios, perhaps because of

Table 3. Oxygen Transmission Rates (OTR) of Cast Silsesquioxane Films [at 20 °C and 65% RH; $cm^3 \cdot 20\ \mu m/m^2 \cdot day \cdot atm\text{-}O_2$, i.e., Standardized to 20 μm Thickness][43]

sample	*N* NH_2:epoxy	initial curing	curing with pressure	OTR (±0.5) ($cm^3 \cdot 20\ \mu m/m^2 \cdot day \cdot atm$)
OAPS/DGEBA	0.5	120 °C/4 h	200 °C/10 h at 0.690 MPa	7
OAPS/DGEBA	0.5	120 °C/4 h	200 °C/10 h at 0.862 MPa	5
OAPS/DGEBA	0.5	120 °C/4 h	200 °C/10 h at 1.03 MPa	3.9
OAPS/TGMX	0.5	100 °C/1 h, 130 °C/4 h	200 °C/4 h at 1.03 MPa	3.2
OAPS/ECHX	0.5	100 °C/1 h, 130 °C/4 h	200 °C/4 h at 1.03 MPa	5.2
OAPS/TGMX	0.5	100 °C/1 h, 130 °C/4 h	200 °C/4 h at 1.03 MPa	1.2
OAPS/ECHX (i) bilayer	0.5	i. 100 °C/1 h, 130 °C/4 h	iii. 200 °C/4 h at 1.03 MPa	0.8
OAPS/TGMX (ii) bilayer	0.5	ii. 100 °C/1 h, 130 °C/4 h		0.8
50%OAPS/PMDA[a]		120 °C/4 h	240 °C/8 h at 1.03 MPa	17
50% OAPS/ODPA[b]		120 °C/4 h	240 °C/8 h at 1.03 MPa	12
EVAL F grade[c]				< 1.0

[a] Pyromellitic dianhydride. [b] oxidiphthalic anhydride. [c] Eval F is 32% ethylene−vinyl alcohol copolymer biaxially orientated (3 × 3) and heat treated to 140 °C.

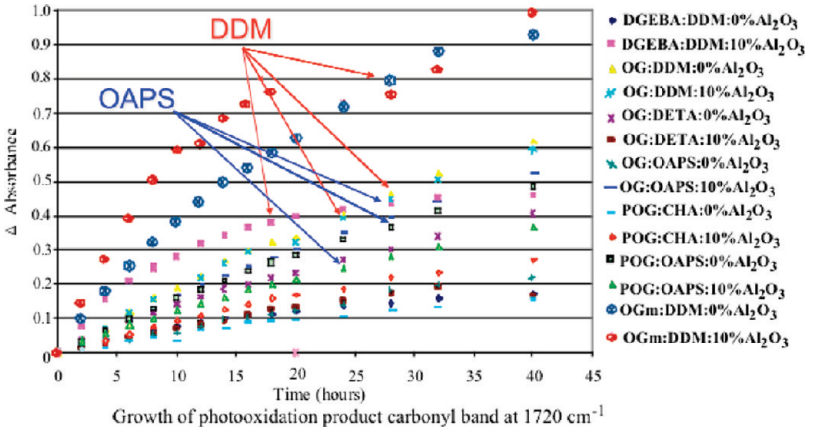

Figure 6. Effects of irradiation as determined by appearance of acidic carbonyl at 1720 cm^{-1}.[85] CHA = di(amino)dicyclohexylmethane, OG = octaglycidyldimethylsiloxyoctasilsesquioxane, POG = polyglycidyldimethylsiloxysilsesquioxane, and OGm:DDM should read as OG:mDDM.

Scheme 6. Reaction of OAPS with PMDA To Form a Nanocomposite with Completely Rigid Components Were First Cast Prior to Heating To Minimize Gel Formation; Thereafter, Complete Curing Obtained Only at Temperatures above 300 °C

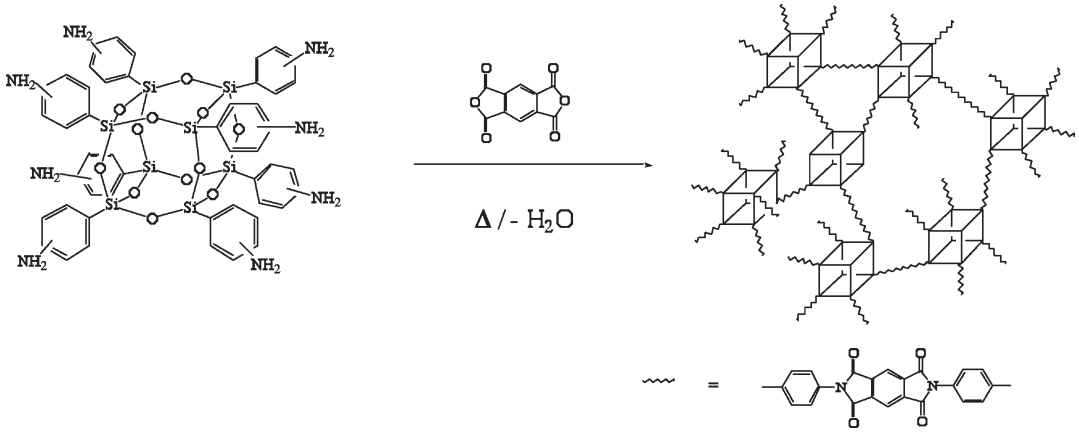

the much higher cross-link densities achieved. The use of bilayer systems and curing with pressure improves barrier properties likely because of removal of bubbles within the cured films and also by generating an interface between the layers. Table 3 also provides data for selected polyimide films whose properties are discussed in the next section.

An additional advantage to using OAPS rather than aromatic amines is demonstrated in Figure 6 where epoxy resin samples of standard thickness were irradiated 40 h at $\lambda > 300$ nm, 60 °C (medium acceleration test) in the presence of oxygen.[85] The chemical evolution of the polymer matrices was followed by infrared and UV−vis spectrometries in transmission. The samples are divided into two groups: aromatic and nonaromatic. For nonaromatic samples, the oxidation is controlled only by O_2 diffusion into the polymer. Thus, for the thickness analyzed, the O_2 diffusion is similar for all samples, and the oxidation is relatively homogeneous throughout the sample thickness. Aromatic samples absorb $\lambda >$ at 300 nm; thus, their degradation is limited by the penetration of light (Beer−Lambert law). Sharp oxidation profiles are observed only for the first 10−30 μm, depending on the structure of the material.

Scheme 7. Imide Tether Formation from OAPS and PDMA (Amine:Anhydride = 1:1)

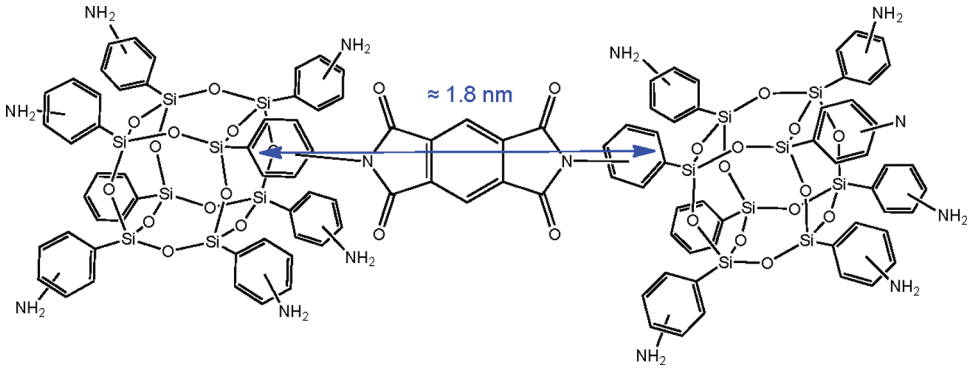

Scheme 8. Imide Extremes: (a) 100% vs (b) OAPS in OAPS/ODPA/ODA Nanocomposites Offer Maximum/Minimum Cross-Link Densities[a]

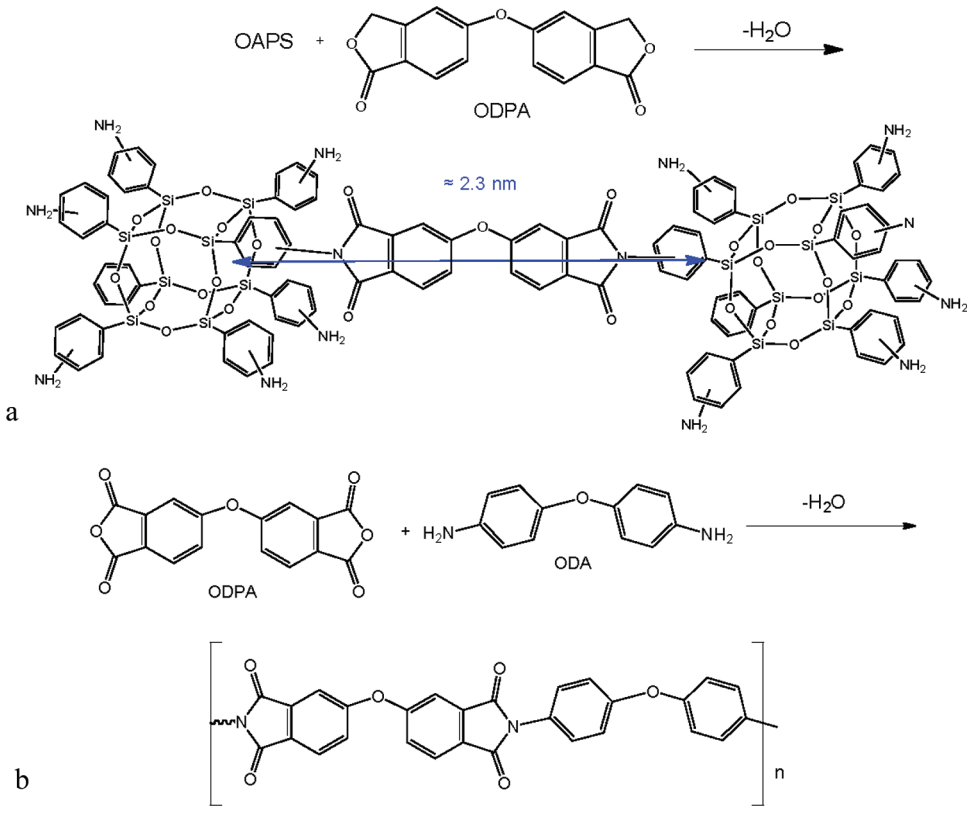

[a] 0% OAPS gives a thermoplastic imide ($T_g \approx 270$°C).[39]

Perhaps the most telling is the change in oxidative stability observed that, as might be expected, corresponds directly to the number of benzyl hydrogens with the 4,4′-diamino-3,3′-dimethyldiphenylmethane (mDDM) having eight compared to only two for 4,4′-diaminodiphenylmethane (DDM) and zero for OAPS.[85] Thus, the photostability of the former is much less than that of the latter.

The nonaromatic amine curing agents are the most stable because they do not absorb UV light. Given that DGEBA:DDM is a common primer for aluminum alloys including aircraft frames, these data are important in understanding the mechanisms whereby such coatings degrade and/or can be repaired or replaced with better materials, including those based on OAPS.

Nagendiran et al.[81] described efforts to create materials with controlled dielectric behavior wherein mixtures of OAPS/4,4′-diaminodiphenyl sulfone (DDS) are reacted with DGEBA and/or tetraglycidyldiaminodiphenylmethane (TGDDM) to form resin systems with improved T_gs and thermal stability.[81] In these systems T_g improvements were seen at loadings up to 3 wt %, reaching 210 °C from 199 °C for OAPS/DGEBA and 275 °C from 260 °C for OAPS/TGDDM. Thereafter, the T_gs dropped by > 20 °C likely because of incomplete curing.[81]

In contrast, the thermal stabilities in both epoxy systems increase with increased OAPS loading up to the point where pure OAPS was used in place of DDS. In part, this must reflect the overall higher cross-link densities. The dielectric constants also decreased with increases in OAPS content from 3.6 for the DDS/DEGBA to 2.6 for the 20 wt % OAPS system. Similar decreases were observed for the TGDDM system as well. Again the changes are ascribed to incomplete curing that results in more free volume, which in turn suggests the possibility of some microporosity; although as noted above, although no microporosity was observed.

SQ-Polyimides

As with epoxy resins, polyimides also are susceptible to UV, oxygen, and hydrolytic degradation.[68,69,85] Thus, efforts to

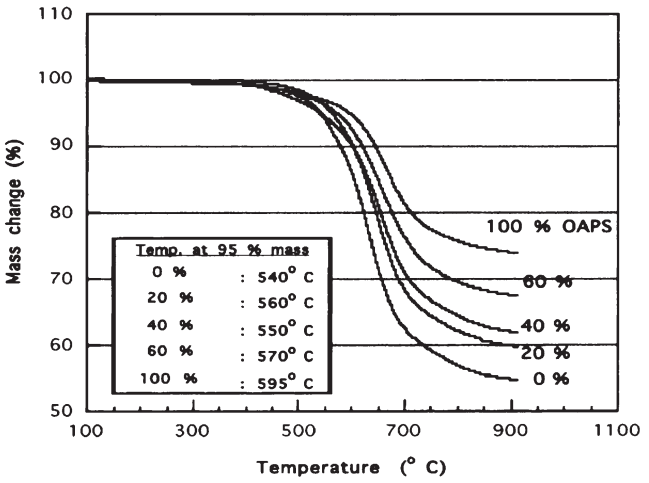

Figure 7. TGA (N_2/10 °C/min) of OAPS/ODPA/ODA nanocomposites with various OAPS loadings cured at 330 °C.[39]

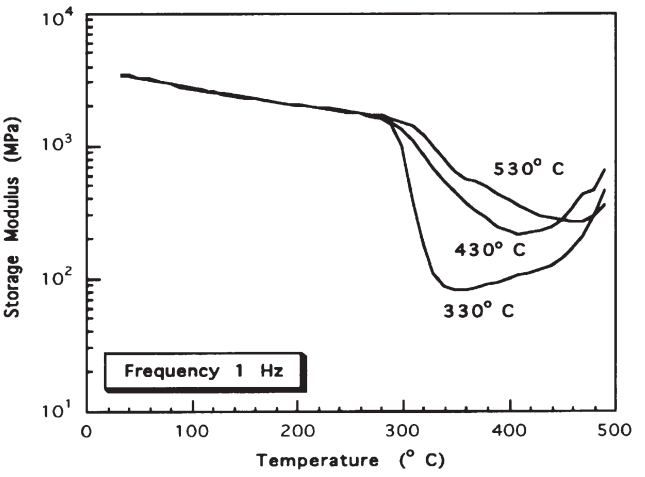

Figure 8. Storage moduli of 20 mol % OAPS/ODPA/ODA nanocomposites cured at selected temperatures, 3 h/N_2.[39]

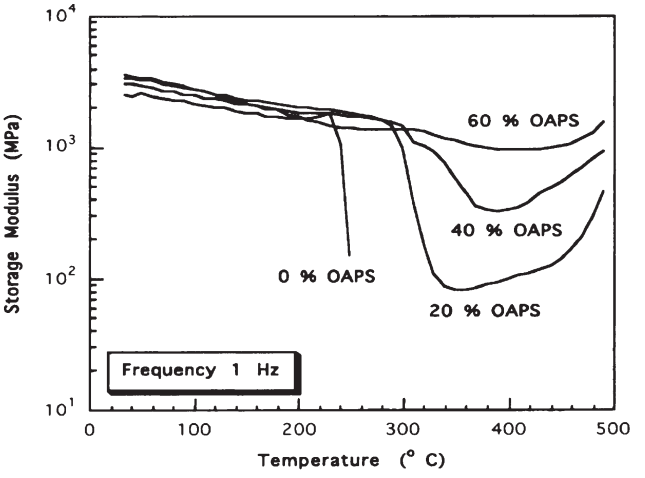

Figure 9. Storage moduli of OAPS/ODPA/ODA nanocomposites with varying OAPS concentrations cured at 330 °C, 3 h/N_2.[39]

improve their properties suggest that OAPS materials with silica cores might offer superior behavior. Indeed, SQ epoxies are much less sensitive to moisture than regular epoxy resins.[23] The downside to using OAPS and DDAPS for polyimide syntheses is the obvious very high cross-link densities that would result if these materials could actually be made to fully imidize. A further issue is that processing of traditional linear polyimides proceeds via an intermediate polyamic acid, reaction 12, which is often soluble and/or melts under the operating conditions of traditional polymer processing methods.

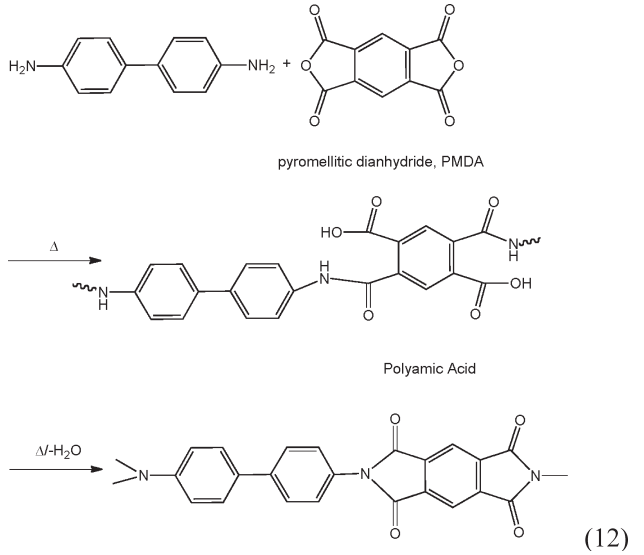

(12)

In contrast, the use of OAPS or DDAPS to form imides will first produce highly cross-linked polyamic acids that are likely only to gel and provide very poor processability. However, one can envision processing OAPS and DDAPS derived imides by codissolution with dianhydrides such as PMDA or oxidiphthalic anhydride (ODPA) in high boiling polar solvents and thereafter processing the resulting viscous solutions prior to driving formation of the corresponding amic acid. Indeed, this is possible; however, the resulting imides are highly cross-linked and quite brittle.[41]

One might anticipate that such properties are unattractive for any type of application, but in fact this is far from correct. First, one must recognize that fiberglass is basically a highly cross-linked flexible inorganic polymer. These and other ceramic fibers resist catastrophic failure because the fiber diameters are small enough that the energy required to induce a surface flaw needed for catastrophic failure to propagate is beyond the energy one can apply mechanically. Indeed, it is possible to make crystalline ceramic fibers that offer exceptional mechanical properties.[87,88]

This same argument holds true for thin films, typically $\leq 1\ \mu$m. However, unlike processing ceramic fibers at temperatures up to 1800 °C, thermally stable, highly cross-linked polyimide fibers should be processable at temperatures < 600 °C. Therefore, they should be much easier to process and will be much lower density than ceramic fibers; however, they should offer almost equivalent mechanical properties of considerable value in aerospace applications.[89] Furthermore, the electronics industry needs materials with good high temperature stability (> 400 °C) with very low CTEs for substrates for electronic and barrier materials.[42,43]

These issues represent some of the motivation for developing routes to OAPS- and DDAPS-derived polyimides. Still another motivation was to determine if the use of very short cross-linking components could introduce microporosity. Thus, a series of studies were conducted to identify conditions for processing PMDA/OAPS (Scheme 6) and ODPA/OAPS materials.[39] To this end, it was determined that NMP was a good processing solvent for forming films of the starting imide tethers. Full curing requires temperatures > 300 °C.

In this system the tether length is estimated to be 1.8 nm, Scheme 7 (Si−C: ≈0.16 nm, Ph: ≈0.25 nm, Ph−N: ≈0.14 nm; and PMDA imide segment: ≈0.67 nm), vs 0.53 nm for the cube body diagonal.[39] Although we can obtain highly cross-linked SQs with surface areas of 400−1200 m^2/g with other systems[32] (see below), the

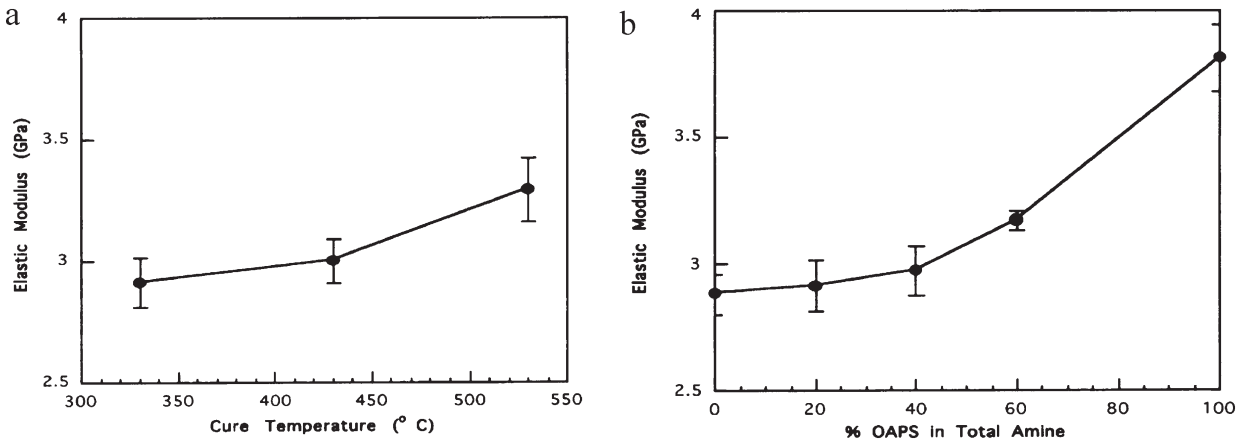

Figure 10. Moduli of (a) 20% OAPS/ODPA/ODA at different cure temperatures and (b) at selected OAPS loadings (cured at 330 °C, 3 h, N_2) measured by nanoindentation.

Scheme 9. Reaction of OAPS/ODA and Bismaliemide (BMI) To Form $T_{d5\%}$ Nanocomposites[78]

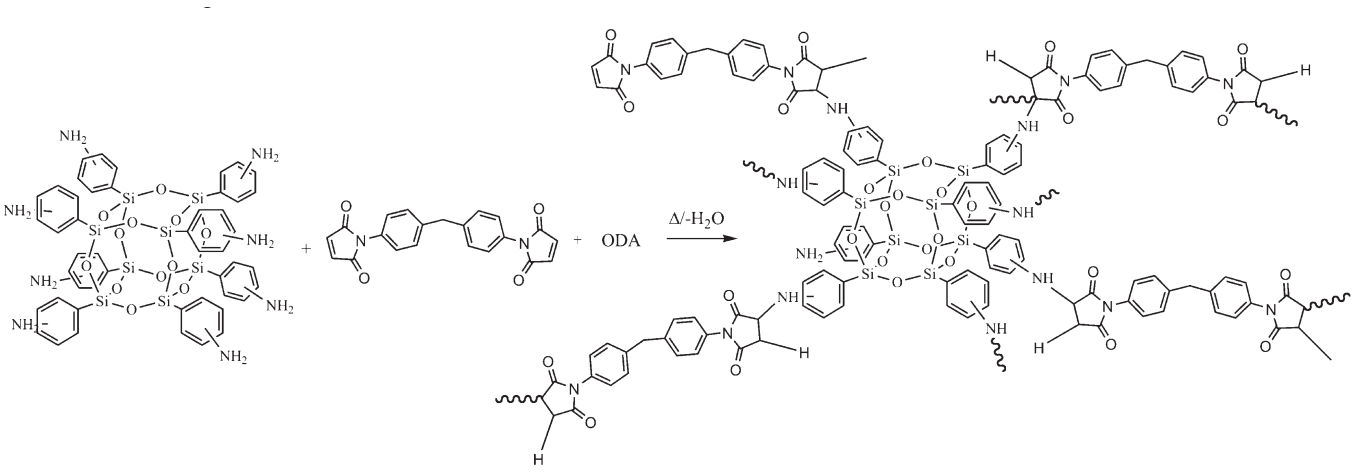

imide materials showed no evidence of microporosity. The PMDA films proved too brittle to work with, and efforts were made to introduce some flexibility by replacing PMDA with ODPA, which is slightly longer (Scheme 8a). In a further effort to explore the effects of high cross-link densities in these polyimides, sets of materials were made diluting OAPS with the diamine oxidianiline or alternatively diluting oxidianiline with incremental amounts of OAPS (Scheme 8b).

Figure 7 indicates that the resulting materials show the anticipated increases in thermal stability as $T_{d5\%}$ for these materials increases by 60 °C on going from 0 to 100% OAPS. However, DMA studies seen in Figure 8 reveal unusual storage moduli for samples cured at 330 °C.

Basically, it appears that at 330 °C curing is incomplete, as higher temperatures lead to higher storage moduli. The argument presented above, stating that high cross-link densities should lead to much higher viscosities, seems to be correct. What is perhaps surprising compared with most organic imidization reactions is that the amic acid intermediates remain sufficiently stable as to permit curing at higher temperatures.

Figure 9 shows that changing ODA to OAPS ratios increases the storage moduli of these materials up to ≈60% OAPS. Thus, the 60% OAPS material offers a storage modulus that is almost constant at 1 GPA up to 500 °C suggesting excellent thermal stabilities.[39] The very high cross-link densities lead to quite good mechanical properties per Figure 10 even at 540 °C.

Unfortunately, all efforts to find microporosity in these materials failed, perhaps because of the lack of open porosity. Furthermore, except as thin films, these materials are quite brittle. However, evidence of microporosity is demonstrated in OAPS-derived materials below.

Maleimides

A number of other groups have explored the development of OAPS based maleimide materials including Zhang et al.,[78] who used it as a reactant with the organic maleimide BMI as seen in Scheme 9. Krisnan and He[75] used OMIPS produced via an alternate route to one we described.[71] The advantage to developing maleimide-based polymers is in the fact that the imidization process occurs before polymerization; consequently, there are no problems with the formation of water which can lead to pores in the cured polymer, and also the possibility of incomplete curing is at least partially avoided.

Zhang et al. simply reacted OAPS/ODA mixtures with BMI via Michael addition per Scheme 9 at 280 °C for an unspecified time to produce amorphous nanocomposites that exhibited increases in T_g of 60 °C in the 400 °C region as the amount of OAPS increased from 0 to 33 wt %.[78] At amounts up to 15 wt %, T_g was observed to increase ≈35 °C and then fall off. Again, this phenomenon is likely a consequence of incomplete curing, suggesting perhaps the use of higher curing temperatures. Unfortunately, no mechanical properties are reported, but this area seems rich in potential for future development.

Krishnan and He report a simplified synthesis of OMIPS.[75] They use acetic anhydride coincident with maleic anhydride which allows them to produce the octamaleimide at 60 °C

Scheme 10. Synthesis of Octacinnamide (OCINPS) from OAPS[73]

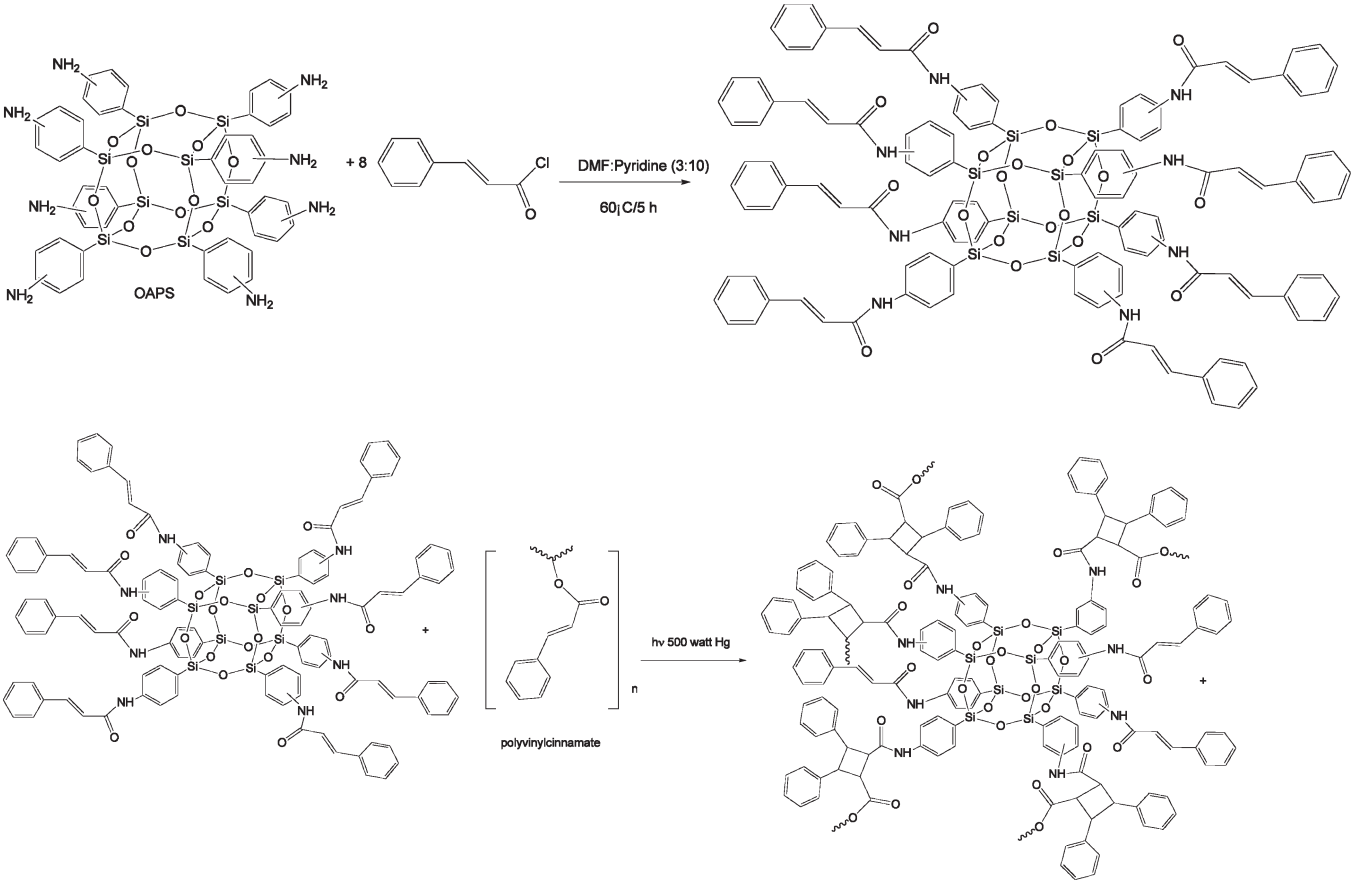

following reaction in ethyl acetate for just 2 h.[75] This is a considerable improvement over our own method.[78]

Krishnan and He also report that OMIPS cures exothermically at temperatures above 100 °C. They produced copolymers with *N,N′-p*-phenylenedimaleimide (PPMI) and urethane methacrylate, demonstrating that incremental addition of OMIPS increases the thermal stability of the copolymers with the highest loadings giving thermal stabilities ($T_{d10\%}$) greater than 450 °C.[75] They also see shifts in the T_g of the resulting copolymers as a function of added OMIPS. What is surprising is that they see a T_g for 100% OMIPS cured at 280 °C, which may suggest that these materials are only partially cured at this temperature, since they should be so highly cross-linked as to show no T_g, as discussed above. Unfortunately, no mechanical properties are reported for these materials.[75]

Ni and Zheng[73] developed an approach that escapes *in situ* imidization by using OAPS as a building block to make photopolymerizable imides by reaction with cinnamoyl chloride as shown in Scheme 10. Photopolymerization offers a cross-linking mechanism that is potentially reversible.

Their studies focused on using the octacinnamide (OCINPS) as a cross-linker for co-photopolymerization with poly(vinyl cinnamate) (PVCIN) at contents up to 40 wt % of the cage compound. Thus, solutions of PVICN with OCINPS in THF (5 wt %) were cast into Petri dishes, dried, and then subjected to a high-pressure mercury lamp (500 W) at a distance of 15 cm from lamp without photoinitiator for periods up to 10 h, where photo-cross-linking was found to be 90% complete. No further cross-linking was observed even for photolysis times up to 50 h. All of the result films were transparent, indicating no phase separation.

They observed slight increases in T_g (78 to 85 °C ± 3 °C) with increasing OCINPS contents but not monotonically which might be attributed to aggregation of the cages. The thermal stability of these materials showed only slight increases above the 185 °C $T_{d5\%}$ at all loadings, suggesting again that segregation of the cages occurred to some extent, but certainly not macroscopically given the transparent nature of the samples. This behavior is hard to explain decisively without mechanical properties studies that might offer more information about nanocomposite properties. To date, only one example of the use of OAPS in the synthesis of phenolic resins has been reported.[76] In this work, Hitco 134A, a commercial resin, was used. This resin is reported to consist of 63−67 wt % oligomeric phenolic components, 13−17 wt % isopropanol, 10 wt % phenol, 3−7 wt % bis(2-hydroxyethyl)-amine, 2−6 wt % water, and 1.1 wt % formaldehyde. Following removal of the water and isopropanol, the resin was dissolved in THF, and 1, 3, 6, or 12 wt % OAPS was added. The solution was cast into containers and solvent removed at 80 °C at 300−350 mmHg. The resulting resin mixtures were then heated to cure the resin, generating a cross-linked product as suggested by reaction 13.

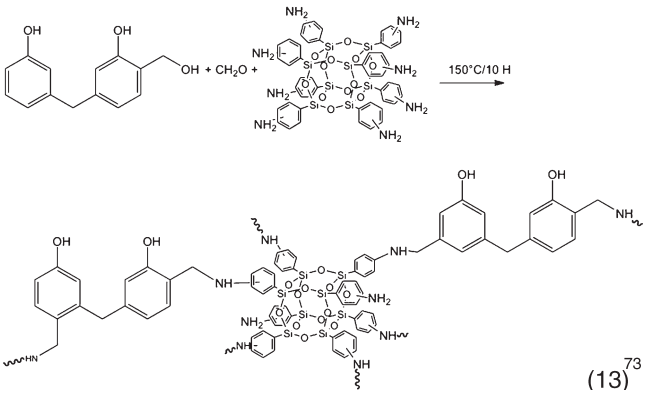

(13)[73]

XRD analyses showed a mostly amorphous resin with a small peak appearing at 5.8° 2θ, corresponding to the OAPS component. The intensity of this peak increases with initial OAPS concentration as well as a typical amorphous hump centered roughly at 20° 2θ. SEM analyses showed fracture surfaces typical of amorphous materials.[76]

DMA studies are as expected for increasing cross-link densities with increasing OAPS contents; values at ambient are just below 1 GPa except for the 12 wt % sample, where it appears that OAPS aggregation within the phenolic resin reduces the mechanical properties. This is confirmed by the XRD results.[76] Thermal stabilities increase only slightly with the addition of OAPS. Indeed at 12 wt % the thermal stability decreases by a small amount from the pure polymer.[76] The tan δ data indicate decreases in T_g from T_{max} at 227 °C for the pure resin to 175 °C for the 12% OAPS, suggesting that the OAPS does not readily form highly cross-linked materials as might be assumed from reaction 13.[76] Alternately, it may be that the OAPS increases the free volume, thereby reducing T_g. This latter conclusion might be supported by the decrease in thermal stability at the higher loadings. Further work will be required to clarify these issues.

OAPS/Polyaniline (PANI)

One of the more exciting possible uses of OAPS is as an initiator for the synthesis of star polyaniline. It is now known that conductivity similar to that seen in polyanilines can be observed in oligomers containing as few as nine or ten aniline units.[91] Thus, one might envision making OAPS-based stars by growing oligoaniline units out from the silsesquioxane core. The potential advantage is that the normal insolubility of rigid PANI chains might be overcome because the star configuration places the chains in a 3-D configuration.

Several papers have now appeared on this subject[80,91] with the earliest work from Xiong et al.[80] These researchers used traditional methods of polymerizing aniline in the presence of OAPS per reaction 14 and then doped the resulting material with either dodecylbenzenesulfonic acid (DBSA) or poly(4-styrenesulfonic acid) (PSS).

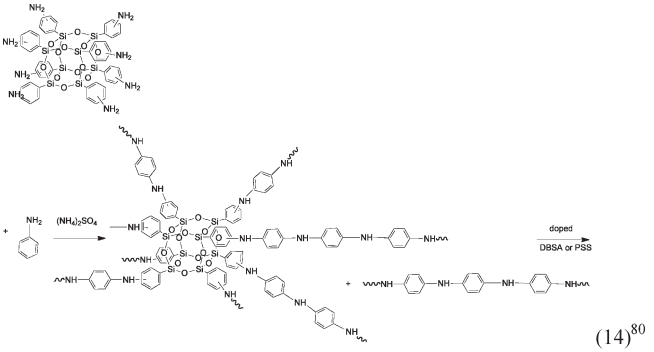

(14)[80]

In their approach, OAPS and aniline were copolymerized as an emulsion in aqueous media by oxidative with ammonium peroxydisulfate (APS) in the presence of DBSA or PSS, respectively, as shown in reaction 14. Molar feed ratios of OAPS to aniline were set at 0.5/95.5 and 1.0/99.0, respectively. The resulting emulsion solutions were then spin-cast onto ITO-coated poly(ethylene terephthalate) (PET) substrates for properties characterization. The DBSA and PSS serve coincidentally as dopants and surfactants.[80]

As expected, the 3-D starlike nature of the products prevents close packing of these materials facilitating ion transport through the films. Because some PANI is coproduced in the process, it is still possible for this material to align with arms of the star materials, leading to some crystallization.[80] Thus, XRD studies reveal the presence of PANI crystallites. TEM studies suggest that the OAPS stars are excluded from these PANI crystallites.[80]

For 0.5% OAPS star/PANI/DBSA composites, the electrical conductivity drops by an order of magnitude from the pure PANI from 2.2×10^{-2} to 1.9×10^{-3} S/cm while the ionic conductivity increases by an order of magnitude from 2.5×10^{-6} to 3.0×10^{-5} S/cm.[80] In contrast, the 0.5% OAPS star/PANI/PSS composite electrical conductivities remain relatively the same with and without OAPS star at $(5-6) \times 10^{-2}$, whereas the ionic conductivity increases from 1.7×10^{-5} to 8.5×10^{-5} S/cm.[80]

Cyclic voltametry studies reveal only slight changes in behavior, which were ascribed to the looser packing for the star composite materials. However, the electrochromic behavior of 230 nm cast films was superior for the composite materials. Thus, absorption changes on scanning from −2.0 to +2.0 V; 0.5% star/PSS has a total change in absorbance (ΔA) of 0.66 at its λ_{max}, whereas ΔA for PANI/PSS is only 0.44 at its λ_{max}.[80] This is a significant enhancement in optical contrast at relatively small doping levels. At applied voltages of 0, 1.0, 1.5, and 2.0 V, λ_{max} values are 770, 750, 700, and 635 nm—shorter wavelengths than those for PANI/PSS, i.e., 775, 755, 715, and 670 nm at the same potentials.[80] The authors ascribe the small blue shift at 0 V to the presence of relatively short PANI chains on the cages. An alternate explanation may be an electronic interaction through the cage itself as discussed below.

These authors also used a three-electrode system to assess the electrochemical stability of the electrochromic thin films in a 0.1 M $LiClO_4$/acetonitrile solution. CV studies under these conditions show the OAPS star systems have significantly higher electrochemical stability than simple PANI/PSS systems prepared the same way.[80]

More recently, this same group conducted similar polymerization studies, using aqueous HCl rather than PSS or DBSA to produce the protonated emeraldine salt, OAPS Star/PANI ES. Triethylamine was used to deprotonate the salt to form the base, OAPS Star/PANI EB. The resulting material could, for the most part, be dissolved in dimethylacetamide (DMAc) with particulates being removed by centrifugation followed by filtration. Thus, 1% solutions of OAPS Star-PANI/poly(2-acrylamidomethane-2-propanesulfonic acid) (PAMPS) were used to process multilayer thin films in DMAc using Langmuir−Blodgett (LB) techniques to create multilayer films. Films up to 50 layers were prepared and then characterized.[80]

The surface morphologies of the multilayer films with the electrochromic layer on top were examined via FESEM. Figure 11a shows densely packed (bright) small islands. In Figure 11b, the islands are surrounded by dark regions tens of nanometers wide, which the authors interpret to mean an interdigitated morphology for 1% OAPS Star/PAMPS multilayer films.

CV studies show sharper peaks for 1% OAPS Star/PAMP than for PANI/PAMPS, suggesting that the introduction of the cage component creates more open pathways allowing more rapid dedoping. This translates to faster color changes, making these types of materials more attractive for practical applications. Complete color change occurs in 4 s for the star system while it takes 6 s for the PANI/PAMP system. However, the LBL films showed somewhat better behavior in part because of the use of a different dopant and in part because the LBL films are made from dilute solutions. In such solutions, it is suggested that the molecules unfold giving greater linearity, which in turn gives more uniformity in the multilayer films. Unfortunately, from a practical standpoint, LB processing cannot be used in commercial applications.

Octa-azide

A recent paper by Ak et al.[79] describes the diazotization of OAPS followed by nucleophilic displacement to form the octa-azide, OAZPS, as shown in reaction 15. As with many of these reactions it is hard to assess the degree to which all of the eight functional groups have been modified, that is, to obtain 100% conversion. Given that the dinitro compound noted above is explosive, OAZPS might also be expected to be explosive. The chemical analysis shows the compound to have slightly lower than expected carbon contents and higher than expected hydro-

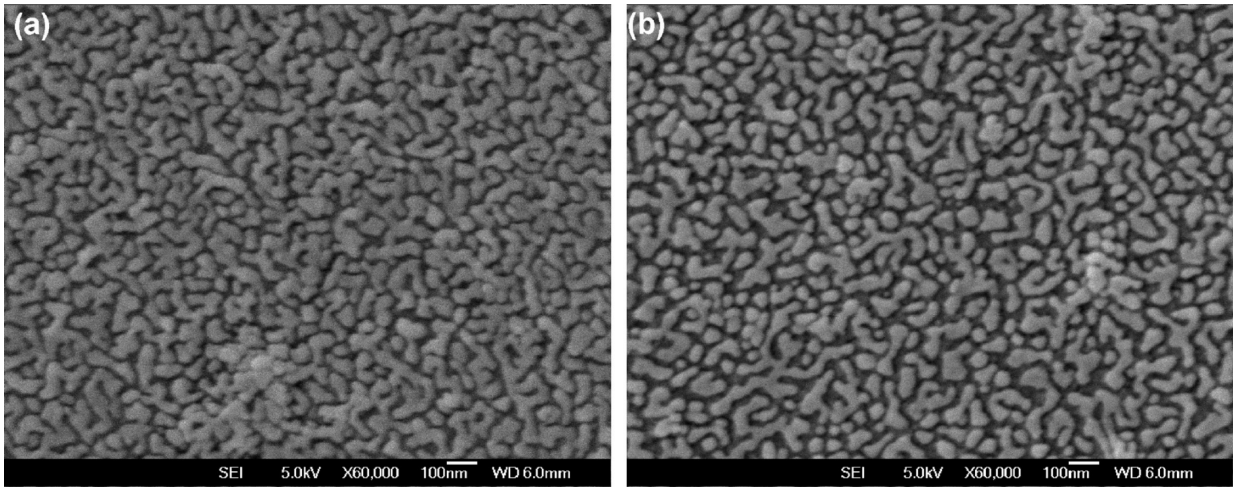

Figure 11. FSEM studies with (a) PANI/PAMPS and (b) 1% OAPS Star/PAMP.

gen contents. One simple explanation is that water is contaminating the products. Other interpretations are possible.

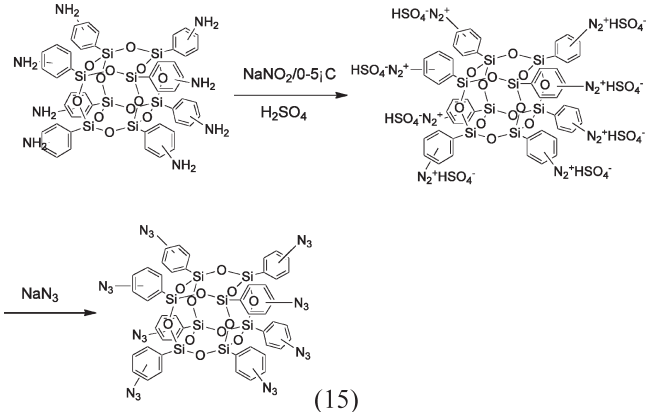

(15)

With OAZPS in hand, these researchers explored its reactions with an alkyne modified thiophene per reaction 16. The next step in this effort was to electropolymerize this 3-D polythiophene, THOPS. Electrochemical polymerization was effected on an ITO-coated glass slide in 10 mL of Py in TBAFB (0.1 M)/CH_2Cl_2 at −0.8 to 1.1 V at 40 mV/s scan rate. The thiophene derivative, THOPS,

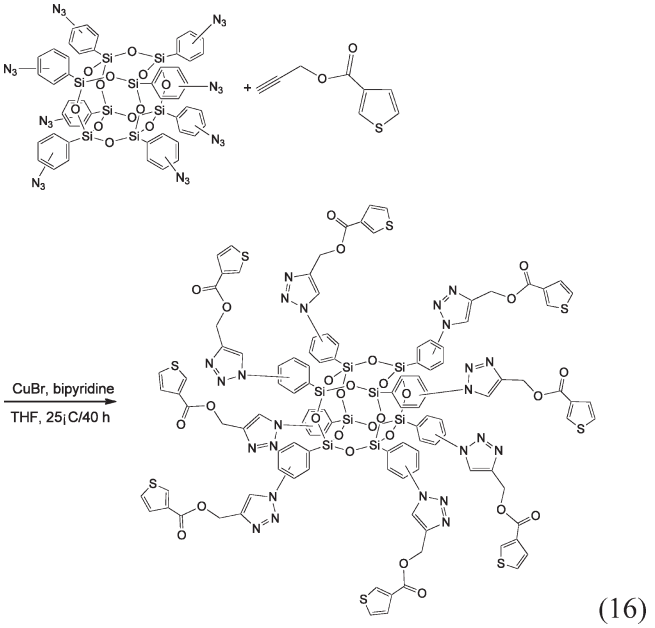

(16)

exhibits electroactivity (E_{ox} 1/41.35 V) in TBAFB/DCM; unfortunately, the current decreases upon repeated cycling perhaps as a consequence of forming an insoluble 3-D polymer.[79]

The addition of pyrrole to the initial polymerization solution greatly changes the properties. As expected, high concentrations of pyrrole relative to THOPS lead to polymers with properties resembling polypyrrole.[79] At lower concentrations, different results are obtained. Thus, for a polymer derived from 50 mg of THOPS and 10 μL of pyrrole, the spectroelectrochemical and electrochromic properties at potentials between −0.8 and 1.1 V in CH_2Cl_2/TBAFB (0.1 M) medium were evaluated. In the neutral state λ_{max} due to $\pi-\pi^*$ transitions for polypyrrole and THOPS/pyrrole copolymer were 351 and 390 nm, respectively. Band-gap transitions were calculated to be 2.35 eV for polypyrrole and 2.25 eV for the THOPS/pyrrole copolymer. Incorporation of THOPS into the polypyrrole backbone, with coincident formation of a 3-D porous and cross-linked structure, greatly improves ion mobilities as seen above with the 1% OAPS Star/PANI/PAMP materials.[79]

For example, the optical contrast at all wavelengths measured showed increases in the transmittance, with ΔT going from 17% to 30% at 730 nm. Again as above, switching times were improved from 1.1 s for polypyrrole to 0.4 s for THOPS−polypyrrole. In addition, the THOPS−polypyrrole films exhibited four different colors in neutral and oxidized states as given in Table 4 compared to polypyrrole. The authors suggest that the introduction of other chromophores could allow still a greater range of colors to be accessed.[79]

Thus, several of the above examples suggest that the incorporation of OAPS or its derivatives into electrochromic films introduces microporosity, which aids in ion transport allowing more rapid color development and switching but also improvements in contrast as well. None of the reports to date discuss lifetimes, which is an important, but as yet unexplored, parameter.

Halogenation

As discussed above, electrophilic aromatic substitution offers an effective route to functionalizing OPS. Furthermore, the nitration studies discussed above show that the inorganic core and the linking C−Si bond are remarkably stable in the presence of strong electrophiles.[47] In this section we discuss the use of electrophiles that allow the selective introduction of Br and I onto the OPS phenyl groups.

Traditionally, halogenation reactions rely on Lewis acid (LA) catalysts to polarize a diatomic halogen, X_2. For example, benzene will not react with bromine without a catalyst.[92,93] Polarization generates electrophilic halogens "X^+" of sufficient reactivity to attack aromatic rings.[92−94] However, phenols and other activated aromatic systems halogenate without a LA catalyst.[92] One might

Table 4. Comparison of Colors for THOPS−Polypyrrole vs Polypyrrole[79]

polymer	potential (V)	color
THOPS−polypyrrole	−1.0	yellow
	10.5	red
	+0.2	green-gray
	+1.0	blue
polypyrrole	−1.0	gray
	1.0	light blue

expect SQ cages to deactivate aromatic substituents with respect to electrophilic attack given Feher et al.'s observation that the cage offers electron-withdrawing character similar to a CF_3 group based on analysis of Hammett constant correlations.[95] Such a substituent can be expected to substantially reduce electrophilic substitution rates.[92]

Thus, LAs (e.g., iron or iron trichloride) will complex with Br_2, generating cationic Br^+ equivalents that react readily with aromatic groups.[92,93] Iron-catalyzed bromination of $[PhSiO_{1.5}]_8$ or OPS was described by Laine et al. (reaction 17),[96] by He et al.,[97] and by Brick et al.[98] The bromination of OPS by IBr was reported by Erben et al.[99]

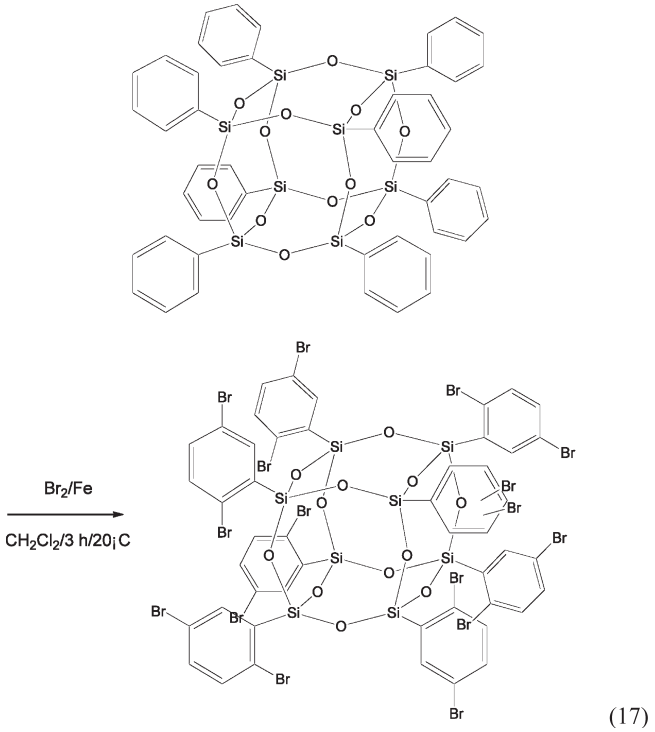

(17)

The substitution pattern for iron-catalyzed bromination was established by Brick et al. using F^-/H_2O_2 to oxidatively cleave Si−C bonds producing a mixture of phenols.[97] GC-MS was used to determine the ratio of *ortho*, *meta*, and *para* isomers. Table 5 contains data obtained for $Br_{5.3}$OPS, suggesting initial bromination was *para*.

As a complication to the LA-catalyzed monobromination studies, we also observed formation of higher bromination products including Br_{16}OPS, where the apparent substitution pattern was 2,5.[98] Most recently, we developed a more definitive route to monobromination with some surprising results.[100]

In contrast to published methods, we find that OPS will react directly with bromine in the absence of LA catalyst.[100] Thus, the careful addition of Br_2 to a suspension of OPS in methylene chloride (1 g OPS/5 mL CH_2Cl_2) at a Br:Ph ratio of 1.65:1, followed by heating to reflux, provides octabrominated OPS with a narrow distribution in substitution number, reaction 18.[100]

If the silsesquioxane cage is an electron-withdrawing substituent, as proposed by Feher et al., significant *meta* substitution should occur due to deactivation of the *ortho* and *para* positions.[95] However in this case, oxidative Si−C cleavage of the isolated octa(bromophenyl)silsesquioxane shows no *meta*-substituted phenols.[100] Most surprisingly, *ortho* substitution is preferred to substitution at the more sterically available *para*-position 85% to 15%.[100]

Table 5. Bromination Pattern for $Br_{5.3}$OPS Based on F^-/H_2O_2 Cleavage To Produce Phenols

major isomers	mole fraction[a] (%)
4-bromo	39
phenyl	37
3-bromo	15
2-bromo	6
dibrominated	3

[a] ±3%.

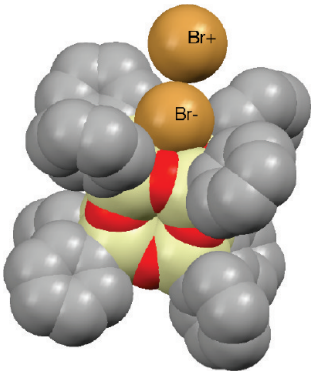

Figure 12. Proposed complexation/polarization of Br_2 at silsesquioxane cage face.[99,100]

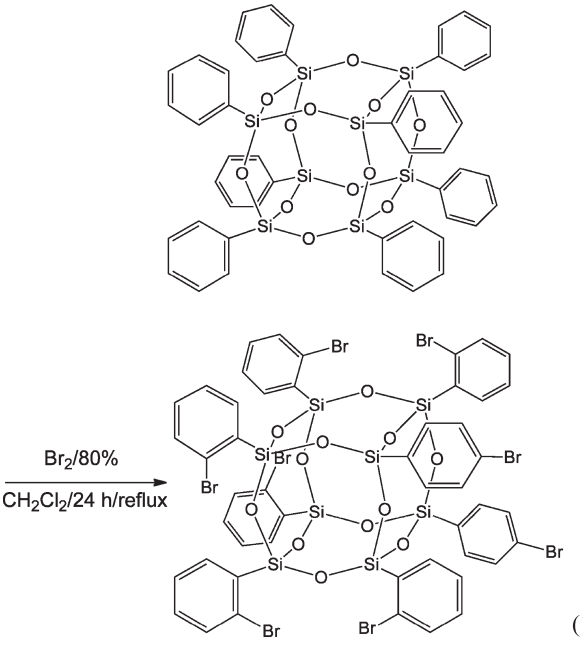

(18)[100]

This unexpected result can be rationalized in light of recent calculations by Park et al., who report that halide ion complexation to cubic silsesquioxanes faces is favored energetically by 10−60 kcal/mol.[101] Thus, in solution at room temperature, we suggest that diatomic bromine spontaneously polarizes at the cage face generating a Br^+ equivalent adjacent to the *ortho* position, as depicted in Figure 12. In other words, it appears that the cage itself drives bromination, acting as a LA.

During work-up of octa(bromophenyl)silsesquioxane, an ethyl acetate insoluble fraction may be isolated comprising up to 40% of the total mass. Recrystallization from *o*-dichlorobenzene gives large colorless, orthorhombic crystals of *o*-Br_8OPS. The remaining soluble material (~85% of the total) is precipitated into cold methanol and isolated as a fine white powder and is determined to be on average Br_8OPS.

X-ray quality crystals of *o*-Br_8OPS were grown by slow cooling of hot, saturated *m*-xylene solutions. Single crystal X-ray diffraction analysis revealed that *o*-Br_8OPS crystallizes in the tetragonal space group *I*4(1)/*a* (Figure 13). The unit cell contains eight molecules with a total volume of 15348.5 Å^3. The 2.5 *m*-xylene solvent molecules are disordered. Two of the solvent molecules were modeled by partial occupancy, while one-half of one *m*-xylene per unit cell was modeled using the SQUEEZE subroutine of the PLATON program suite.[102]

It is possible to further increase the degree of substitution, in this process simply by adding more bromine; however, experimentally that the average degree of bromination does not exceed 14. Given that iron powder used as a LA catalyst dramatically accelerates the reaction, it can be used to increase the average substitution to 16.[98] As the degree of substitution number reaches 16, the product precipitates from the reaction solution, allowing it to be isolated in near-quantitative yields.[98]

However, once isolated, the product is insoluble in most traditional laboratory solvents, including ethyl acetate, toluene, THF, and acetone. Fortunately, Olson and Gronwall reported bromination of the octathiophenesilsesquioxane some 40 years earlier and found it to be soluble in carbon disulfide.[103] Br_{16}OPS is also soluble in carbon disulfide.

Optimization studies determined that slow addition of Br_2 to a stirring suspension of OPS and $FeBr_3$ (used as a homogeneous LA) in methylene chloride at 0 °C leads to an instantaneous, vigorous reaction (19).[100]

X-ray quality crystals of 2,5-Br_{16}OPS·CS_2 can be grown by slow evaporation of a 1:1:1 carbon disulfide/dichloromethane/dodecane solution. Single crystal X-ray diffraction analysis reveals a triclinic space group *P*-1 (Figure 14). The unit cell contains one molecule with a total volume of 1699.3 Å^3 and a density of 2.318 g/cm^3. This is an unusually high density for a compound containing no metal atoms. The single CS_2 solvent is disordered.[100]

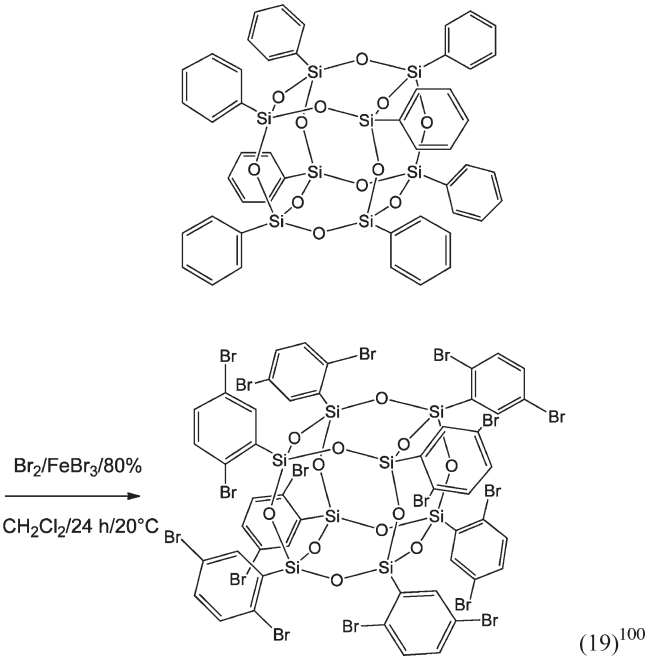

(19)[100]

The addition of the $FeBr_3$ catalyst after an initial stage of bromination without catalyst increases the degree of bromination beyond 16, reaction 20, providing highly insoluble white powders. Attempts to increase the degree of bromination to 24 led to significant Si−C cleavage as a side reaction, leaving a silanol functionalized corner, as detected in the crude reaction products by MALDI-TOF.[99] It appears that the tribrominated corners are readily cleaved[100]under the highly acidic (due to HBr produced), oxidizing (due to excess Br_2) conditions. Repeated recrystallization of the reaction product from hot *o*-dichlorobenzene removes the cleaved products and allows isolation of crystalline material in low yields, < 10%.[99]

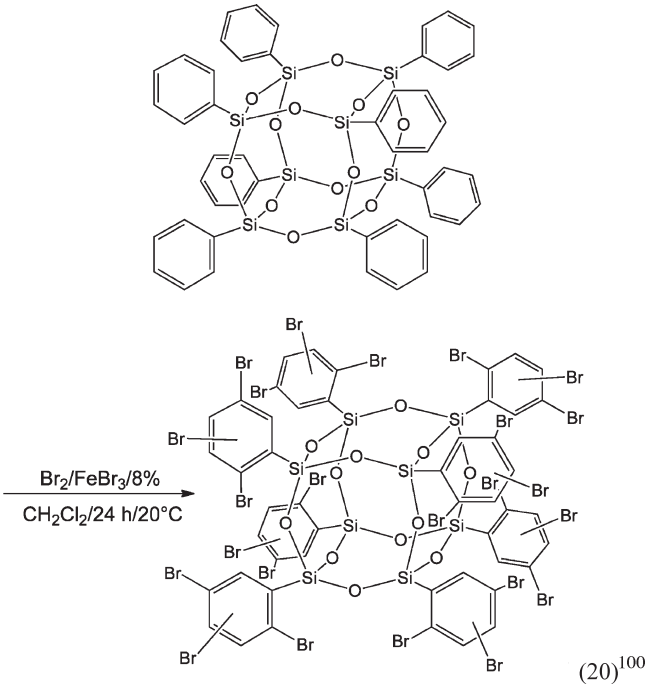

(20)[100]

Single crystals suitable for X-ray diffraction were grown from dilute solutions of hot *o*-dichlorobenzene. The refined crystal structure shows a solid solution, with multiple substitution patterns (Figure 15). The partial filling factors indicate an average of 24 bromines. The crystal structure is relatively open, hosting disordered *o*-dichlorobenzene solvents, and having a lower density (2.0 g/cm^3) than the Br_{16}OPS.

DSC analysis shows melting points range from 250 to 400 °C. While the as-prepared Br_8OPS melts at ca. 260 °C, the crystalline octa-*ortho*-brominated OPS melts at ca. 360 °C, almost 100 deg higher.[100] This is presumably due to the higher degree of crystallinity. The hexadecabrominated OPS melts at ca. 375 °C.[100] Together, these melting points are below or far below where mass losses are observed in the TGA.[100] The tetraicosa-brominated OPS has a melting point close to the decomposition temperature. Under nitrogen, the octa-brominated compound shows a mass loss akin to a boiling/sublimation at ca. 450 °C. The TGA traces of the hexadeca- and tetraicosa-brominated compounds show > 500 °C stability in air. The TGA trace of Br_{16}OPS under nitrogen does not show evidence of sublimation.[100]

Functionalization of $Br_{5.3}$OPS

Initial efforts to functionalize the $Br_{5.3}$OPS produced via reaction 17, where the substituent distribution of Br groups on the phenyls was well understood, were undertaken to demonstrate the utility of these species for generating a wide variety of 3-D functionalized SQs. Scheme 11 provides a list of functionalization

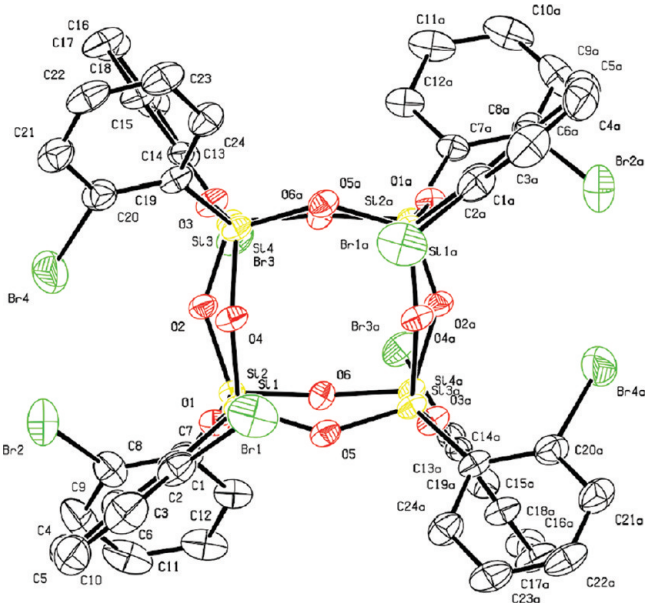

Figure 13. 50% thermal ellipsoid plots of octa(*o*-bromophenyl)-silsesquioxane·2.5*m*-xylene. Hydrogen atoms and *m*-xylene solvates are omitted for clarity.[100]

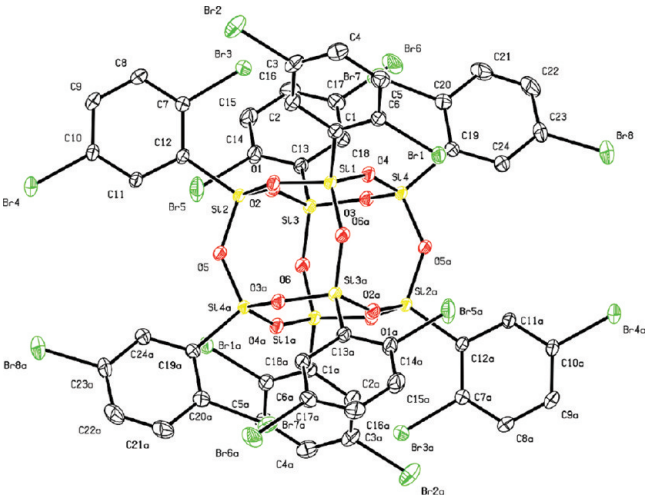

Figure 14. 50% thermal ellipsoid plots of octa(2,5-dibromophenyl)silsesquioxane carbon disulfide solvate. Hydrogen atoms and carbon disulfide solvates are omitted for clarity.[100]

reactions surveyed. The yields and analytical data for each compound are found in Table 6.

Of note is the fact that in the alkyne and amine heterocoupling reactions significant amounts of aryl bromide are retained in the final product. In part, this is because heterocoupling is inefficient in these reactions. In part, this is a consequence of the product containing some portion of *ortho*-bromo groups, which are difficult to functionalize as discussed just below.

Alkyne and Alkene Syntheses (Sonogashira and Heck Reactions)

In the case of the alkyne reactions, we frequently observed double alkynation.[118] The most reasonable explanation for this result is via the back-reaction of the HBr byproduct with the alkyne, as suggested in reaction 21.[118] For this reason, plus the complications that arise because of the mix of substituent sites and the presence of 3−5% dibromo products, the iodo compounds proved to more useful for alkyne coupling studies, as discussed below.[118]

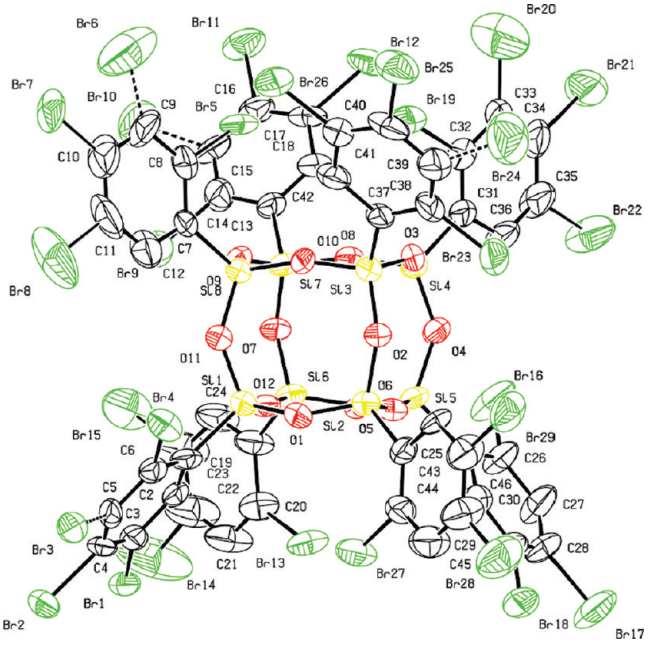

Figure 15. 50% thermal ellipsoid plots of tetraicosabrominated OPS·5*o*-dichlorobenzene (*R*-factor of 6.3%). Hydrogen atoms and *o*-dichlorobenzene solvates are omitted for clarity. Dashed bonds indicate partially occupied bromine sites.[100]

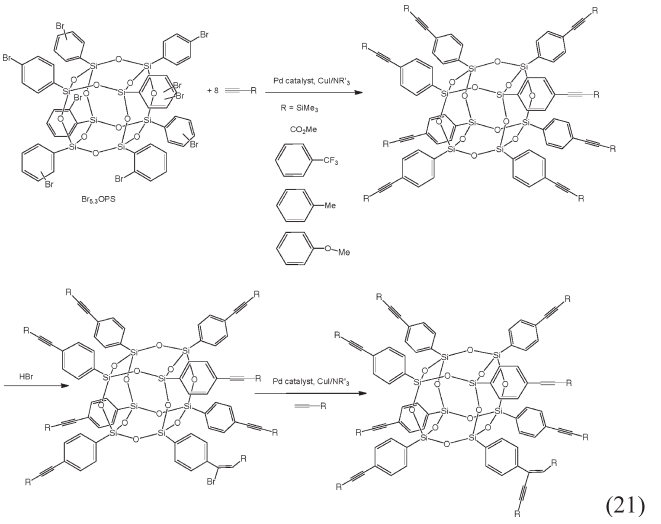

(21)

Polyaromatic Syntheses (Suzuki Reactions)[119]

As noted throughout this review, the 3-D nature of these molecules allows one to attach oligomeric groups that are poorly soluble or insoluble by themselves. However, by forcing the individual units to be symmetrically disposed on the cage surface, their ability to order for example by extended $\pi-\pi$ interactions can be diminished and their solubility and ease of purification much improved.[119] This is particularly problematic for polyaromatics. Given our continuing interest in making materials for organic electronic applications, we sought to explore use of the Suzuki coupling to produce polyaromatics. Thus, we chose to synthesize a series of compounds according to Scheme 12 with analytical data contained in Table 7. Note that $Br_{5.3}$ represents the average degree of substitution,

While in the course of running these studies, another group published a paper making several of the same compounds prepared using a Br_xOPS with a poorly defined number of bromines.[97] This work[97] reports finding that these compounds exhibit organic quantum dot like properties.

Scheme 11. Functionalization of $Br_{5.3}$OPS via (i, iv) Heck, (ii) Songashira−Miura, (iii) Suzuki, and (v) Amine Heterocoupling Reactions[98]

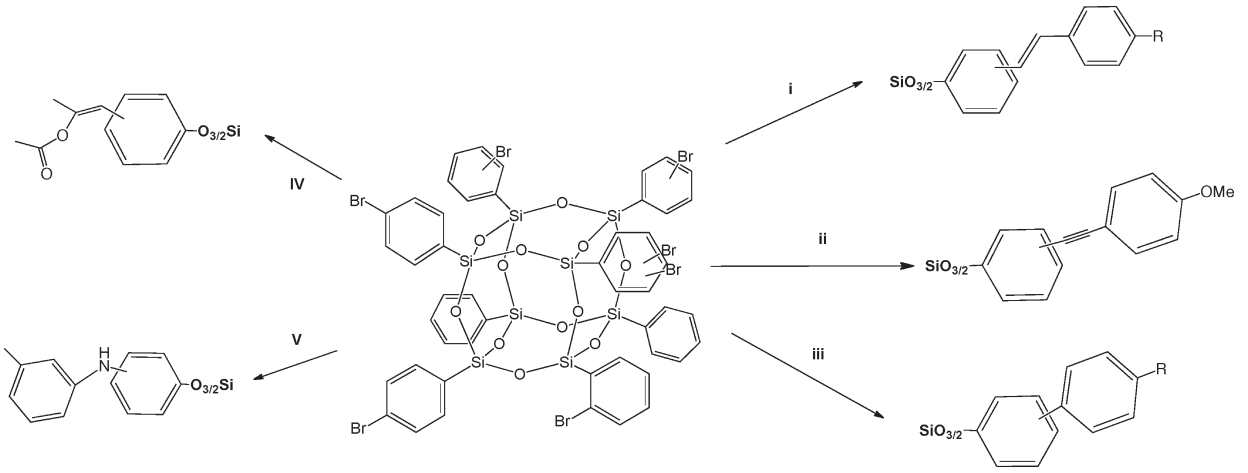

Table 6. Characterization Data for $Br_{5.3}$OPS (Average Degree of Substitution) Derivatives[98]

		GPC			TGA		MALDI-TOF (Ag^+ adduct)		
cmpd	conv (%)[a]	M_n	M_w	PDI	found %	calc %	most common isotope	found	calc
$Br_{5.3}$OPS		921	928	1.01	32.4	33.1	$Br_6Si_8O_{12}C_{48}H_{34}$	1614.1	1614
i	99	1669	1786	1.07	27.0	29.2	$Si_8O_{12}C_{48}H_{34}(C_9H_9)_6$	1839.4	1838
ii	51	1118	1194	1.07	30.3	31.1	$Si_8O_{12}C_{48}H_{34}(C_9H_7)_4Br_2$	1754.8	1755
iii	99	1983	2027	1.02	32.6	33.5	$Si_8O_{12}C_{48}H_{34}(C_6H_5)_6$	1597.3	1597
iv	99	2450	3015	1.23	28.3	30.8	$Si_8O_{12}C_{48}H_{34}(C_5H_7O_2)_6$	1728.8	1729
v	63	1591	1862	1.17	28.5	31.2	$Si_8O_{12}C_{48}H_{34}(C_7H_8N)_4Br_2$	1718.0	1718

[a] Conversion represents the fraction of aryl bromides reacted in the final product.

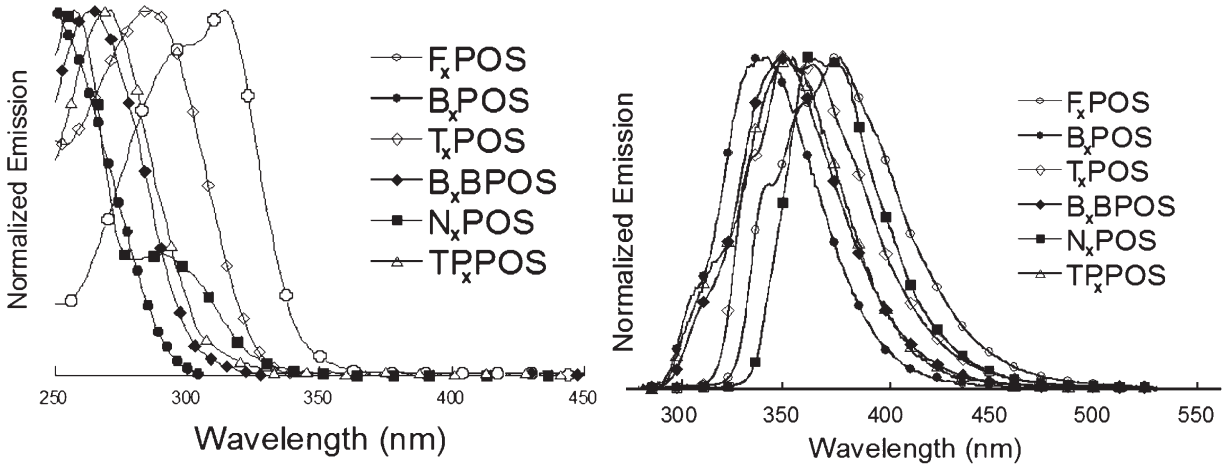

Figure 16. (a) UV−vis and (b) PL emission spectra (dilute THF) of $Ar_{5.3}$OPS.

The emission spectra appear to be very narrow. The same paper also claimed that Suzuki coupling did not work, and thus an Ar−Br coupling reaction was effected using a palladium catalyst. Both results were surprising to us, given that we got reasonable, unoptimized yields from Suzuki coupling per Table 7. In addition, we see emission peaks that are typical of polyaromatics as shown in Figure 16 with no apparent emission narrowing. Finally, both efforts find that these compounds are highly soluble, air-stable to >400 °C, and emission quantum efficiencies, Φ_{PL}, can be up to 98% (Table 8). Of particular importance is the fact that the 9,9-dimethylfluorene derivative is very soluble. There is no need to attach long chain branched alkyl groups for solubility. Such groups are excellent points for oxidative degradation at the branch point.

Alkenes via Heck Coupling

The recent discovery of methods of obtaining quite pure bromination products, as shown above, has allowed us to revisit some of these reactions especially given that we can make pure *ortho* derivatives and compare them with pure *para* derivatives as discussed in the next section.

To this end, we recently began a series of efforts to functionalize the *o*-Br_8OPS, $[2,5\text{-}Br_2PhSiO_{1.5}]_8$, and $[Br_3PhSiO_{1.5}]_8$ systems with the objective of assessing their photophysical properties for reasons discussed below.[104] Scheme 13 provides an overview of all of the reaction chemistries assessed for these three compounds.[104]

As implied above, Heck coupling at the ortho site is relatively slow, and as a consequence, most of the reactions were run at 70 °C/24 h,[104] in contrast to our earlier studies where the reactions were run at room temperature (48 h).[98] The acetoxy derivatives

Table 7. Mass Spectroscopy, GPC, and TGA Data for Ar_xOPS Compounds ($x \approx 6-8$)[119]

		MALDI Ar_6POS (Ag^+)		GPC				TGA	
molecule	yield (%)	found	calc	M_n	M_w	PDI	$T_{d5\%}$	CY[a]	calc
F_xOPS	59	2295.0	2294.5	1521	1594	1.05	480	22.8	25.0
B_xOPS	49	1597.2	1597.2	904	920	1.02	440	35.2	33.5
T_xOPS	38	2054.0	2054.3	1231	1256	1.02	440	33.4	26.1
BBOPS	41	1934.2	1934.5	1312	1412	1.08	400	29.1	27.8
NP_xOPS	28	1896.8	1898.3	1181	1256	1.06	450	38.9	28.3
TP_xOPS	52	1632.7	1632.9	987	1018	1.03	510	26.4	32.8

[a] CY = ceramic yield.

are potentially quite interesting as they offer, via hydrolysis, access to phenolic species per reaction 22. These compounds in turn offer many opportunities for further functionalization for diverse applications.

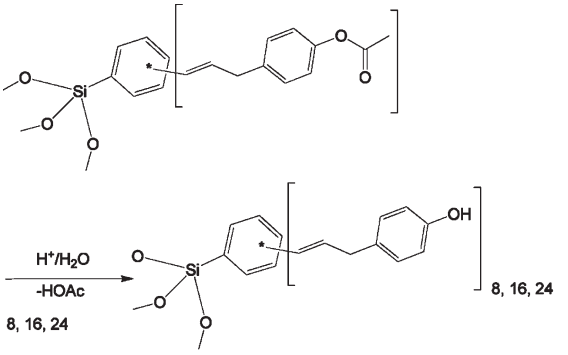

(22)[104]

Likewise, removal of the BOC protecting group will produce a polyamine as suggested in reaction 23. However, in our preliminary studies, we find the resulting free amines to be quite susceptible to oxidation. Furthermore, the resulting cage compound is expected to be highly hygroscopic as noted above for the hexadecaanilino SQ and also quite basic. In the latter case, hydroxide generated from trace amounts of water may cause cage Si−O bond scission. Thus, we suggest the use of alkyl-functionalized aminostyrene in reactions such as those shown in Scheme 13. Given their novel photophysical properties, we believe this is a worthwhile area to pursue, as discussed below.

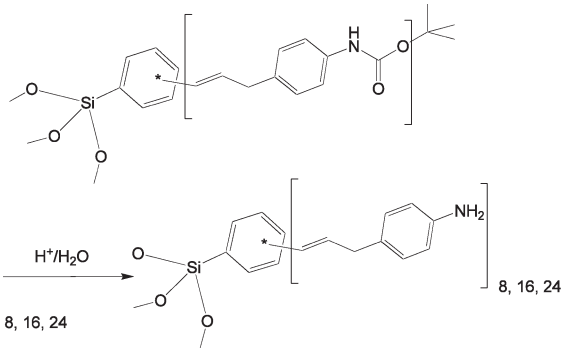

(23)[104]

Iodination

As with bromination, the halogen cation electrophile is the active species. An oxidizing agent is typically used to generate I^+ in situ.[92−94] Vogel suggests using nitric acid as an oxidant in benzene iodination.[93] The expensive hypervalent iodine reagent bis-(trifluoroacetoxy)iodobenzene was used as an oxidant in the synthesis of tetra(*p*-iodophenyl)adamantane[105] and hexa(*p*-iodophenyl)benzene.[106] In contrast, the less expensive iodine monochloride (ICl) is permanently polarized due to the higher electronegativity of chlorine, acting effectively as a stable I^+ source.[60,107] ICl is commercially available in methylene chloride solution, the best solvent for OPS, which reduces the heterogeneity of the reaction.[60,107]

Scheme 12. Synthesis of Arylated Phenyloctasilsesquioxanes from $Br_{5.3}OPS$ ($Ar_{5.3}OPS$)

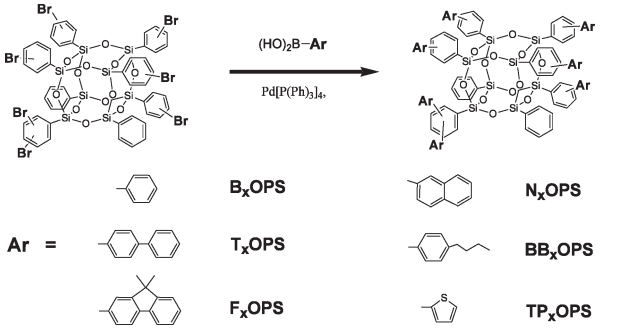

As described previously,[60,107] for operational simplicity, initial reactions of OPS with ICl in methylene chloride (reaction 24) were conducted at room temperature, but we were surprised to discover that iodination of OPS with ICl at −40 to −60 °C followed by recrystallization from ethyl acetate provided 30−40 mol % colorless crystals of $(IPhSiO_{1.5})_8$ (or I_8OPS) and I_7OPS and following filtration, based on octa-substitution. The remaining noncrystalline fraction (70−60%) is recovered by precipitation into methanol.

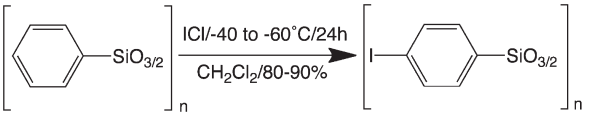

(24)[105]

Though initial NMR data suggested *para* substitution, oxidative cleavage using fluoride was used to produce the iodophenols, allowing the substitution patterns of the crystalline and oil fractions to be quantified.[107] Recrystallization, giving 30−40% of the theoretical yield by mass, is found to remove the I_9OPS isomer and GC/MS analysis of the resulting iodophenols shows *p*-iodophenol and only traces of phenol or other iodophenols.[107] Coincidentally, the same approach permits iodination of $(PhSiO_{1.5})_{10}$ and $(PhSiO_{1.5})_{12}$ per reaction 22.[60] Single crystals suitable for diffraction studies were grown by slow cooling of hot, saturated ethyl acetate. Figure 17 depicts the single crystal X-ray structure.[60]

$(IPhSiO_{1.5})_{10}$, (or $I_{10}dPS$), because of its high solubility, is difficult to isolate.[60] Analogous to the high solubility of the $(PhSiO_{1.5})_{10}$ in toluene/methanol solutions, precipitation of $I_{10}dPS$ into methanol leads to somewhat lower yields. Recrystallization from ethyl acetate gives deca(*p*-iodophenyl)silsesquioxane as single crystals suitable for X-ray diffraction (Figure 18).[60]

$(para\text{-}IPhSiO_{1.5})_{12}$ (or $I_{12}DPS$) is recovered in 90% yield, and the symmetrically substituted material is obtained by recrystallization from *m*-xylene in 20% yield.[60] The remaining ~70% of the reaction product is isolated as a white powder after precipitation into methanol, shown by MALDI-TOF to be a mixture of $I_{10}DPS-I_{13}DPS$ isomers.[60] Single crystals of the dodecamer,

Table 8. Photophysical Data for $Ar_{5.3}OPS$ and Related Materials

compound	ext coeff[a]	UV max (nm)	PL max (nm)	Φ_{PL} (%)[a]
F_xOPS	1.17×10^5	312	377	98
B_xOPS	3.43×10^4	250	342	10
T_xOPS	5.46×10^4	285	349	23
BB_xOPS	3.06×10^4	263	348	35
N_xOPS	2.13×10^5	291	362	38
TP_xOPS	3.81×10^4	271	350	9

[a] Measured at maximum absorption wavelength in THF.

Table 9. Characterization Data for Selected $RStilbene_xOS$[104]

		m/z (Ag^+ adduct)	GPC			ceramic yield (%)		
R group	x	MALDI	M_n	M_w	PDI	actual	calc	$T_{d5\%}$ (°C)
Me	8	2068.6	1212	225	1.011	24.6	24.5	367
	16	2890.4	2032	2057	1.012	17.2	16.6	417
	23	3812	2522	2565	1.011	13.5	13	386
acetoxy	8	2422.2	1535	1570	1.023	20.3	20.8	397
	16	3702.7	2542	2614	1.029	13	13.4	359
	23		3593	3893	1.083	5.7	10.2	344

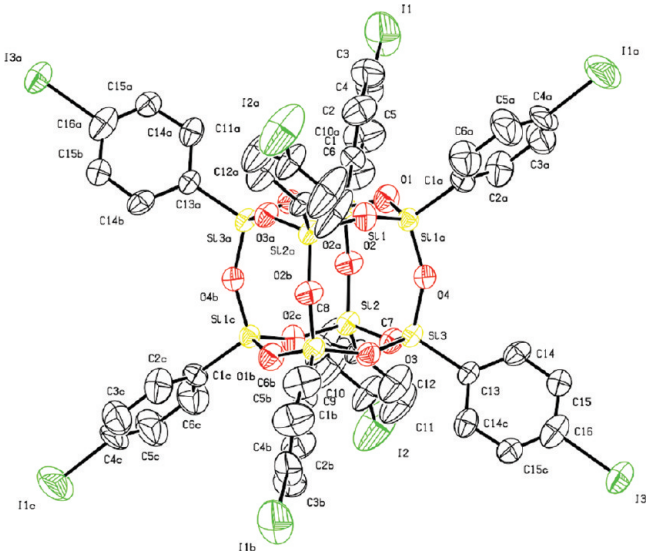

Figure 17. 50% thermal ellipsoid plots of I_8OPS. Hydrogen atoms are omitted for clarity.[60,108]

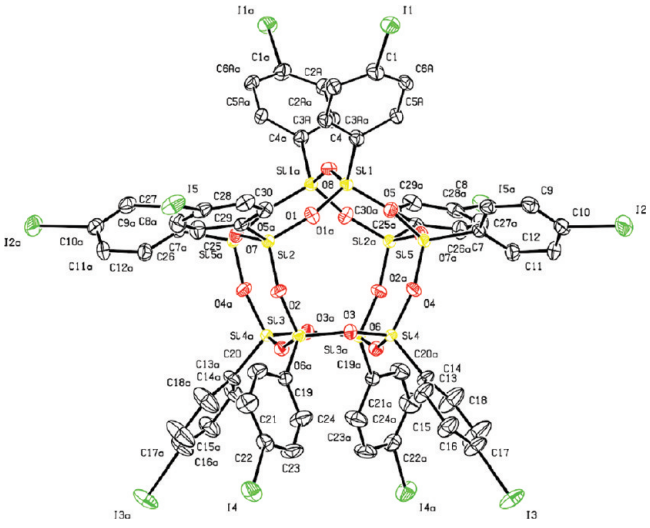

Figure 18. 50% thermal ellipsoid plots of $I_{10}dPS$. Hydrogen atoms are omitted for clarity.[60]

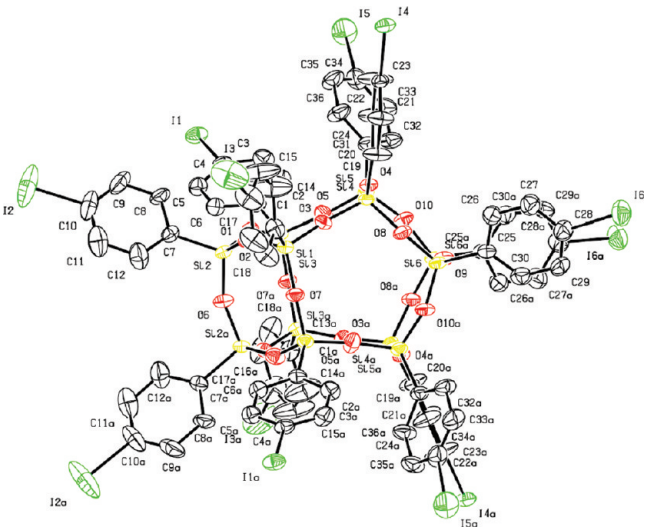

Figure 19. 50% thermal ellipsoid plots of dodeca(*p*-iodophenyl)-silsesquioxane. Hydrogen atoms and *m*-xylene solvents are omitted for clarity.[60]

Table 10. Characterization Data for $NBocStilbene_xOS$[104]

	m/z (Ag^+ adduct)[a]	GPC		
x	MALDI	M_n	M_w	PDI
8	1969.2[b]	2382	2431	1.021
16	3013.9	3749	3809	1.016
23		4290	4390	1.023

	ceramic yield (%)			Boc group mass loss %	
x	actual	calc	$T_{d5\%}$ (°C)	actual	theoretical
8	15.4	17.3	177/~400	29	29.2
16	11.5	10.2	190/~440	35	35.9
23	7	8	184/~450	38	38.6

[a] As deprotected species ($NH_2Stilbene_xOS$). [b] H^+ adduct.

prepared identically to the other iodophenyl cages, were grown from hot *m*-xylene. The single crystal structure is presented in Figure 19. Table 11 compares the crystallographic data for all three $(para\text{-}IPhSiO_{1.5})_{n=8,10,12}$ structures. Note that the octamer unit cell is tetragonal but quite close to cubic symmetry as might be expected given its high symmetry. This also indicates that its crystal packing is almost cubic. In the Introduction, we argue that

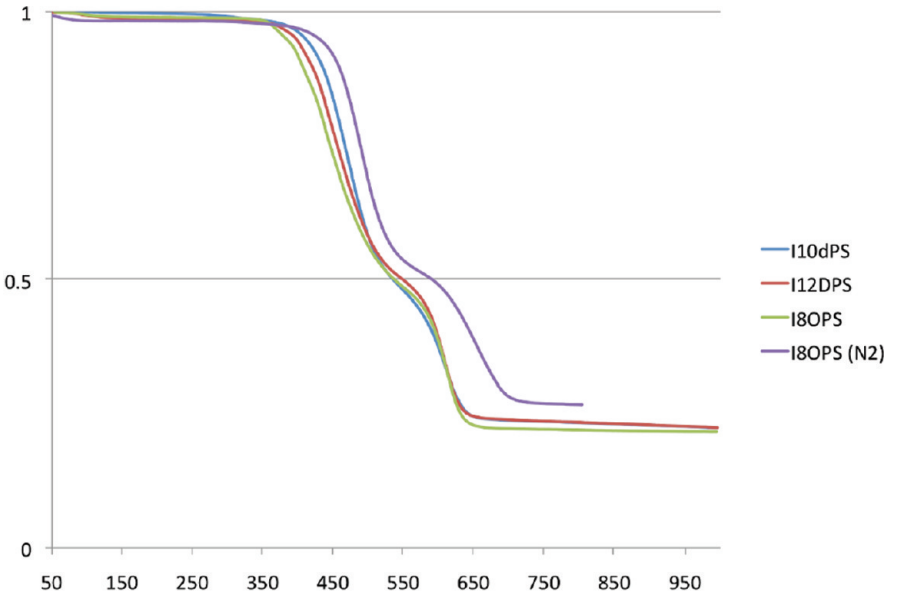

Figure 20. TGA of the homologous iodophenylsilsesquioxanes.[60]

this kind of packing is needed to obtain nearly perfect assembly in 3-D at much larger length scales. In contrast, the symmetry of other two crystal structures is far from cubic. These differences explain observations made below on the thermolysis of these compounds.

In and of themselves, the I_8OPS, I_{10}dPS, and I_{12}DPS compounds exhibit novel thermal behavior that is not evident by simply examining the TGA ceramic yields of these compounds. TGA studies in air and nitrogen indicate that these compounds all undergo an ~50% mass loss on heating above 420 °C, as seen in Figure 20. These equivalent mass losses occur with the evolution of I_2 (49 wt % theory) as evidenced by the formation of I_2 crystals as bulk samples are heated to this temperature. This likely suggests the reaction shown in (25).

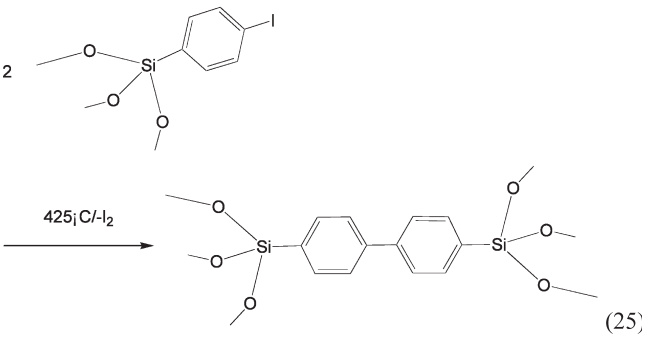

(25)

The FTIR of the starting and heat-treated materials (Figure 21) suggests retention of the cage structure as well as the aromatic ring structure. Unfortunately, whether this is simply a highly cross-linked aromatic char or an ordered materials arising out of reaction 25 is not obvious. However, more detailed studies do suggest that reaction 25 has occurred. The thermolysis products are labeled as T-T8 for I_8OPS, T-T10 for I_{10}dPS, and T-T12 for I_{12}DPS.

The T_8 compound alone crystallizes in a tetragonal space group with $a = b = 20$ Å and $c = 21.5$ Å, nearly cubic with four molecules per unit cell. If reaction 25 is operative, then we might expect this crystal structure to be close to the desired perfect 3-D NB packing. If packing is preserved in the thermolysis products, it should produce a nanostructured material with cubic symmetry. Figure 22 strongly suggests that this has happened. In addition, one might anticipate that the high symmetry would lead to microporosity.

This is indeed the case. Table 13 provides both the TGA and the microporosity data for the individually thermolyzed materials, indicating that the most symmetrical nanobuilding block gives the highest surface area. This seems to be indicative of the highest 3-D order at larger length scales compared to the other two thermolysis products as supported by the XRD studies of Figure 23 wherein T-T_8 offers the most ordered structure at larger length scales. This is one of the first examples where ordered molecular packing at nanometer length scales leads to nanostuctured materials were this order is retained.

I_8OPS Derivatives

The $[p\text{-IPhSiO}_{1.5}]_{8,10,12}$ compounds offer the potential to build 3-D nanostructures with a variety of symmetries allowing novel structure−property relationships at nanometer length scales. As noted above, $[PhSiO_{1.5}]_{10}$ is difficult to isolate in large quantities, whereas the $[p\text{-IPhSiO}_{1.5}]_{8,12}$ compounds are not. In this section, we concentrate primarily on $[p\text{-IPhSiO}_{1.5}]_8$, I_8OPS.

Iodinated aromatics, including I_8OPS, tetra(*p*-iodophenyl)-adamantane[105] and the hexa(*p*-iodophenyl)benzene,[106] can be expected to be quite useful 3-D precursors for the synthesis of complex molecular and supramolecular systems, like our targeted nanobuilding blocks. One reason is the extensive development of catalytic C−C and C−heteroatom bond forming reactions via cross-coupling over the past few decades which has multiplied the types of functionality that can be incorporated.[106−117]

Some examples of C−C bond formation based on C−halogen functionalization include the Sonogashira,[106] Suzuki,[107] Heck,[108] and Stille[114] coupling reactions. The incorporation of heteroatoms, multiplying the accessible functionality, can be accomplished through amination,[111,115,116] phosphonation,[114] etherfication,[113] and thioetherification.[115] We have previously discussed examples of such reactions, as shown in Scheme 14. It is worth noting we have found the Suzuki coupling conditions described for the bromo derivatives (Scheme 11)[119] may also be extended to the iodo derivatives. Here we focus on two particular areas: the alkyne-functionalized materials and their derivatives and the stilbene-functionalized materials.

Scheme 13. Heck Coupling Studies on *o*-Br_8OPS, 2,5-Br_{16}OPS, and Br_{24}OPS; Preparation of Selected Functionalized Stilbenes for Comparison of Photophysical Properties[104]

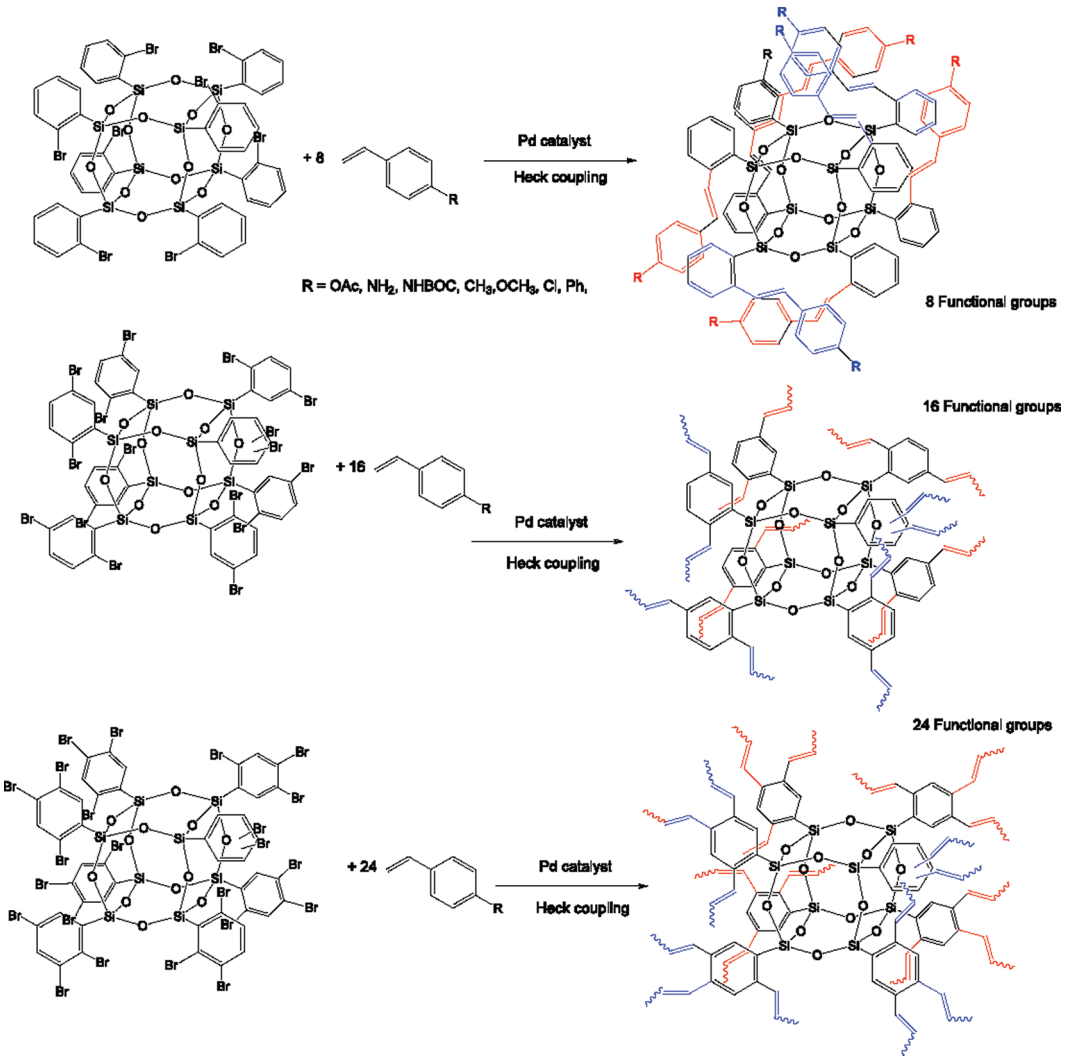

In the former case, we are interested in using the octa-alkynes as building blocks for larger scale compounds and also for microporous materials.

As noted above, our original efforts to synthesize alkyne derivatives using $Br_{5.3}$OPS were fraught with complications arising from what appears to be addition of HBr byproduct to the product alkynes leading to reaction 21 with the formation of an enyne. In these new efforts, a modified catalyst system, composed of the commercially available bis(tri-*tert*-butylphosphine)Pd(0) and $CuI(PPh_3)_3$, was used to improve yields and purity of the final products.[118] Table 14 compares the analytical data for these two substrates. Figure 24 provides the single crystal structure of the octa-diphenylacetylene.

Thermolysis of these compounds (N_2) appears to induce alkyne polymerization,[118] analogous to processes observed in the thermolysis of alkynyl-functionalized tetraphenyladamantanes.[120] Table 15 provides $T_{d5\%}$ for the compounds synthesized via reaction 26.

Continuing with efforts to build 3-D structures, a collaborative effort was undertaken to use the trimethylsilylalkyne compound of reaction 26 as a starting point for oxidative homocoupling of the demasked alkyne as suggested in reaction 27.[121] Note that this would be a silsesquioxane analogue of the cubane structure illustrated in Figure 1b. In theory, if perfect coupling were achieved, then a 3-D structure as shown in Figure 25 would arise. This structure was calculated to offer a specific surface area of 6400 m^2/g.

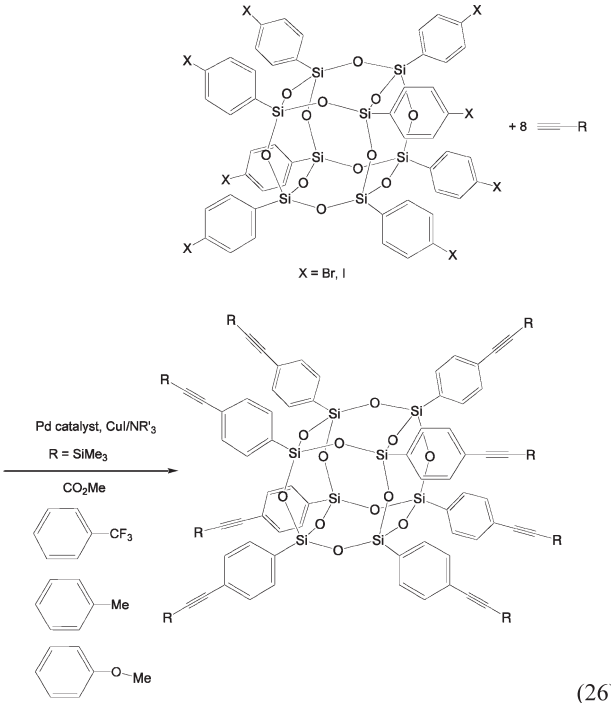

(26)[118]

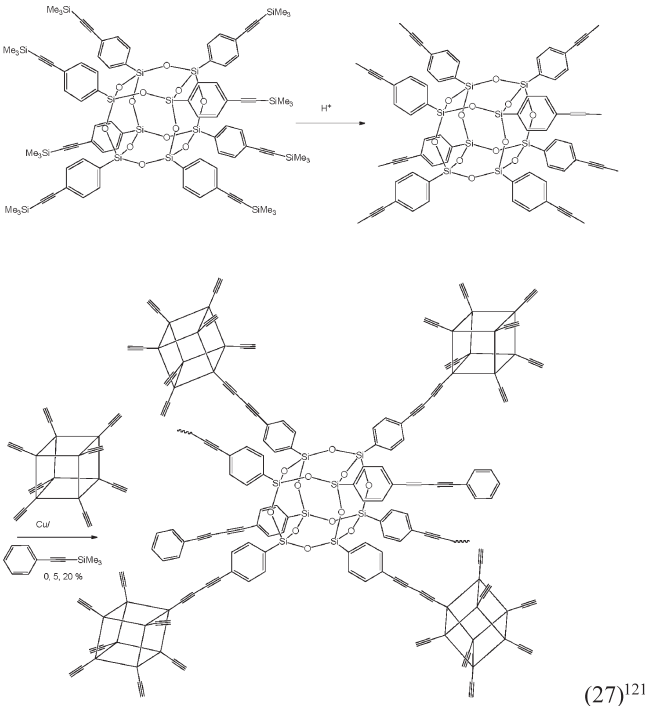

(27)[121]

This approach, while not fully ideal in that it does not allow for bond equilibration during homocoupling, still provides materials with quite high surface areas for simple covalent organic frameworks. Thus, surface areas approaching 1100 m^2/g were obtained when small amounts (5 mol %) of end-capping trimethysilylethynylbenzene are added. These materials, because of the inherent thermal stability of the cage, exhibit essentially no mass loss on heating to 500 °C in nitrogen.[121] Finally, extensive exposure to water did not have any effect on the surface areas, again pointing to the robust nature of these materials compared to metal organic framework materials.[121]

We have also taken advantage of these alkynyl-functionalized silsesquioxanes to prepare much larger single structures via Diels−Alder condensation with tetraarylcyclopentadienones to generate the octa(hexaarylbenzene)silsesquioxanes (Figure 26).[122] The reader is directed to the original reference for more details on the Diels−Alder reaction. The octa(hexaphenylbenzene)silsesquioxane (MW 4685 Da) crystallizes readily from hot, saturated solutions of *m*-xylene giving an approximately triclinic unit cell with edge lengths of ~2 nm and $Z = 1$.[122] In addition, the crystal structure is found to contain a network of voids comprising *55%* of the unit cell, occupied by disordered solvent molecules and connected by a 2-D network of infinite channels in the *ab* plane.[123] Subsequent dehydrogenative cyclization reactions in the manner of Müllen et al. were used to convert the hexaphenylbenzene groups to hexa-*peri*-benzocoronene moieties as suggested by Figure 27.[122] The 15 Å spacing noted below is seen in the powder X-ray diffraction data for these products given in ref 122.

Acylation and Alkylation

In this final section on electrophilic substitution, we briefly address the acylation reaction and focus on alkylation studies. In efforts to effect acylation, it was possible to obtain good acylation in only one case, using acetyl chloride as suggested in reaction 28.[123] Efforts to acylate with other simple acyl compounds failed under the same conditions. Given the success with the alkylation discussed below, perhaps this area should be revisited.

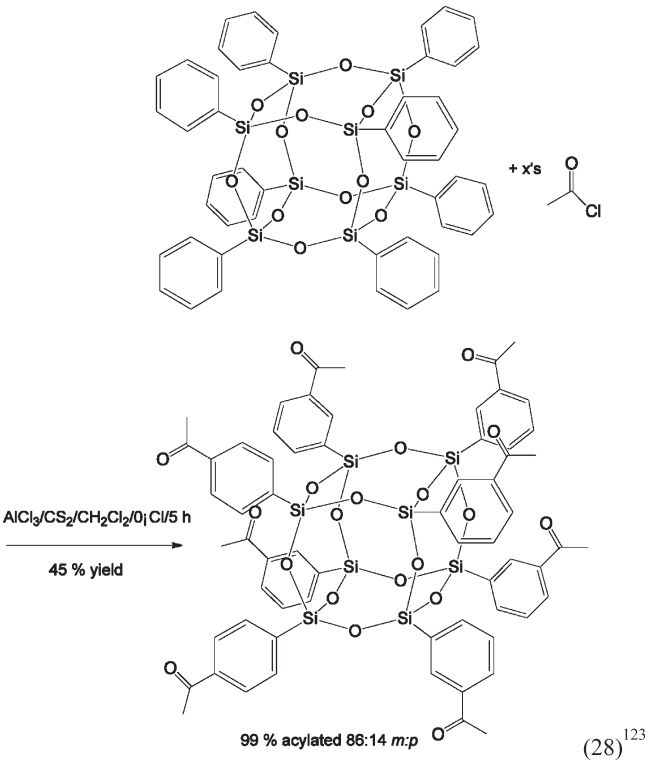

(28)[123]

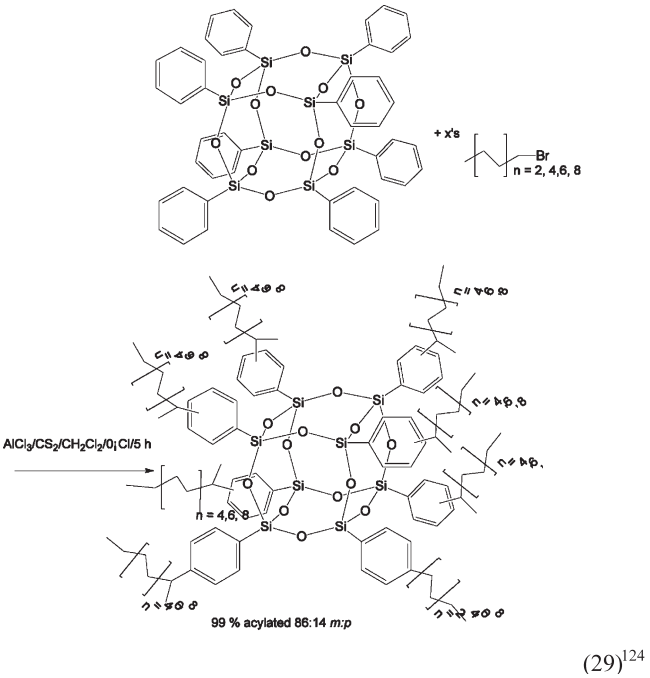

(29)[124]

In contrast to the acylation studies, it was quite easy to alkylate OPS using similar reaction conditions per reaction 29, which shows a generalized reaction.[124] As anticipated from traditional Friedel−Crafts chemistry, a primary cation is generated initially that can either effect electrophilic substitution or first rearrange to the more stable secondary cation which then reacts.

Alkylation is less discriminating than acylation leading to mixtures of *ortho*, *meta*, and *para* that are difficult to distinguish analytically. Thus, alkylation leads to a plethora of products for each linear alkyl bromide used. Furthermore, degrees of substitution vary distinctly with the amounts and size of the alkyl chain. Figure 28 provides examples from MALDI-ToF analyses of separate alkylation experiments. Table 16 provides

Table 11. Crystal Structure Data for the Iodophenylsilsesquioxanes[60]

	I_8OPS	I_{10}dPS	I_{12}DPS
space group	*I*4/, tetragonal	*C*2/*c*, monoclinic	*C*2/*c*, monoclinic
unit cell dimensions	a = 20.0403(11) Å b = 20.0403(11) Å c = 21.4606(12) Å α, β, γ = 90°	A = 28.054(2) Å b = 15.6168(11) Å c = 22.3246(16) Å α, γ = 90; b = 108.859(1)°	a = 32.082(9) Å b = 14.704(4) Å c = 28.755(8) Å α, γ = 90; β = 118.438(4)°
unit cell volume	8618.9 Å^3	9255.7 Å^3	11927.9 Å^3
Z	4, 1.641 mg/m^3	4, 1.831 mg/m^3	4, 1.941 mg/m^3
R-factor	7.4% (9.7%)[a]	4.6% (6.6%)[a]	9.2

[a] Before use of SQUEEZE to account for disordered solvent.[60]

Table 12. Characterization of the Homologous Iodophenylsilsesquioxanes

compound	yield (%)	GPC M_n (Da)	GPC PDI	CY calc	CY[a] found	MALDI calc (Da)	MALDI found (Da)
I_8OPS	90	1159	1.01	23.5	22	2148.6 (Ag^+)	2148
I_{12}DPS	90			23.5	24	3168.9	3167.3
I_{10}dPS	80			23.5	23	2658.72	2657

[a] CY = ceramic yield in air/10 °C/min.

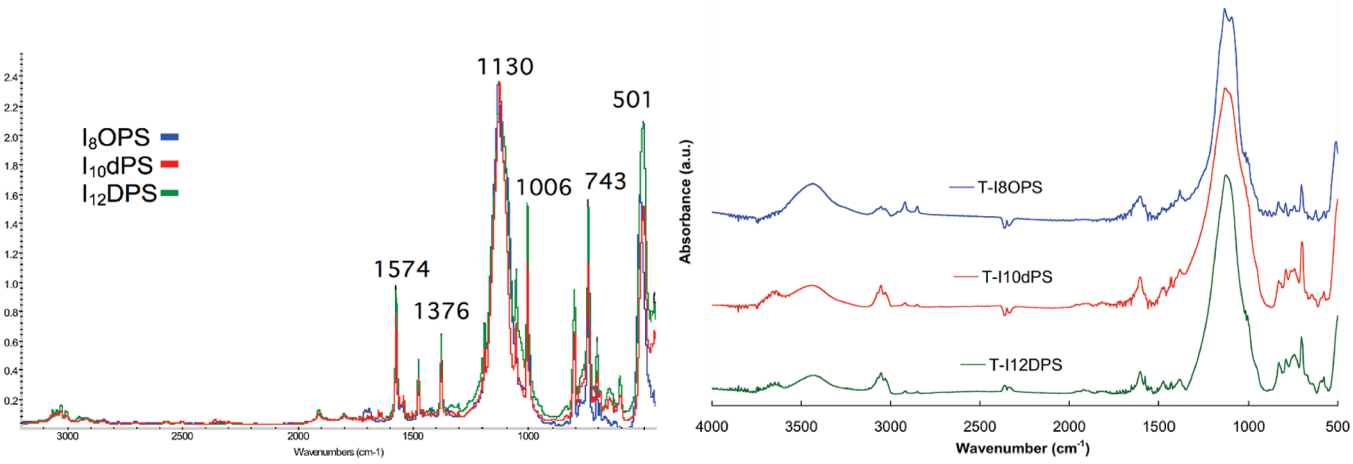

Figure 21. FTIRs of (a) homologous and (b) 425 °C thermolyzed iodophenylsilsesquioxanes T-T_8, T-T_{10}, and T-T_{12}. Note that both the aromatic νC−H and νSi−O−Si peaks remain.[60]

GPC data for alkylation under standard conditions for set reaction times. These data are captured in the GPCs shown in Figure 29.

The dimers come from small amounts of solvent (CH_2Cl_2) alkylation. The melting points of all of these materials after purification were recorded and are plotted in Figure 30. Several novel results are revealed by the data in Figure 30. First, in most instances, the addition of greater amounts of alkyl groups at first lowers T_m, but in several instances thereafter the T_m actually rises. As might be expected, the greater the chain length, the more difficult it is to alkylate beyond a certain limit most likely due to steric factors inhibiting the approach of the cationic species. Still more interesting are the results obtained for the $T_{d5\%}$ and after 12 h shown in Figure 31. The most important point is that the butyl and hexyl compounds are air stable to >400 °C for the most of the products isolated. In contrast, most of the octyl and decyl compounds exhibit $T_{d5\%}$ values closer to 325 °C on average. This disparity is greater in the 12 h/250 °C oxidation studies of Figure 31b.

We know from Figure 30 that these temperatures are well above the melting temperatures of these molecules. Additionally, DSC studies show almost no obvious phase transitions occur on heating or cooling, suggesting that these materials are perhaps amorphous. However, detailed XRD studies show that these materials are reasonably well ordered as seen in Figure 32. These data strongly suggest that at least for the butyl and hexyl compounds these materials are interdigitated both in the liquid state (hence the improved oxidation resistance) and in the solid state as determined by the XRD data. This also explains the increase in T_m as more alkyl groups are added. Indeed, modeling studies suggest that both the butyl and hexyl materials are interdigitated whereas the longer chain compounds act more like simple alkanes, exhibiting typical chain−chain interactions and packing as seen in Figure 33.

The apparent interdigitation in the solid and especially the liquid states suggests that more carefully designed analogues might be expected to act as nanogears in some form of nanomachine.

Alternately, when fixed to a surface, one might envision these types of interdigitated formats to offer "Velcro"-like properties, allowing one to fix an object to a surface and by raising the temperature to a point where the object can be shifted on the surface without ever leaving and then cooled to re-establish a fixed position.

Properties of StilbeneSQs

Initial functionalization studies with $Br_{5.3}$OPS targeted the introduction of aromatic groups in an effort to create luminescent centers especially for organic light-emitting diode components.[98,119,125] For reasons justified here, these studies were extended to iodo-derived materials. The original intent was to develop standard routes to luminescent materials that take advantage of the robustness of the SQ core. In addition, the 3-D nature of the system and the relative ease of synthesis and high solubility offered the potential for rapid purification of the resulting compounds.

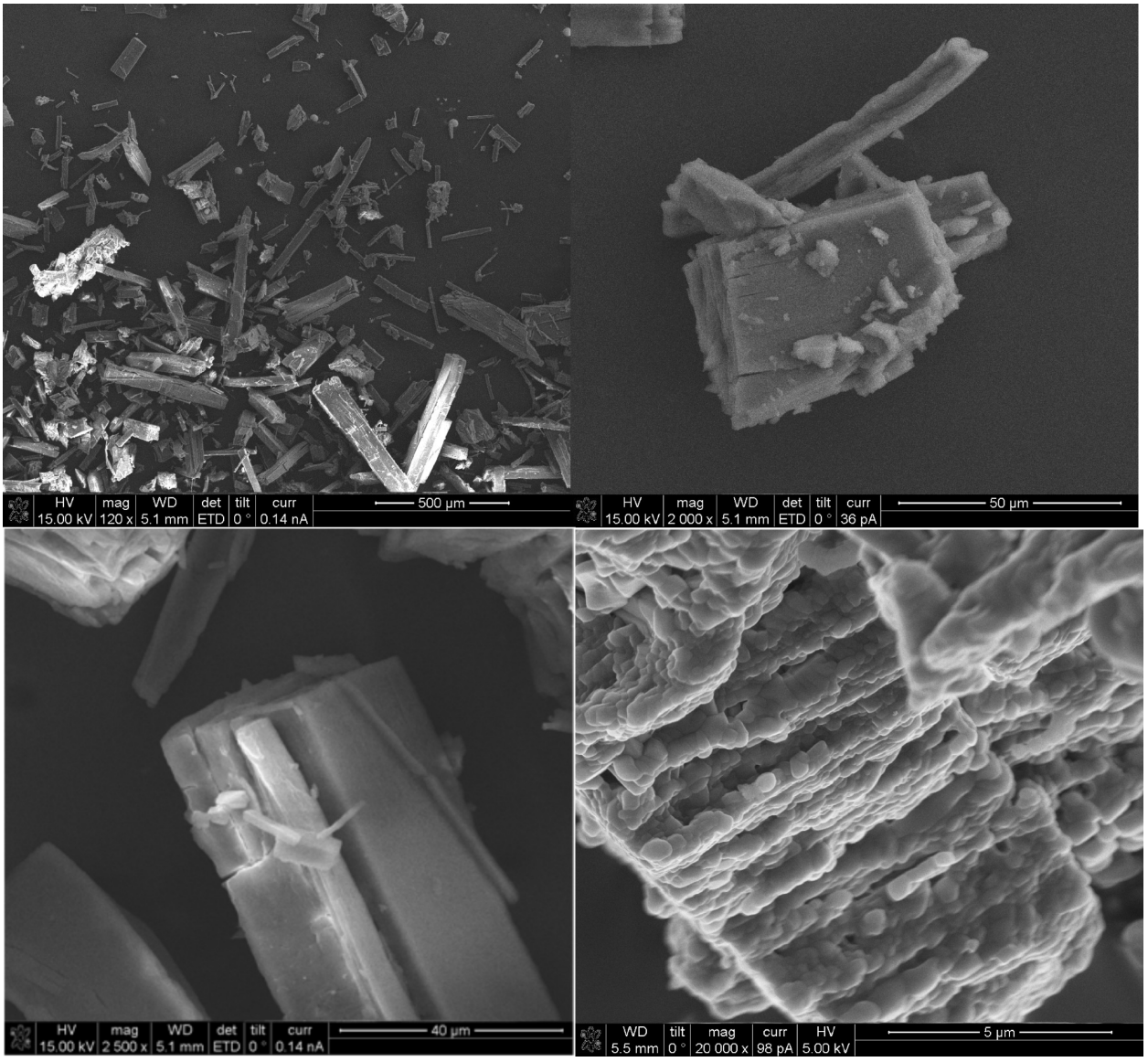

Figure 22. SEMs of T-T_8 suggesting retention of the original crystal morphology.[60]

Table 13. Characterization Data for T-T_8, T-T_{10}, and T-T_{12} (CY = Ceramic Yield)

compound	mass yield (%)	CY calc (%)	CY found (%)	SA (m^2/g) Langmuir	SA (m^2/g) BET	pore volume (cm^3/g)
T-T_8	55	47	45	830	555	0.31
T-T_{12}	56	47	45	670	455	0.26
T-T_{10}	52	47	44	740	500	0.27

Table 14. Alkyne Product Yields, Conversions, and GPC Data from $Br_{5.3}$OPS and I_8OPS[118]

	$Br_{5.3}$OPS				I_8OPS				
acetylene	yield (%)[a]	% conv[b] (NMR)	GPC PDI	ceramic yield (%)	yield (%)[a]	% conv[b](NMR)	GPC PDI	ceramic yield (%)	ceramic yield (%) (theory)
phenylacetylene	90	n/a	1.14	25.4	90	n/a	1.02	26.4	27.0
4-ethynyltoluene	86	130	1.09	22.5	89	>99	1.01	24.5	25.4
4-ethynylanisole	87	130	1.15	21.2	90	>99	1.01	22.6	23.8
4-ethynyl-α,α,α-trifluorotoluene	64	120	1.21	22.5	70	>99	1.15	21.1	20.7
trimethylsilylacetylene	80	110	1.23	17.8	81	>99	1.02	27.6	27.5
methylpropiolate	56	110	1.23	17.8	67	>99	1.02	29.3	29.3

[a] Isolated yield calculated relative to complete conversion of aryl halide. [b] Conversion calculated as ratio of aromatic to nonaromatic protons in ^{1}H NMR compared to the theoretical ratio.

To this end, we investigated the synthesis of stilbene systems via Heck coupling and polyaromatic systems relying on Suzuki coupling.[119] The reason for starting with the stilbene compounds (Scheme 11, Table 17) is that the photophysics of stilbene is well

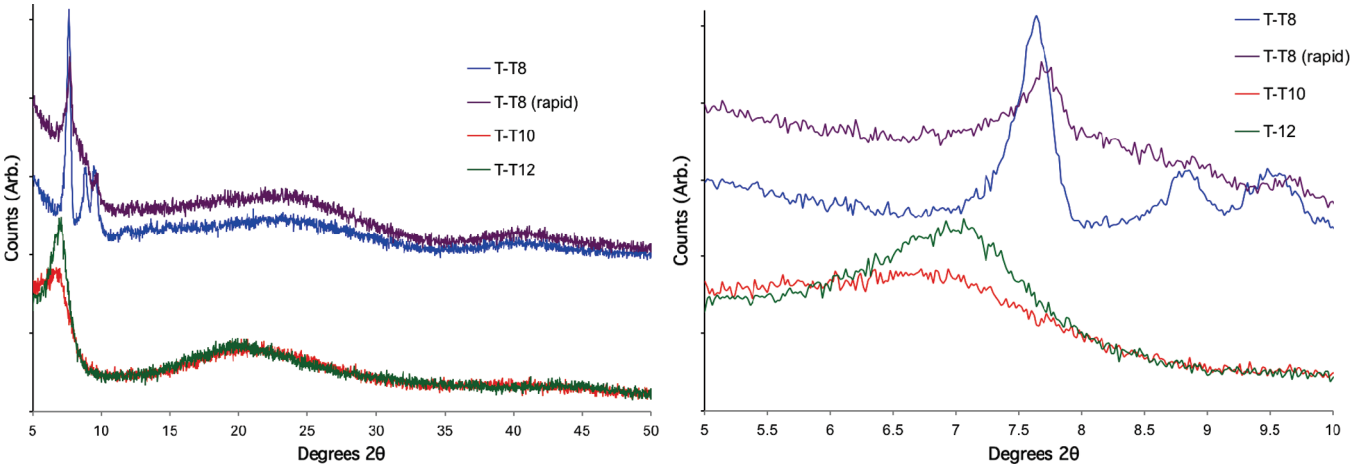

Figure 23. XRD Powder patterns of T-T_8, T-T_{10}, and T-T_{12}: (a) full scale; (b) expanded.[60]

Scheme 14. Functionalization of I_8OPS Using Standard Heterocoupling Chemistries[107]

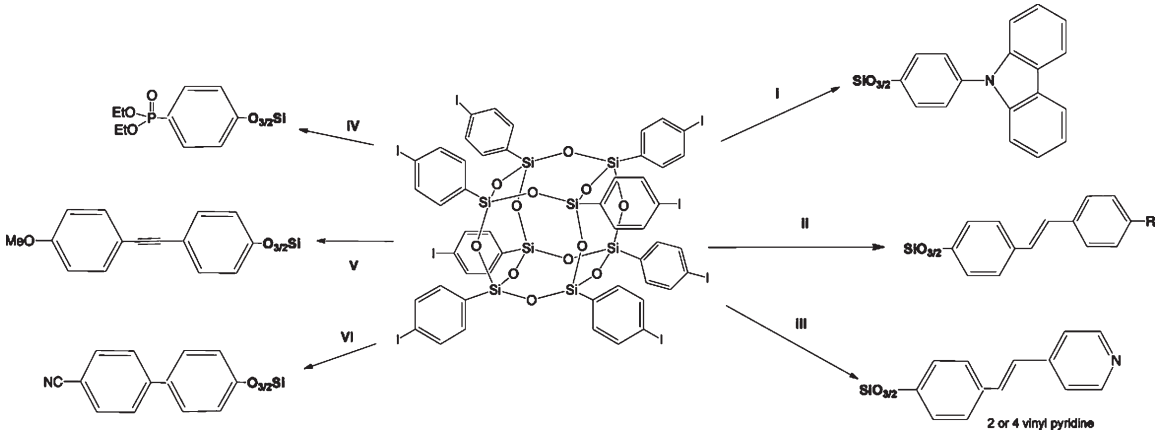

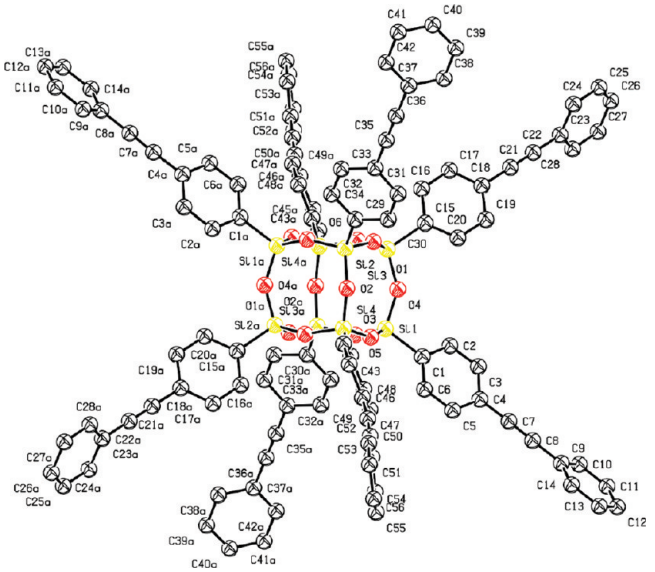

Figure 24. 50% thermal ellipsoid plots of octa(diphenylacetylene)-silsesquioxane·*m*-xylene solvate. Hydrogen atoms and *m*-xylene solvates are omitted for clarity.

studied, and it represents the monomer unit for polyphenylene-vinylene (PPV). PPV is noted to be an outstanding blue emitter but suffers from the fact that it is quite insoluble.[126]

With this in mind, we were able to synthesize a wide variety of [*p*-RstilbeneSi$O_{1.5}$]$_8$ compounds as suggested in Tables 17 and 18.[127] In this instance, we used $Br_{5.6}$OPS, [*p*-I_8PhSi$O_{1.5}$]$_8$, and [*p*-$I_{6.3}$PhSi$O_{1.5}$]$_8$ substrates. The reason for this latter material will become evident shortly. The respective UV−vis absorption and emission data for the $Br_{5.6}$OPS are shown in Figure 34.[127]

Table 15. $T_{d5\%}$ for Octa-alkynes from I_8OPS (in Air)[118]

R	$T_{d5\%}$ (°C)
—C≡C—	526
—C≡C— CH_3	475
—C≡C— OCH_3	508
F_3C —C≡C—	423
—C≡C—$Si(CH_3)_3$	418
—C≡C—$COOCH_3$	403

The key features observed are that all of the stilbene derivatives absorb at wavelengths typical of both *trans*-stilbene and *para*-substituted *trans*-stilbenes. In the latter case, electron-donating groups red shift both the absorptions and emissions equally by 10−20 nm. However, the most surprising discovery was that the emissions are red-shifted compared to *trans*-stilbene or the model compound *p*-trimethoxysilylstilbene by 60−80 or 40−60 nm.[127]

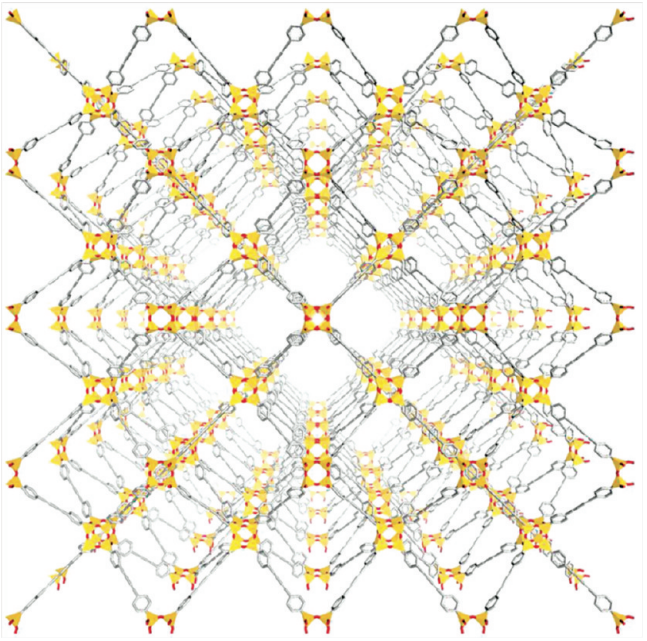

Figure 25. Idealized model structure of the homocoupling of [alkynylPhSiO$_{1.5}$]$_8$.[121]

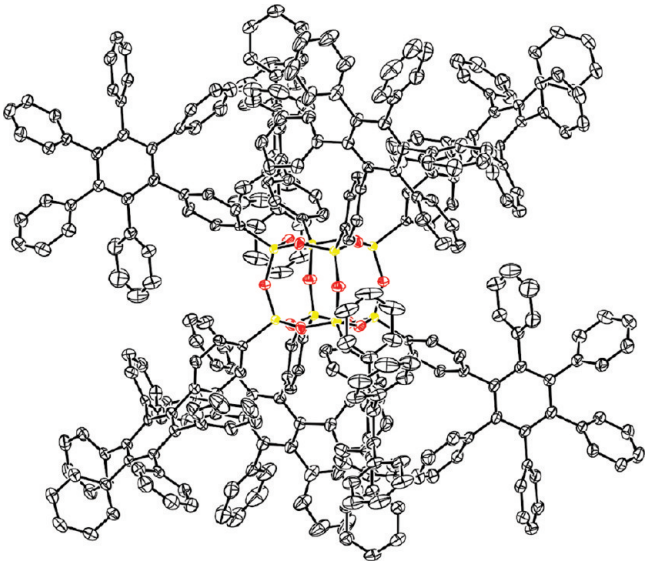

Figure 26. 50% thermal ellipsoid plots of 56aryl·18toluene. Labels and hydrogen atoms not shown for clarity.

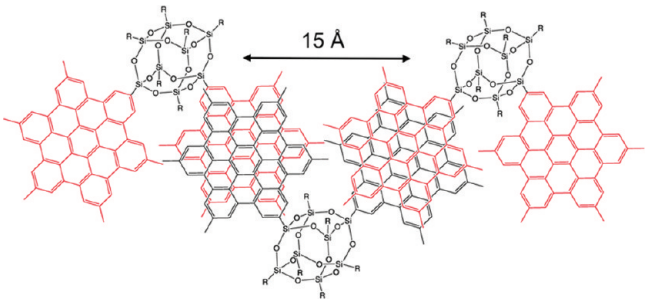

Figure 27. Schematic of octagraphene packing.[122]

Such red shifts are normally obtained by extending the conjugation in stilbene for example by adding a second styrenyl group. An additional finding for the Br$_{5.6}$OPS-derived materials

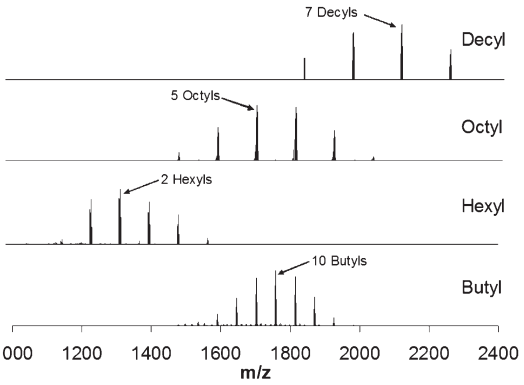

Figure 28. Representative MALDI-TOF spectra of selected alkylated OPS (Ag^+ ions).[125]

Table 16. GPC Data for Alkylated OPS at Various Reaction Times[125]

R	time (h)	M_w	M_n	PDI
butyl	1	852	913	1.07
	5	1035	1058	1.02
	10	1116	1196	1.07
	24	1215	1288	1.06
hexyl	1	1021	1102	1.08
	5	1184	1204	1.02
	10	1298	1394	1.07
	24	1416	1574	1.11
octyl	1	950	1002	1.05
	5	1063	1120	1.05
	10	1253	1302	1.04
	24	1592	1775	1.11
decyl	1	911	952	1.05
	5	1414	1516	1.07
	10	1649	1738	1.05
	24	2160	2459	1.14

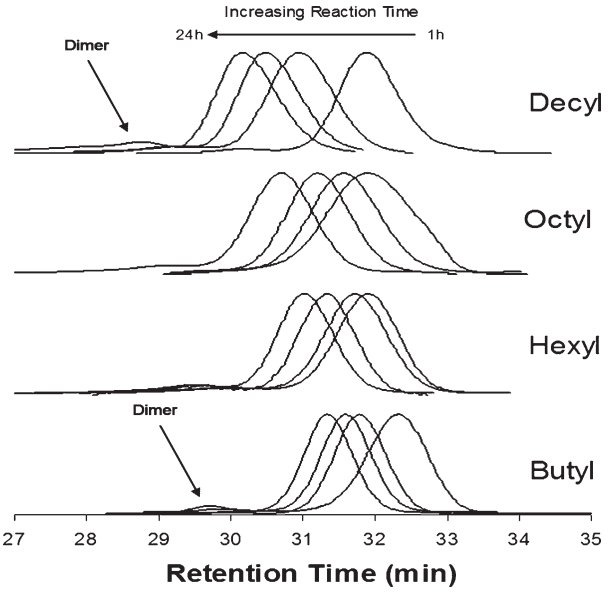

Figure 29. GPCs of alkylated OPS as a function of reaction time and alkyl chain length after 1, 5, 10, and 24 h of reaction time.[122]

was that the Φ_{PL} values for these compounds were 5−10 times higher than those normally seen for *trans*-stilbenes, which typically run 5−7%.[123] Recognizing that these compounds contained 3−5% dibromo groups, it seemed likely that a significant fraction of the molecules would contain at least one divinylbenzene substitutent. As we show below, Heck

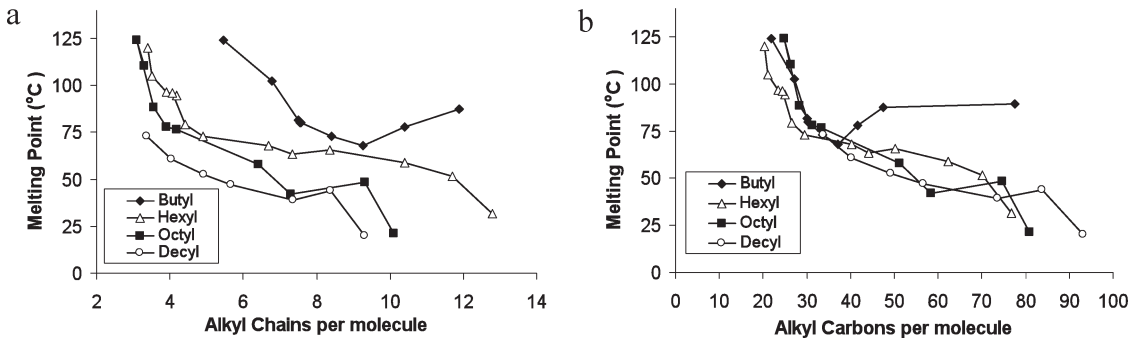

Figure 30. Melting points of alkylphenylsilsesquioxanes as a function of the (a) number of chains/cage and (b) number of carbons/cage.[122]

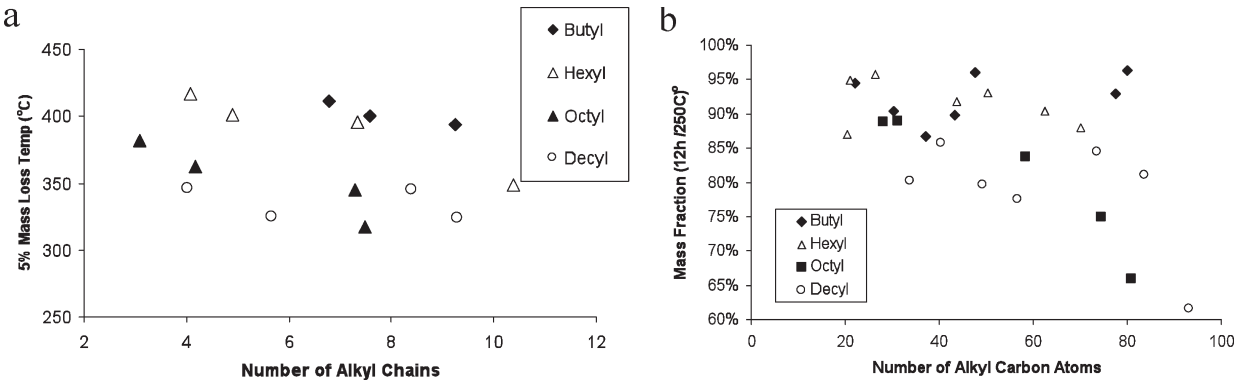

Figure 31. (a) $T_{d5\%}$ vs alkyl chain number. (b) Mass loss in air (12 h/250 °C).[122]

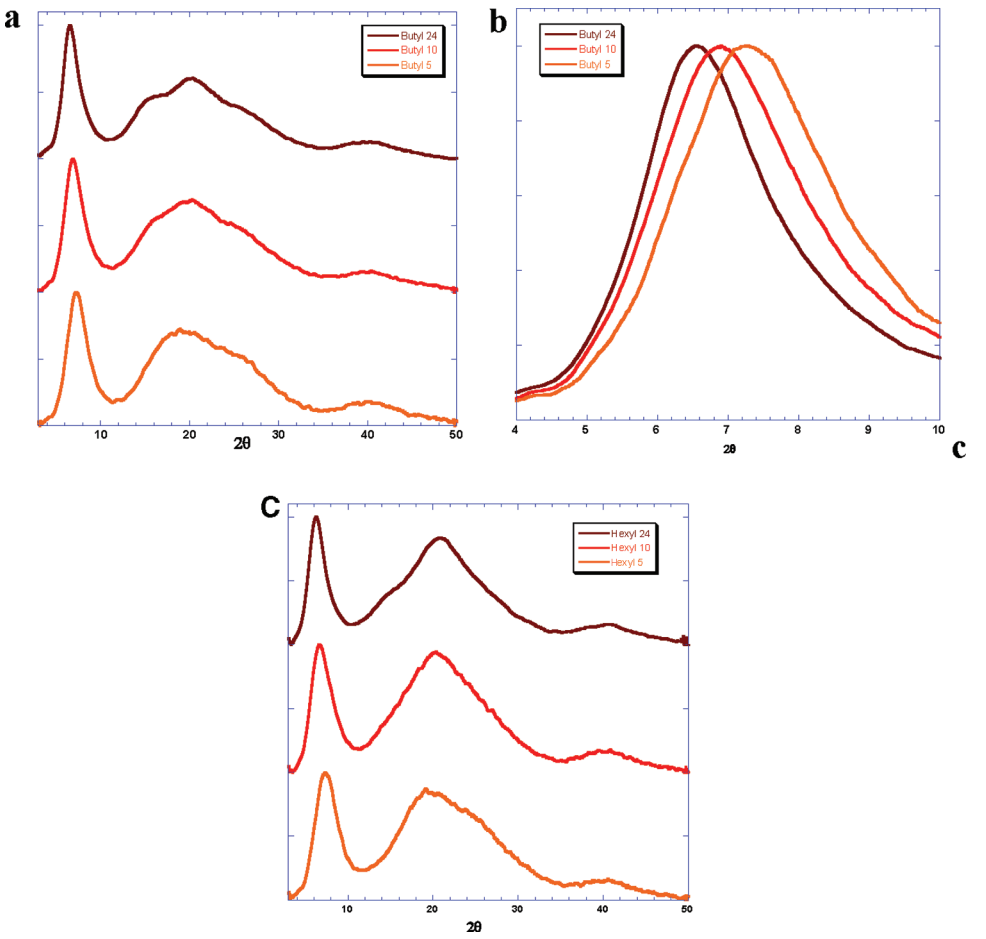

Figure 32. XRD of (a) butyl$_x$OPS, (b) expanded XRD of butyl$_x$OPS, and (c) XRD of hexyl$_x$OPS showing peak shifts as a function of reaction times.

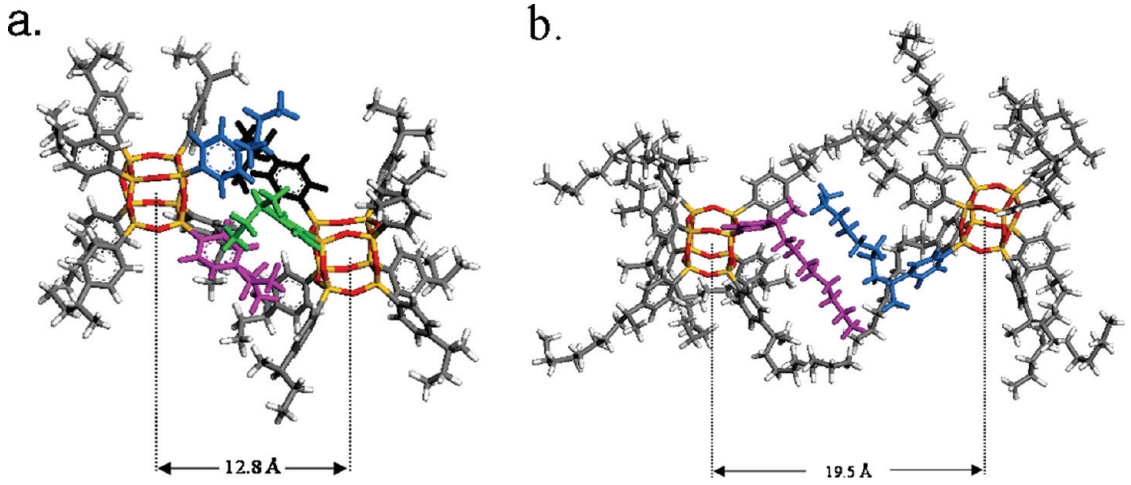

Figure 33. Molecular modeling of R_xOPS [R = Bu (a), decyl (b), $x = 8$]. Simulations run at 150 °C to capture liquid state behavior.[125]

Table 17. GPC, TGA, and MALDI-TOF Data for Br_xOPS and $RStil_xOS$ Compounds[127]

		Br_xOPS	$Stil_xOS$	$MeStil_xOS$	$MeOStil_xOS$	$ClStil_xOS$
GPC	M_n	1009	1330	1669	1667	1756
	M_w	1040	1404	1786	1771	1864
	PDI	1.03	1.06	1.07	1.06	1.06
TGA	ceramic yield (%)	31.0	29.2	27.0	27.0	24.0
	theory (%)	31.9	29.1	27.8	26.3	26.0
	$T_{d5\%}$ (°C)	460	414	404	401	420
MALDI-ToF	mass ($X = 6$)	1499.5	1644.3	1728.4	1824.4	1848.1
	X_{ave}	5.7	6.0	5.8	5.9	5.5

Table 18. GPC, TGA, and MALDI-TOF Data for *p*-I_xOPS, *o*-Br_8OPS, Selected *p*-$RStil_xOS$ Compounds, and *o*-$MeStil_8OS$[127]

		$I_{6.4}OPS$	$Stil_8OS$	$MeStil_8OS$	*o*-$MeStil_8OS$	Me_2NStil_8OS	$Me_2NStil_{6.3}OS$
GPC	M_n	918	1609	1852	1201	2010	1797
	M_w	929	1641	2007	1217	2048	1873
	PDI	1.01	1.02	1.08	1.01	1.02	1.04
TGA	ceramic yield (%)	24.0	26.3	26.3	25.9	21.5	24.1
	theory (%)	25.1	26.0	24.5	24.5	21.9	23.4
	$T_{d5\%}$ (°C)	429	410	429	404	325	318
MALDI-ToF	mass	2022	1958	2071	2069	2193	2050
	($X = 8$)	(Ag^+, $x = 7$)	(Ag^+)	(Ag^+)	(Ag^+)	(H^+)	(H^+, $x = 7$)
	X_{ave}	6.4	8	8	8	8	6.3

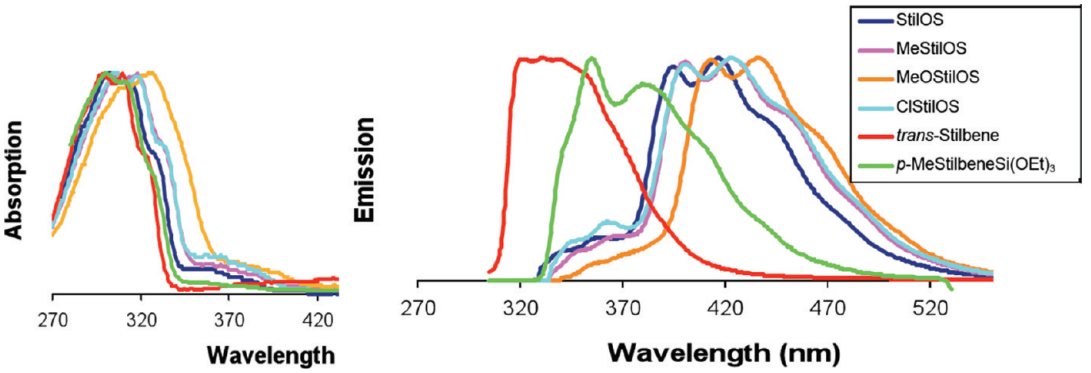

Figure 34. $RStil_{5.7}Ph_{2.3}OS$ and *trans*-stilbene: (a) UV−vis and (b) emission spectra (THF). Absorptions normalized to 1.[127]

coupling of [2,5-$Br_2PhSiO_{1.5}$]$_8$ leads to significant red shifts and significant improvements in Φ_{PL}. Consequently, we first ascribed the significant red shift to the presence of one divinylbenzene per cage or less.[127] This led to the conclusion that in these systems, rapid energy transfer occurs between moieties on the cage such that energy absorbed by simple stilbene units is rapidly transferred to the single divinylbenzene and then emitted.

The synthesis of essentially pure [*p*-$IPhSiO_{1.5}$]$_8$ allowed us to test the source of this red shift. Thus, efforts were made to prepare both pure [*p*-$MeStilbeneSiO_{1.5}$]$_8$ {(*p*-MeStil)$_8$OS} and also [*p*-$MeStilbeneSiO_{1.5}$]$_{6.8}$[$PhenylSiO_{1.5}$]$_{1.2}$ {(*p*-MeStil)$_x$(Ph)$_{8-x}$OS} to determine if the red shift was derived from small quantities of divinylbenzene units or from some other source. Figure 35 shows that the emission red shift is still observed for (*p*-MeStil)$_8$OS whereas the emission structure changes for (*p*-MeStil)$_{6.8}$(Ph)$_{1.2}$OS.

For both these compounds, Φ_{PL} is reduced to ≈0.05, indicating that efficient energy transfer to the small quantities of divinylbenzene moieties was the reason for the high Φ_{PL} values observed in the earlier work.[127] This has implications for use of these materials as antennae for light harvesting.

Nonetheless, the large red shift still remains to be explained. Studies at increasingly greater dilutions did not change the shift, indicating that exciplexes were not involved. The fact that the emission band is structured indicates that emission was not from a charge-transfer transition. This was also supported by solvent studies that showed no dependence on solvent polarity.[127]

A potential explanation was identified based on theoretical studies. Silsesquioxanes in general have been the subject of a large number of theoretical studies.[128−139] Most of the studies find that the highest occupied molecular orbital (HOMO) involves 2p lone pair states of A_{2g} symmetry on the oxygen atoms which is not surprising. However, these same studies find that the lowest unoccupied molecular orbital (LUMO) has $4A_1$ symmetry and involves contributions from all Si and oxygen atoms and the organic substituents, is spherical, and resides in the core center.

These states are depicted in Figure 36, and some exemplary DFT calculations are provided in Table 19. This LUMO is considered to be highly electrophilic and is the reason that it is possible to encapsulate F^- ions in a wide variety of these compounds providing that the organic substituents are at least mildly electron withdrawing.[135] Indeed, it is also likely that this electrophilic character is responsible for the *ortho* bromination pattern discussed above.

It is not uncommon for DFT-calculated band gaps to overestimate experimental results. Thus, Marsmann et al.[131] demonstrated that band gap calculations on the $[RSiO_{1.5}]_8$ cages are high, reporting that $[XSiO_{1.5}]_8$ where X = CH_3−, CH_3CH_2, ..., decyl) absorb 3.8 eV (325 nm) light and emit at ≈2.8−3.5 eV (330−370 nm). Their calculations suggest a 6.0 eV band gap for $[HSiO_{1.5}]_8$, but the experimental value was 4.4 eV, which is 1.6 eV lower.

In our calculations, we see that the energy differences between the HOMO and the core (core gap) drop to ≈4.23 eV for $[p\text{-MeStilSiO}_{1.5}]_8$ from a calculated value of 7.0 eV for $[HSiO_{1.5}]_8$. This drop alone is significant and points to some form of interaction between the stilbene groups and the cage. If our calculated gaps are also high by 1.6 eV as in Marsmann et al.'s calculations, then the actual core-based band gap is close to 2.6 eV, roughly the same as that calculated for the $\pi-\pi^*$ transition for stilbene (Figure 36). Thus, one can suggest that in the excited state the cage-centered or "core" orbital is the same energy as the π^*-state of stilbene. The implication is the existence of 3-D conjugation through the core.

This leads to the potential for many exciting opportunities including the development of SQ-based single molecule transistors,[127] the use of SQs with both donor and acceptor groups on the same cage as moieties that allow for charge separation from absorbed photons, and also for electron and hole transport.

Indeed, it is possible to demonstrate that in some SQs, excitation generates strong and stable charge transfer (CT) transitions. Thus, solvatochromism studies of $[p\text{-NH}_2\text{StilSiO}_{1.5}]_8$ (Figure 37) indicate that while absorption is not affected by changes in solvent polarity, emissions are indeed stabilized, and red shifts of 30−40 nm can be observed on going from THF to acetonitrile.

Perhaps the most important observation here is that the quantum efficiencies of $[p\text{-NH}_2\text{StilSiO}_{1.5}]_8$ for fluorescence are quite low, as would be associated with C-T behavior. Proof of CT in the excited state comes from two-photon (TPA) cross-section studies

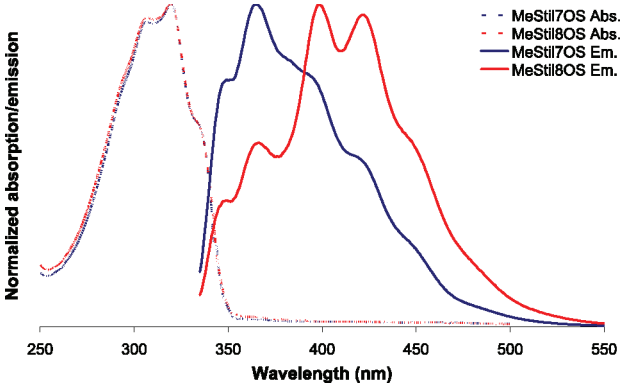

Figure 35. UV−vis absorption and PL spectra of $(p\text{-MeStil})_x(Ph)_{8-x}OS$ in THF.[127]

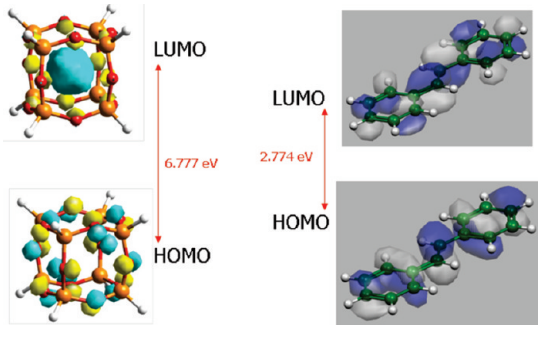

Figure 36. LUMO and HOMO of $[XSiO_{1.5}]_8$.[127]

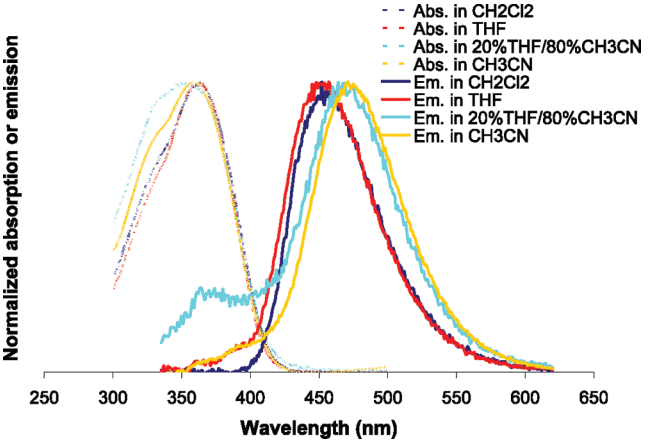

Figure 37. Solvatochromism of $[p\text{-NH}_2\text{StilSiO}_{1.5}]_8$ in selected solvents.[127]

Table 19. DFT HOMO−LUMO Calculations for Various $[XSiO_{1.5}]$ (all Values in eV)[127]

	$[HSiO_{1.5}]_8$	$[FSiO_{1.5}]_8$	$[HOSiO_{1.5}]_8$	$[NH_2SiO_{1.}]_8$	OPS	$StiSi(OSiMe_3)_3$	$Stil_1[SiO_{1.5}]_8$	$Stil_8OS$
HOMO	−7.52 (O)	−8.79 (O)	−7.38 (O_{cube})	−5.75 (N)	−5.53	−5.165	−5.47	−4.52
core/LUMO	−0.54 (H,Si)	−2.33 (F)	−1.218 (H,Si)	−0.56 (H)	−0.035	−0.213 (SiO_3)	−0.41	−0.29
organic/LUMO					−0.86	−2.46	−2.77	−1.91
core gap	6.978	6.46	6.166	5.18	5.56	4.95	5.06	4.79
organic gap					4.66	2.70	2.70	2.61

Table 20. TPA Properties of Silsesquioxane Derivatives[127]

sample	δ (GM)	δ/moiety (GM)	λ_{max} nm
[*p*-MeStilSiO$_{1.5}$]$_8$	11	1.2	735
[*p*-NH$_2$StilSiO$_{1.5}$]$_8$	211	26	755
[StilCH=CHSiO$_{1.5}$]$_8$	25	3	705
[*p*-MeOStilCH=CHSiO$_{1.5}$]$_8$	110	14	705
[*p*-NH$_2$StilCH=CHSiO$_{1.5}$]$_8$	810	101	720

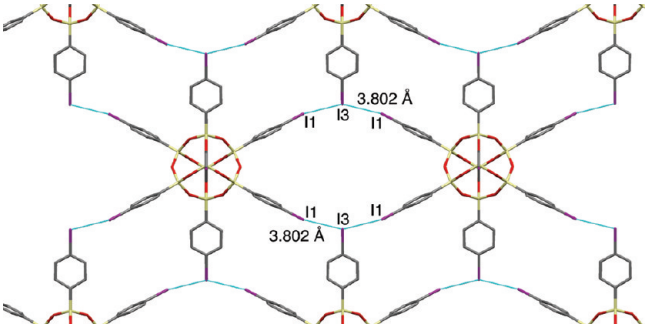

Figure 38. Coplanar [*p*-IPhSiO$_{1.5}$]$_8$ molecules coordinated via I1···I3 short contacts (3.802 Å).

listed in Table 20. *Para* NH$_2$ groups in both the stilbene and vinyl stilbene systems, [NH$_2$StilCH=CHSiO$_{1.5}$]$_8$, lead to quite high cross sections with higher cross sections obtaining where conjugation is extended by a vinyl group. These numbers are greater than the TPA values listed above for the 8, 16, and 23 derivatives, especially the NBoC (*N*-*tert*-butylcarbamate) system. As noted above, this protecting group is quite electron withdrawing, and as such, further studies with deprotected NH$_2$ or NR$_2$ substituents are warranted vis-à-vis controlling charge transport in these systems and charge separation. There appears to be great potential for new compounds for use in OLEDs and organic photovoltaics.

Crystal Packing Structures for [*p*-IPhSiO$_{1.5}$]$_8$, [*o*-BrPhSiO$_{1.5}$]$_8$, and [2,5-Br$_2$PhSiO$_{1.5}$]$_8$

We will now discuss some features of the crystal structures of the halogenated phenylsilsesquioxanes. These molecular systems show a number of halogen−halogen short contacts, or halogen bonding motifs, which are as short or shorter than published examples from small molecule systems. While a paper documenting these results is in preparation,[140] we present here some important examples.

The crystal structure of [*p*-IPhSiO$_{1.5}$]$_8$ reveals a continuous network of channels, comprising ≈40 vol % of the unit cell, occupied by disordered ethyl acetate solvates as calculated by PLATON.[141] The *para*-substituted iodine bonds strongly to other halogens.[142] One might anticipate any halogen bonding interactions would be intermolecular, minimizing the potential for $\pi-\pi^*$ driven interdigitation of the aromatic rings. This in turn can be anticipated to result in accessible voids close to cage faces. Lastly, such coordination might also serve as "host" crystal structures, which could be infiltrated with a desired "guest". This then represents a novel area for future research.

The crystal structure of [*p*-IPhSiO$_{1.5}$]$_8$ shows examples of I···I motifs as well as C···I short contacts. The iodine van der Waals radius given by Bondi is 2.04 Å, so an I···I short contact would be <4.08 Å.[131] Figure 38 shows two pairs of type II contacts (3.8 Å) found in the I$_8$OPS structure. Though there are three coordinating iodines, the 90° coordination angles are best described by a type II contact, not an I$_3$ motif. In Figure 39, the combination of four one-dimensional ArC···I short contacts in I$_8$OPS forms a square pore between adjacent molecules.

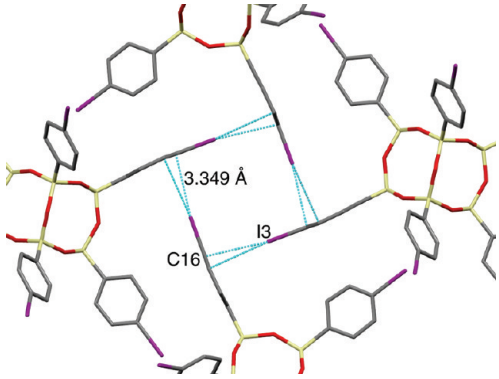

Figure 39. Four coplanar C16···I3 short contacts (3.349 Å) as seen in [*p*-IPhSiO$_{1.5}$]$_8$.

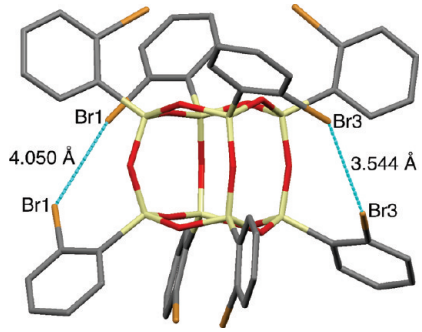

Figure 40. Intramolecular bromine short contacts in *o*-Br$_8$OPS.

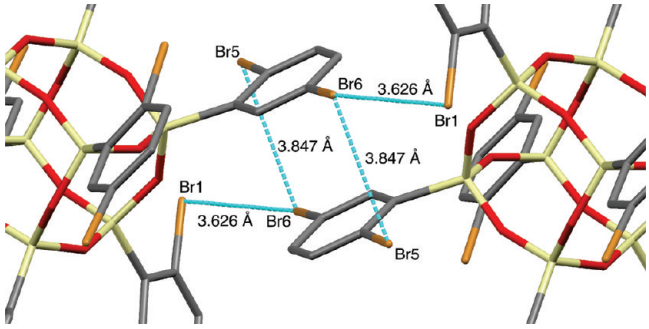

Figure 41. Br···Br short contact pairs in Br$_{16}$OPS.

Figure 40 shows the octa(*o*-bromophenyl)silsesquioxane crystal structure, which has several unique *intra*molecular coordination features due to the *ortho* substitution pattern. Type I coordination is found in two pairs of bromophenyls on opposite sides of the molecule. One of these Br···Br interactions is a short-contact using the van der Waals radius (3.7 Å), while the other is shorter than the sum of the *n*-polar radius (4.08 Å).[132] Each molecule is paired with a second through a tetrahedral "Br$_4$" synthon. Along orthogonal axes, there are additional contacts. Figure 41 shows coplanar aromatic rings with multiple coordinating Br···Br short contacts. Though the type II Br1···Br6 contacts are below the sum of the vdW radii, the Br5···Br6 contacts are only shorter than the sum of the "*n*-polar" radii.

These findings are important in that these compounds have the unique ability to demonstrate intra- and intermolecular coordination structures with very high symmetry.[142,143] Such coordination can be used to coordinate reactive species in addition to the formation of guest−host species.[145] For instance, porous crystal structures could be used as models to examine the dynamics of

enclosed probe species. Given the transparency of these crystals, correlation of colored tracer diffusion rates could be possible or the trapping of polymer species.

Future Directions

We have attempted to note some possible areas of future study above but believe that the recent development of methods of controlled halogenation of PhenylSQs discussed above will allow a great many new compounds to be made and nanostructured materials from them

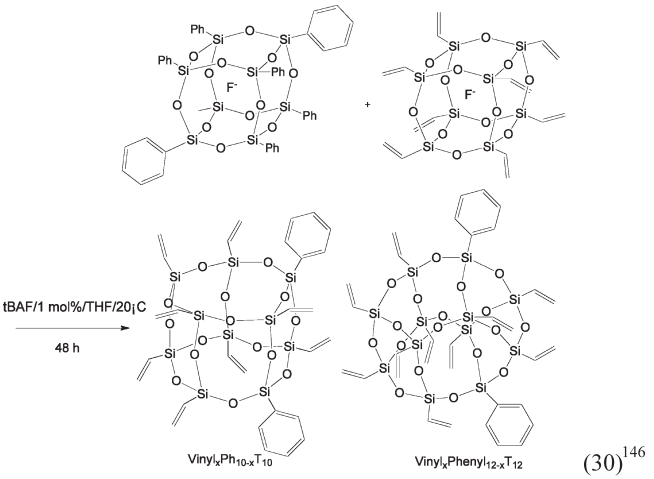

(30)[146]

This review is by no means complete, and other sections are now being created in multiple laboratories around the world. As an example of this, we recently reported the synthesis of mixed functional phenylSQs as illustrated in reaction 30.[146] The F^--catalyzed exchange provides access to phenyl compounds with other functionality in the same cage and also access to T_{10} and T_{12} cages that have hitherto been quite difficult to form. We anticipate this type of reaction creating a whole new chapter in silsesquioxane chemistry and in nanocomposite materials made therefrom.

Acknowledgment. We thank NSF, AFRL, USDA, ONR, U.S. Army Natick, Canon Ltd, Delphi Inc., Nippon Shokubai, and Mayaterials Inc. for support of work reported here from our research group. We also thank DOE Center Grant Award No. DE-SC0000957 for support of the more recent work especially on photoluminescent compounds. We are also grateful to the extensive efforts of our reviewers, as their comments have served to improve this review. We thank Springer-Verlag for permission to reprint Scheme 3 and Figures 3 and 30−32.

References and Notes

(1) Lanznaster, M.; Heeg, M. J.; Yee, G. T.; McGarvey, B. R.; Verani, C. N. Design of Modular Scaffolds Based on Unusual Geometries for Magnetic Modulation of Spin-Diverse Complexes with Selective Redox Response. *Inorg. Chem.* **2007**, *46*, 72–8.

(2) (a) Addicott, C.; Das, N.; Stang, P. J. Self-Recognition in the Coordination Driven Self-Assembly of 2-D Polygons. *Inorg. Chem.* **2004**, *43*, 5335–38. (b) Seidel, S. R.; Stang, P. J. High-Symmetry Coordination Cages via Self-Assembly. *Acc. Chem. Res.* **2002**, *35*, 972–83.

(3) Mastalerz, M. The Next Generation of Shape-Persistant Zeolite Analogues: Covalent Organic Frameworks. *Angew. Chem., Int. Ed.* **2008**, *47*, 445–447.

(4) Yang, H.-B.; Ghosh, K.; Arif, A. M.; Stang, P. J. The Synthesis of New 60 Organometallic Subunits and Self-Assembly of Three-Dimensional M_3L_2 Trigonal-Bipyramidal Cages. *J. Org. Chem.* **2006**, *71*, 9464–9.

(5) (a) Yaghi, O. M.; Li, H.; Davis, C.; Richardson, D.; Groy, T. L. Synthetic strategies, structure patterns, and emerging properties in the chemistry of modular porous solids. *Acc. Chem. Res.* **1998**, *31*, 474–84. (b) Yaghi, O. M.; Li, Q. Reticular Chemistry and Metal-Organic Frameworks for Clean Energy. *MRS Bull.* **2009**, *34*, 682–690.

(6) Menzel, H.; Mowery, M. D.; Cai, M.; Evans, C. E. Fabrication of Noncovalent and Covalent Internal Scaffolding in Monolayer Assemblies Using Diacetylenes. *Macromolecules* **1999**, *32*, 4343–50.

(7) Morris, R. E. Modular materials from zeolite-like building blocks. *J. Mater. Chem.* **2005**, *15*, 931–8.

(8) (a) Broutman, L. J.; Agarwhal, B. D. A theoretical study of the effect of an interfacial layer on the properties of composites. *Polym. Eng. Sci.* **1974**, *14*, 581–8. (b) Li, T.; Zhang, M.; Zhang, K.; Zeng, H. The dependence of the fracture toughness of thermoplastic composite laminates on interfacial interaction. *Compos. Sci. Technol.* **2000**, *60*, 465–76.

(9) Lipic, P. M.; Hillmyer, M. A.; Bates, F. S. Nanostructured thermosets templated from self-assembled amphiphilic block copolymer epoxy resin mixtures. *J. Am. Chem. Soc.* **1998**, *120*, 8963–70.

(10) Detken, A.; Zimmermann, H.; Haeberlen, U.; Poupko, R.; Luz, Z. Molecular Reorientation and Self-Diffusion in Solid Cubane by Deuterium and Proton NMR. *J. Phys. Chem.* **1996**, *100*, 9598–604.

(11) Eaton, P. E. Cubanes: Starting Materials for the Chemistry of the 1990s and the New Century. *Angew. Chem., Int. Ed. Engl.* **1992**, *31*, 1421–36.

(12) Yildrim, T.; Yildirim, P. M. G.; Neumann, D. A.; Eaton, P. E.; Emrick, T. Solid Cubane: A Brief Review. *Carbon* **1998**, *36*, 809–15.

(13) Voronkov, M. G.; Lavrent'yev, V. I. Polyhedral oligosilsesquioxanes and their homo derivatives. *Top. Curr. Chem.* **1982**, *102*, 199–236.

(14) Baney, R. H.; Itoh, M.; Sakakibara, A.; Suzuki, T. *Silsesquioxanes*. *Chem. Rev.* **1995**, *95*, 1409–30.

(15) Loy, D. A.; Shea, K. J. Bridged Polysilsesquioxanes. Highly Porous Hybrid Organic-Inorganic Materials. *Chem. Rev.* **1995**, *95*, 1431–42.

(16) (a) Calzaferri, G. Silsesquioxanes. In *Tailor-made Silicon-Oxygen Compounds, from molecules to materials*; Corriu, R., Jutzi, P., Eds.; Publ. Friedr. Vieweg & Sohn mbH: Braunshweig/Weisbaden, Germany, 1996; pp 149−169. (b) Kannan, R. Y.; Salacinski, H. J.; Butler, P. E.; Seifalian, A. M. Polyhedral Oligomeric Silsesquioxane Nanocomposites: The Next Generation Material for Biomedical Applications, *Acc. Chem. Res.* **2005**, *38*, 879−884.

(17) Lichtenhan, J. Silsesquioxane-based Polymers. In *Polymeric Materials Encyclopedia*; Salmone, J. C., Ed.; CRC Press: New York, 1996; Vol. *10*, pp 7768−77.

(18) Provatas, A.; Matisons, J. G. Synthesis and applications of silsesquioxanes. *Trends Polym. Sci.* **1997**, *5*, 327–32.

(19) Li, G.; Wang, L.; Ni, H.; Pittman, C. U. Polyhedral Oligomeric Silsesquioxane (POSS) Polymers and Copolymers: A Review. *J. Inorg. Organomet. Polym.* **2001**, *11*, 123–151.

(20) Duchateau, R. Incompletely Condensed Silsesquioxanes: Versatile Tools in Developing Silica-Supported Olefin Polymerization Catalysts. *Chem. Rev.* **2002**, *102*, 3525–3542.

(21) Abe, Y.; Gunji, T. Oligo- and polysiloxanes. *Prog. Polym. Sci.* **2004**, *29*, 149–182.

(22) Phillips, S. H.; Haddad, T. S.; Tomczak, S. J. Developments in Nanoscience: polyhedral oligomeric silsesquioxane (POSS)-polymers. *Curr. Opin. Solid State Mater. Sci.* **2004**, *8*, 21–29.

(23) Laine, R. M. Nano-building blocks based on the $[OSiO_{1.5}]_8$ silsesquioxanes. *J. Mater. Chem.* **2005**, *15*, 3725–44.

(24) Lickiss, P. D.; Rataboul, F. Fully Condensed Polyhedral Silsesquioxanes: From Synthesis to Application. *Adv. Organomet. Chem.* **2008**, *57*, 1–116.

(25) Chan, K. L.; Sonar, P.; Sellinger, A. Cubic silsesquioxanes for use in solution processable organic light emitting diodes (OLED). *J. Mater. Chem.* **2009**, *19*, 1–19.

(26) Cordes, D. B.; Lickiss, P. D.; Rataboul, F. Recent Developments in the Chemistry of Cubic Polyhedral Oligosilsesquioxanes. *Chem. Rev.* **2010**, *10*, 2081–2173.

(27) (a) Feher, F. J.; Newman, D. A.; Walzer, J. F. Silsesquioxanes as models for silica surfaces. *J. Am. Chem. Soc.* **1989**, *111*, 1741. (b) Feher, F. J.; Budzichowski, T. A.; Blanski, R. L.; Weller, K. J.; Ziller, J. W. Facile syntheses of new incompletely condensed polyhedral oligosilsesquioxanes: $[(c\text{-}C_5H_9)_7Si_7O_9(OH)_3]$, $[(c\text{-}C_7H_{13})_7Si_7O_9(OH)_3]$, $[(c\text{-}C_7H_{13})_6Si_6O_7(OH)_4]$. *Organometallics* **1991**, *10*, 2526–8. (c) Maschmeyer, T.; Klunduk, M. C.; Martin, C. M.; Shephard, D. S.; Thomas, J. M.; Johnson, B. F. G. Modelling the active sites of heterogeneous titanium-centred epoxidation catalysts

with soluble silsesquioxane analogues. *Chem. Commun.* **1997**, 1847–8.
(28) (a) Feher, F. J.; Blanski, R. L. Olefin polymerization by vanadium-containing silsesquioxanes: synthesis of a dialkyl-oxo-vanadium (V) complex that initiates ethylene polymerization. *J. Am. Chem. Soc.* **1992**, *114*, 5886–7. (b) Feher, F. J.; Budzichowski, T. A. Silasesquioxanes as Ligands in Inorganic and Organometallic Chemistry. *Polyhedron* **1995**, *14*, 3239–53. (c) Severn, J. R.; Duchateau, R.; van Santen, R. A.; Ellis, D. D.; Spek, A. L. Homogeneous Models for Chemically Tethered Silica-Supported Olefin Polymerization Catalysts. *Organometallics* **2002**, *21*, 4–6. (d) Duchateau, R.; Abbenhuis, H. C. L.; van Santen, R. A.; Meetsma, A.; Thiele, S.K.-H.; van Tol, M. F. H. Half-Sandwich Titanium Complexes Stabilized by a Novel Silsesquioxane Ligand: Soluble Model Systems for Silica-Grafted Olefin Polymerization Catalysts. *Organometallics* **1998**, *17*, 5222–4.
(29) Maxim, N.; Magusin, P. C. M. M.; Kooyman, P. J.; van Wolput, J. H. M. C.; van Santen, R. A.; Abbenhuis, H. C. L. Synthesis and Characterization of Microporous Fe-Si-O Materials with Tailored Iron Content from Silsesquioxane Precursors. *J. Phys. Chem. B* **2002**, *106*, 2203–6.
(30) Bonhomme, C.; Toledano, J. P.; Maquet, J.; Livage, J.; Bonhomme-Coury, L. Studies of octameric vinylsilasilsesquioxane by carbon-13 and silicon-29 cross polarization magic angle spinning and inversion recovery cross polarization nuclear magnetic resonance spectroscopy. *J. Chem. Soc., Dalton Trans.* **1997**, 1617–26.
(31) (a) Bassindale, A. R.; Pourny, M.; Taylor, P. G.; Hursthouse, M. B.; Light, M. E. Fluoride-Ion Encapsulation within a Silsesquioxane Cage, *Angew. Chem., Int. Ed.* **2003**, *42*, 3488. (b) Bassindale, A. R.; Parker, D. J.; Pourny, M.; Taylor, P. G.; Horton, P. N.; Hursthouse, M. B. Fluoride Ion Entrapment in Octasilsesquioxane Cages as Models for Ion Entrapment in Zeolites. Further Examples, X-ray Crystal Structure Studies, and Investigations into How and Why They May Be Formed. *Organometallics* **2004**, *23*, 4400–5.
(32) Zhang, C.; Babonneau, F.; Bonhomme, C.; Laine, R. M.; Soles, C. L.; Hristov, H. A.; Yee, A. F. Highly Porous Polyhedral Silsesquioxane Polymers. Synthesis and Characterization. *J. Am. Chem. Soc.* **1998**, *120*, 8380–91.
(33) Choi, J.; Harcup, J.; Yee, A. F.; Zhu, Q.; Laine, R. M. Organic/inorganic hybrid composites from cubic silsesquioxanes. *J. Am. Chem. Soc.* **2001**, *123*, 11420–11430.
(34) Sellinger, A.; Laine, R. M. Silsesquioxanes as synthetic platforms. Thermally curable and photocurable inorganic/organic hybrids. *Macromolecules* **1996**, *29*, 2327.
(35) Sellinger, A.; Laine, R. M. Silsesquioxanes as synthetic platforms. 3. Photocurable, liquid epoxides as inorganic/organic hybrid precursors. *Chem. Mater.* **1996**, *8*, 1592–1593.
(36) Laine, R. M.; Choi, J. W.; Lee, I. Organic-inorganic nanocomposites with completely defined interfacial interactions. *Adv. Mater.* **2001**, *13*, 800–803.
(37) Choi, J.; Kim, S. G.; Laine, R. M. Organic/inorganic hybrid epoxy nanocomposites from aminophenylsilsesquioxanes. *Macromolecules* **2004**, *37*, 99–109.
(38) Choi, J.; Yee, A. F.; Laine, R. M. Organic/inorganic hybrid composites from cubic silsesquioxanes. Epoxy resins of octa(dimethylsiloxyethylcyclohexylepoxide) silsesquioxane. *Macromolecules* **2003**, *36*, 5666–82.
(39) Choi, J. W.; Tamaki, R.; Kim, S. G.; et al.Organic/inorganic imide nano-composites from aminophenylsilsesquioxanes. *Chem. Mater.* **2003**, *15*, 3365–3375.
(40) Laine, R. M.; Zhang, C.; Sellinger, A.; Viculis, L. Polyfunctional Cubic Silsesquioxanes as Building Blocks for Organic/Inorganic Hybrids. *J. Appl. Organometal. Chem.* **1998**, *12*, 715–23.
(41) Tamaki, R.; Choi, J. W.; Laine, R. M. A polyimide nanocomposite from octa(amino-phenyl)silsesquioxane. *Chem. Mater.* **2003**, *15*, 793–797.
(42) Sulaiman, S.; Brick, C.; De Sana, C. M.; Katzenstein, J. M.; Laine, R. M.; Basheer, R. A. Tailoring the Global Properties of Nanocomposites. Epoxy Resins with Very Low Coefficients of Thermal Expansion. *Macromolecules* **2006**, *39*, 5167–9.
(43) Asuncion, M. Z.; Laine, R. M. Silsesquioxane Barrier Materials. *Macromolecules* **2007**, *40*, 555–62.
(44) Barry, A. J.; Daudt, W. H.; Domicone, J. J.; Gilkey., J. W. Crystalline organo-silsesquioxanes. *J. Am. Chem. Soc.* **1955**, *77*, 4248–4252.
(45) Sprung, M. M.; Guenther, F. O. *J. Polym. Sci.* **1958**, *28*, 17.
(46) Olsson, K. An Improved method to prepare octa-(alkylsilsesquioxanes), *Ark. Kemi* **1958**, *13*, 367.
(47) Olsson, K.; Gronwall, C. On octa-(arylsilsesquioxanes), $(ArSi)_8O_{12}$. 1. The phenyl, 4-tolyl, and 1-naphthyl compounds. *Ark. Kemi* **1961**, *17*, 529–540.
(48) Brown, J. F., Jr.; Vogt, L. H., Jr.; Prescott, P. I. Preparation and Characterization of the Lower Equilibrated Phenylsilsesquioxanes. *J. Am. Chem. Soc.* **1963**, *86*, 1120–1125.
(49) Brown, J. F., Jr. The Polycondensation of Phenylsilanetriol. *J. Am. Chem. Soc.* **1965**, *87*, 4317–4324.
(50) Brown, J. F., Jr. Double Chain Polymers and Nonrandom Crosslinking. *J. Polym. Sci., Part C* **1963**, *1*, 83–97.
(51) Frye, C. L.; Klosowski, J. M. Concerning the So-called "Ladder Structure" of Equilibrated Phenylsilsesquioxane. *J. Am. Chem. Soc.* **1971**, *93*, 4599–4601.
(52) Unno, M.; Suto, A.; Takada, K.; Matsumoto, H. Synthesis of Ladder and Cage Silsesquioxanes from 1,2,3,4-Tetrahydroxycyclotetrasiloxane, *Bull. Chem. Soc. Jpn.* **2000**, *73*, 215.
(53) Unno, M.; Suto, A.; Matsumoto, H. Pentacyclic Laddersiloxane. *J. Am. Chem. Soc.* **2002**, *124*, 1574.
(54) Unno, M.; Takada, K.; Matsumoto, H. Formation of Supermolecule by Assembling of Two Different Silanols, *Chem. Lett.* **2000**, 242–3.
(55) Yamamoto, S.; Yasuda, N.; Ueyama, A.; Adachi, H.; Ishikawa, M. Mechanism for the Formation of Poly(phenylsilsesquioxane). *Macromolecules* **2004**, *37*, 2775–2778.
(56) Feher, F.; Schwab, J. J.; Soulivong, D.; Ziller, J. W. Synthesis, Characterization and Reactivity of *cis-cis-cis* $[(C_6H_5)_4Si_4O_4(OH)_4]$ *Main Group Chem* **1997**, *2*, 123–32.
(57) Shchegolikhina, O. I.; Pozdnyakova, Y. A.; Molodtsova, Y. A.; Korkin, S. D.; Bukalov, S. S.; Leites, L. A.; Lyssenko, K. A.; Peregudov, A. S.; Auner, N.; Katsoulis, D. E. Synthesis and Properties of Stereoregular Cyclic Polysilanols: *cis*-$[PhSi(O)OH]_4$, *cis*-$[PhSi(O)OH]_6$, and Tris-*cis*-tris-*trans*-$[PhSi(O)OH]_{12}$. *Inorg. Chem.* **2002**, *41*, 6892–6904.
(58) Kim, S.-G.; Sulaiman, S.; Fargier, D.; Laine, R. M. Simple syntheses of octaphenyloctasilsesquoxane and polyphenylsilsesquioxane. Starting point for aromatic nanocomposites with complete control of physical and chemical properties at nanometer length scales. In *Materials Syntheses. A Practical Guide*; Schubert, U., Hüsing, N. , Laine, R., Eds.; Springer-Verlag: Wien, 2008; pp 179−182.
(59) Brown, Jr., J. F. Organopolysiloxane Composition, U.S. Patent 3 000 858, 1962.
(60) Roll, M. F.; Kampf, J. W.; Kim, Y.; Yi, E.; Laine, R. M. Nano-Building Blocks via Iodination of $[PhSiO_{1.5}]_n$ forming [p-I-C6H4SiO1.5]$_n$ where n = 8, 10, 12 and a new route to high surface area, thermally stable, microporous materials via thermal elimination of I_2. *J. Am. Chem. Soc.* **2010**, *132*, 10171–10183.
(61) Shchegolikhina, O.; Pozdniakova, Y.; Antipin, M.; Auner, N.; Katsoulis, D. E.; Herrschaft, B. Synthesis and Structure of Sodium Phenylsiloxanolate. *Organometallics* **2000**, *19*, 1077–1082.
(62) Asuncion, M. Z.; Ronchi, M.; Abu-Seir, H.; Laine, R. M. Synthesis, Functionalization and Properties of Incompletely Condensed "Half Cube" Silsesquioxanes as a Potential Route to Nanoscale Janus Particles. *C. R. Chem.*, **2010**, *13*, 270−281.
(63) Morimoto, Y.; Watanabe, K.; Ootake, N.; Inagaki, J. Yoshida, K.; Ohguma, K. Silsesquioxane Derivatives and Process or Production Therefor. U.S. Patent Application 20040249103A1, Sept 2002.
(64) Li, Z.; Kawakami, Y. Formation of Incompletely Condensed Oligosilsesquioxanes by Hydrolysis of Completely Condensed POSS via Reshuffling. *Chem. Lett.* **2008**, *37*, 804–05.
(65) Seino, M.; Hayakawa, T.; Ishida, Y.; Kakimoto, M.; Watanabe, K.; Oikawa, H. Hydrosilylation Polymerization of Double-Decker-Shaped Silsesquioxane Having Hydrosilane with Diynes. *Macromolecules* **2006**, *39*, 3473–3475.
(66) Yoshida, K.; Hattori, T.; Ootake, N.; Tanaka, R.; Matsumoto, H. Silsesquioxane-Based Polymers: Synthesis of Phenylsilsesquioxanes with Double-Decker Structure and Their Polymers. In *Silicon Based Polymers*; Ganachaud, F., Boileau., S., Boury, B., Eds.; Springer: Dordrecht, The Netherlands, 2008; pp 205−211.
(67) Hoque, Md. A.; Kakihana, Y.; Shinke, S.; Kawakami, Y. Polysiloxanes with Periodically Distributed Isomeric Double-Decker Silsesquioxane in the Main Chain. *Macromolecules* **2009**, *42*, 3309–3315.
(68) Wu, S.; Hayakawa, T.; Kikuchi, R.; Grunzinger, S. J.; Kakimoto, M.; Oikawa, H. Synthesis and Characterization of Semiaromatic Polyimides Containing POSS in Main Chain Derived from Double-Decker-Shaped Silsesquioxane. *Macromolecules* **2007**, *40*, 5698–5705.

(69) Brunsvold, A. L.; Minton, T. K.; Gouzman, I.; Grossman, E.; Gonzalez, R. Investigations of the Resistance of Polyhedral Oligomeric Silsesquioxane Polyimide to Atomic Oxygen. *High Perform. Polym.* **2004**, *16*, 303–318.

(70) Ding, Yi. X.; Weber, W. P. Regio- and stereospecific 1,4-polymerization of 2-(triethylsilyl)- 1,3-butadiene *Macromolecules* **1988**, *21*, 2672–2674

(71) Tamaki, R.; Tanaka, Y.; Asuncion, M. Z.; Choi, J.; Laine, R. M. Octa(aminophenyl)-silsesquioxane as a Nanoconstruction Site. *J. Am. Chem. Soc.* **2001**, *123*, 12416–7.

(72) Takahashi, K.; Sulaiman, S.; Katzenstein, J. M.; Snoblen, S.; Laine, R. M. New Aminophenylsilsesquioxanes, Synthesis, Properties and Epoxy Nanocomposites. *Aust. J. Chem.* **2006**, *59*, 564–70.

(73) Ni, Y.; Zheng, S. A Novel Photocrosslinkable Polyhedral Oligomeric Silsesquioxane and Its Nanocomposites with Poly(vinyl cinnamate). *Chem. Mater.* **2004**, *16*, 5141–5148.

(74) Kim, S. G.; Choi, J.; Tamaki, R.; Laine, R. M. Synthesis of amino-containing oligophenylsilsesquioxanes. *Polymer* **2005**, *46*, 4514–4524.

(75) Krishnan, P. S. G.; He, C. Octa(maleimido phenyl) Silsesquioxane Copolymers. *J. Polym. Sci., Part A: Polym. Chem.* **2005**, *43*, 2483–2494.

(76) Zhang, Y.; Lee, S. H.; Yoonessi, M.; Toghiani, H.; Pittman, C. U., Jr. Phenolic Resin/Octa(aminophenyl)-T8-Polyhedral Oligomeric Silsesquioxane (POSS) Hybrid Nanocomposites: Synthesis, Morphology, Thermal and Mechanical Properties. *J. Inorg. Organomet. Polym. Mater.* **2007**, *17*, 159–171.

(77) Xiong, S.; Xiao, Y.; Ma, J.; Zhang, L.; Lu, X. Enhancement of Electrochromic Contrast by Tethering Conjugated Polymer Chains onto Polyhedral Oligomeric Silsesquioxane Nanocages. *Macromol. Rapid Commun.* **2007**, *28*, 281–285.

(78) Zhang, J.; Xu, R.-W.; Yu, D.-S. A Novel and Facile Method for the Synthesis of Octa(aminophenyl)silsesquioxane and Its Nanocomposites with Bismaleimide-Diamine Resin. *J. Appl. Polym. Sci.* **2007**, *103*, 1004–1010.

(79) Ak, M.; Gacal, B.; Kiskan, B.; Yagci, Y.; Toppare, L. Enhancing electrochromic properties of Polypyrrole by silsesquioxane nanocages. *Polymer* **2008**, *49*, 2202–2210.

(80) Xiong, S.; Jia, P.; Mya, K. Y.; Ma, J.; Boey, F.; Lu, X. Star-like polyaniline prepared from octa(aminophenyl) silsesquioxane: Enhanced electrochromic contrast and electrochemical stability. *Electrochim. Acta* **2008**, *53*, 3523–3530.

(81) Nagendiran, S.; Alagar, M.; Hamerton, I. Octasilsesquioxane-reinforced DGEBA and TGDDM epoxy nanocomposites: Characterization of thermal, dielectric and morphological properties. *Acta Mater.* **2010**, *58*, 3345–3356.

(82) Sulaiman, S.; Brick, C. M.; De Sana, C. M.; Katzenstein, J. M.; Laine, R. M.; Basheer, R. A. Tailoring the Global Properties of Nanocomposites. Epoxy Resins with Very Low Coefficients of Thermal Expansion. *Macromolecules* **2006**, *39*, 5167–69.

(83) Tamaki, R.; Laine, R. M. Unpublished results.

(84) Evans, R. C.; Douglas, P.; Winscom, C. J. Coordination complexes exhibiting room-temperature phosphorescence: Evaluation of their suitability as triplet emitters in organic light emitting diodes. *Coord. Chem. Rev.* **2006**, *250*, 2093–2126.

(85) Mailhot, B., Frezet, L. Unpublished work.

(86) Holmes, G. A.; Rice, K.; Snyder, C. R. Review Ballistic fibers: A review of the thermal, ultraviolet and hydrolytic stability of the benzoxazole ring structure. *J. Mater. Sci.* **2006**, *41*, 4105–4116.

(87) Liu, Y.; Zhang, Z.-F.; Halloran, J.; Laine, R. M. Yttrium Aluminum Garnet Fibers from Metalloorganic Precursors. *J. Am. Ceram.* **1998**, *81*, 629–645.

(88) Zhang, Z.-F.; Scotto, C. S.; Laine, R. M. Processing stoichiometric silicon carbide fibers from polymethylsilane. Part 1. Precursor fiber processing. *J. Mater. Chem.* **1998**, *8*, 2715–2724.

(89) Walker, K. A.; Markoski, L. J.; Deeter, G. A.; Spilman, G. E.; Martin, D. C.; Moore, J. S. Crosslinking chemistry for high-performance polymer networks. *Polymer* **1994**, *35*, 5012–5017.

(90) Lu, F.-L.; Wudl, F.; Nowak, M.; Heeger, A. J. Phenyl-Capped Octaaniline (COA): An Excellent Model for Polyaniline. *J. Am. Chem. Soc.* **1986**, *108*, 8311–8313.

(91) Jia, P.; Argun, A. A.; Xu, J.; Xiong, S.; Ma, J.; Hammond, P. T.; Lu, X. Enhanced Electrochromic Switching in Multilayer Thin Films of Polyaniline-Tethered Silsesquioxane Nanocage. *Chem. Mater.* **2009**, *21*, 4434–4441.

(92) Morrison, R. T.; Boyd, R. N. *Organic Chemistry*, 2nd ed.; Allyn and Bacon: Boston, 1966.

(93) Vogel, A. *Practical Organic Chemistry*; John Wiley and Sons: New York, 1966.

(94) Galli, C. Aromatic Iodination: Evidence of reaction Intermediate and of the *sigma*-Complex Character of the Transition State. *J. Org. Chem.* **1991**, *56*, 3238–45.

(95) Feher, F. J.; Budzichowski, T. A. Syntheses of highly-functionalized polyhedral oligosilsesquioxanes. *J. Organomet. Chem.* **1989**, *379*, 33–40.

(96) Laine, R. M.; Tamaki, R.; Choi, J. Well-Defined Nanosized Building Blocks for Organic/Inorganic Nanocomposites. U.S. Patent 6,927,301, Aug 2005.

(97) He, C. B.; Xiao, Y.; Huang, J. C.; Lin, T. T.; Mya, K. Y.; Zhang, X. H. Highly efficient luminescent organic clusters with quantum dot-like properties. *J. Am. Chem. Soc.* **2004**, *126*, 7792–3.

(98) Brick, C. M.; Tamaki, R.; Kim, S.-G.; Asuncion, M. Z.; Roll, M.; Nemoto, T.; Ouchi, Y.; Chujo, Y.; Laine, R. M. Spherical, Polyfunctional Molecules Using Poly(bromo-phenylsilsesquioxane)s as Nanoconstruction Sites. *Macromolecules* **2005**, *38*, 4655–60.

(99) Erben, C.; Grade, H.; Goddard, G. D. Bromination of octaphenylsilsesquioxane. *Silicon Chem.* **2006** (DOI: 10.1007/s11201-005-9000-5).

(100) Roll, M. R.; Takahashi, K.; Mathur, P.; Kampf, J. W.; Laine, R. M. $[PhSiO_{1.5}]_8$ autocatalytically brominates to produce $[o\text{-}BrPhSiO_{1.5}]_8$. Further bromination gives crystalline $[2,5\text{-}Br_2PhSiO_{1.5}]_8$ with a density of 2.38 g/cm^3 and calculated refractive index of 1.7 (RI of sapphire is 1.76) or the tetraisocosa bromo compound $[Br_3PhSiO_{1.5}]_8$. Submitted for publication.

(101) Park, S. S.; Xiao, C.; Hagelberg, F.; Hossain, D.; Pittman, C. U., Jr.; Saebo, S. Endohedral and Exohedral Complexes of Polyhedral Double Four-Membered-Ring (D4R) Units with Atomic and Ionic Impurities. *J. Phys. Chem. A* **2004**, *108*, 11260–72.

(102) PLATON Reference: Spek, A. L. PLATON, A Multipurpose Crystallographic Tool, Utrecht University, Utrecht, The Netherlands, 2008.

(103) Olsson, K.; Axen, C. On octa-(arylsilsesquioxanes), (ArSi)8O12. 2. Octa- and dodeca-(2-thienylsilsesquioxane), and their perbromo derivatives. *Ark. Kemi* **1963**, *22*, 237–244.

(104) Sulaiman, S.; Zhang, J.; Goodson, T.; Laine, R. M.: Synthesis, Characterization and Photophysical Properties of PolyfunctionalPhenylsilsesquioxanes: $[o\text{-}RPhSiO_{1.5}]_8$, $[2,5\text{-}R_2PhSiO_{1.5}]_8$, and $[R_3PhSiO_{1.5}]_8$. Submitted for publication.

(105) Reichert, V. R.; Mathias, L. J. Expanded Tetrahedral Molecules from 1,3,5,7-Tetraphenyladamantane. *Macromolecules* **1994**, *27*, 7015–23.

(106) Kobayashi, K.; Kobayashi, N.; Ikuta, M.; Therrien, B.; Sakamoto, S.; Yamaguchi, K. Syntheses of Hexakis(4-functionalized-phenyl)-benzenes and Hexakis[4-(4′-functionalized-phenylethynyl)phenyl]-benzenes Directed to Host Molecules for Guest-Inclusion Networks. *J. Org. Chem.* **2005**, *70*, 749–52.

(107) Roll, M. F.; Asuncion, M. Z.; Kampf, J.; Laine, R. M. para-Octaiodophenylsilsesquioxane, $[p\text{-}IC_6H_4SiO_{1.5}]_8$, a Nearly Perfect Nano-Building Block. *ACS Nano* **2008**, *2*, 320–6.

(108) Negishi, E.; Anastasia, L. Palladium-Catalyzed Alkynylation. *Chem. Rev.* **2003**, *103*, 1979–2018.

(109) Miyaura, N.; Suzuki, A. Palladium-Catalyzed Cross-Coupling Reactions of Organoboron Compounds. *Chem. Rev.* **1995**, *95*, 2457–83.

(110) Nicolaou, K. C.; Bulger, P. G.; Sarlah, D. Palladium-Catalyzed Cross-Coupling Reactions in Total Synthesis. *Angew. Chem., Int. Ed.* **2005**, *44*, 4442–89.

(111) Barrios-Landeros, F.; Carrow, B. P.; Hartwig, J. F. Effect of Ligand Steric Properties and Halide Identity on the Mechanism for Oxidative Addition of Haloarenes to Trialkylphosphine Pd (0) Complexes. *J. Am. Chem. Soc.* **2009**, *131*, 8141–54.

(112) Hartwig, J. F.; Kawatsura, M.; Hauck, S. I.; Shaughnessy, K. H.; Alcazar-Roman, L. M. Room-Temperature Palladium-Catalyzed Amination of Aryl Bromides and Chlorides and Extended Scope of Aromatic C-N Bond Formation with a Commercial Ligand. *J. Org. Chem.* **1999**, *64*, 5575–80.

(113) Vorogushin, A. V.; Huang, X.; Buchwald, S. L. Use of Tunable Ligands Allows for Intermolecular Pd-Catalyzed C-O Bond Formation. *J. Am. Chem. Soc.* **2005**, *127*, 8146–9.

(114) Balthazor, T. M.; Grabiak, R. C. Nickel-Catalyzed Arbuzov Reaction: Mechanistic Observations. *J. Org. Chem.* **1980**, *45*, 5425–6.

(115) Fernandez-Rodriguez, M. A.; Hartwig, J. F. A General, Efficient, and Functional-Group-Tolerant Catalyst System for the Palladium-Catalyzed Thioetherification of Aryl Bromides and Iodides. *J. Org. Chem.* **2009**, *74*, 1663–72.
(116) Babudri, F.; Farinola, G. M.; Naso, F. Synthesis of conjugated oligomers and polymers: the organometallic way. *J. Mater. Chem.* **2004**, *14*, 11–34.
(117) Wolfe, J. P.; Buchwald, S. L. Room Temperature Catalytic Amination of Aryl Iodides. *J. Org. Chem.* **1997**, *62*, 6066–8.
(118) Asuncion, M. Z.; Roll, M. F.; Laine, R. M. Octaalkynylsilsesquioxanes, Nano Sea Urchin Molecular Building Blocks for 3-D-Nanostructures. *Macromolecules* **2008**, *41*, 8047–52.
(119) Brick, C. M.; Ouchi, Y.; Chujo, Y.; Laine, R. M. Robust Polyaromatic Octasilsesquioxanes from Polybromophenylsilsesquioxanes, Br_xOPS, via Suzuki Coupling. *Macromolecules* **2005**, *38*, 4661–5.
(120) Reichert, V. R.; Mathias, L. J. Highly Cross-Linked Polymers Based on Acetylene Derivatives of Tetraphenyladamantane. *Macromolecules* **1994**, *27*, 7030–7034.
(121) Kim, Y.; Koh, K.; Roll, M. F.; Laine, R. M.; Matzger, A. J. Porous Networks Assembled from Octaphenylsilsesquioxane Building Blocks. *Macromolecules* **2010**, *43*, 6995–7000.
(122) Roll, M. F.; Kampf, J. W.; Laine, R. M. Crystalline Polyphenylene Macromolecular Clusters From Octaalkynylsilsesquioxanes, their Crystal Structures and Dehydrogenative Cyclization Products. Submitted for publication.
(123) Brick, C. Functionalization of Phenylsilsesquioxane. Ph.D. Dissertation, University of Michigan, 2005.
(124) Brick, C.; Chan, E. R.; Glotzer, S. C.; Martin, D. C.; Laine, R. M. Self-lubricating nano ball bearings. *Adv. Mater.* **2007**, *19*, 82–86.
(125) Sellinger, A.; Laine, R. M. Organic-Inorganic Hybrid Light Emitting Devices (HLED). U.S. Patent, 6,517,958, Feb 11, 2003.
(126) Nalwa, H. S. *Handbook of Advanced Electronic and Photonic Materials and Devices*; Academic Press: San Diego, 2001; pp 6−10.
(127) Laine, R. M.; Sulaiman, S.; Brick, C.; Roll, M.; Tamaki, R.; Asuncion, M. Z.; Neurock, M.; Filhol, J.-S.; Lee, C.-Y.; Zhang, J.; Goodson, T., III; Ronchi, M.; Pizzotti, M.; Rand, S. C.; Li, Y. Synthesis and photophysical properties of stilbeneoctasilsesquioxanes. Emission behavior coupled with theoretical modeling studies suggest a 3-D excited state involving the silica core. *J. Am. Chem. Soc.* **2010**, *132*, 3708–3722.
(128) Calzaferri, G.; Hoffman, R. The Symmetrical Octasilasesquioxanes $X_8Si_8O_{12}$: Electronic Structure and Reactivity. *J. Chem. Soc., Dalton Trans.* **1991**, 917–28. (b) Calzaferri, G. Silsesquioxanes. In *Tailor-made Silicon-Oxygen Compounds, from molecules to materials*; Corriu, R., Jutzi, P., Eds.; Publ. Friedr. Vieweg & Sohn mbH: Braunshweig/Weisbaden, Germany, 1996; pp 149−169.
(129) Schneider, K. S.; Zhang, Z.; Banaszak-Holl, M. M.; Orr, B. G.; Pernisz, U. C. Determination of Spherosiloxane Cluster Bonding to Si(100)-2 × 1 by Scanning Tunneling Microscopy. *Phys. Rev. Lett.* **2000**, *85*, 602–605.
(130) Chen, Y.; Schneider, K. S.; Banaszak Holl, M. M.; Orr, B. G. Simulated scanning tunneling microscopy images of three-dimensional clusters $H_8Si_8O_{12}$ on Si(100)-2 × 1. *Phys. Rev. B* **2004**, *70*, 085402.
(131) (a) Ossadnik, C.; Veprek, S.; Marsmann, H. C.; Rikowski, E. Photolumineszenzeigenshaften von substituierten Silsesquioxanen der Zusammensetzung $R_n(SiO_{1.5})_n$. *Monatsh. Chem.* **1999**, *130*, 55–68. (b) Azinovic, D.; Cai, J.; Eggs, C.; Konig, H.; Marsmann, H. C.; Veprek, S. Photoluminescence from silsesquioxanes $R_8(SiO_{1.5})_8$. *J. Lumin.* **2002**, *97*, 40–50.
(132) Xiang, K.-H.; Pandy, R.; Pernisz, U. C.; Freeman, C. Theoretical Study of Structural and Electronic Properties of H-Silsesquioxanes. *J. Phys. Chem. B* **1998**, *102*, 8704–8711.
(133) Cheng, W.-D.; Xiang, K.-H.; Pandey, R.; Pernisz., U. C. Calculations of Linear and Nonlinear Optical Properties of H-Silsesquioxanes. *J. Phys. Chem. B* **2000**, *104*, 6737–6742.
(134) Lin, T.; He, C.; Xaio, Y. Theoretical Studies of Monosubstituted and Higher Phenyl-Substituted Octahydrosilsesquioxanes. *J. Chem. Phys. B* **2003**, *107*, 13788–13792.
(135) Anderson, S. E.; Bodzin, D. J.; Haddad, T. S.; Boatz, J. A.; Mabry, J. M.; Mitchell, C.; Bowers, M. T. Structural Investigation of Encapsulated Fluoride in Polyhedral Oligomeric Silsesquioxane Cages Using Ion Mobility Mass Spectrometry and Molecular Mechanics. *Chem. Mater.* **2008**, *20*, 4299–4309.
(136) Park, S. S.; Xiao, C.; Hagelberg, F.; Hossain, D.; Pittman, C. U., Jr.; Saebo, S. Endohedral and Exohedral Complexes of Polyhedral Double Four-Member-Ring (D4R) Units with Atomic and Ionic Impurities. *J. Phys. Chem. A* **2004**, *108*, 11260–11272.
(137) (a) Li, H.-C.; Lee, C.-Y.; McCabe, C.; Striolo, A.; Neurock, M. Ab Initio Analysis of the Structural Properties of Alkyl-Substituted Polyhedral Oligomeric Silsesquioxanes. *J. Phys. Chem. A* **2007**, *111*, 3577–3584. (b) Striolo, A.; McCabe, C.; Cummings, P. T. Thermodynamic and Transport Properties of Polyhedral Oligomeric Silsesquioxanes in Poly(dimethyl-siloxane. *J. Phys. Chem. B* **2005**, *109*, 14300–14307.
(138) Ionescu, T. C.; Qi, F.; McCabe, C.; Striolo, A.; Kieffer, J.; Cummings, P. T. Evaluation of Force Fields for Molecular Simulation of Polyhedral Oligomeric Silsesquioxanes. *J. Phys. Chem. B* **2006**, *110*, 2502–2510.
(139) Cummings, P.; Glotzer, S.; Kieffer, J.; McCabe, C.; Neurock, M. Multiscale Simulation of the Synthesis, Assembly and Properties of Nanostructured Organic/Inorganic Hybrid Materials. *J. Comp. Theor. Nanosci.* **2004**, *1*, 265–279.
(140) Roll, M. F.; Kampf, J. W.; Laine, R. M. To be submitted.
(141) PLATON Reference: Spek, A. L. PLATON, A Multipurpose Crystallographic Tool, Utrecht University, Utrecht, The Netherlands, 2008.
(142) Desiraju, G. R.; Parthasarathy, R. The Nature of Halogen-Halogen Interactions: Are Short Halogen Contacts Due to Specific Attractive Forces or Due to Close Packing of Nonspherical Atoms? *J. Am. Chem. Soc.* **1989**, *111*, 8725–6.
(143) Bondi, A. van der Waals Volumes and Radii. *J. Phys. Chem.* **1964**, *68*, 441–51.
(144) Ganguly, P.; Desiraju, G. R. Van der Waals and Polar Intermolecular Contact Distances: Quantifying Supramolecular Synthons. *Chem.—Asian J.* **2008**, *3*, 868–80.
(145) Chae, H. K.; Siberio-Perez, D. Y.; Kim, J.; Go, Y.; Eddaoudi, M.; Matzger, A. J.; O'Keeffe, M.; Yaghi, O. M. A route to high surface area, porosity and inclusion of large molecules in crystals. *Nature* **2004**, *427*, 523–527.
(146) Asuncion, M. Z.; Laine, R. M. Fluoride Rearrangement Reactions of Polyphenyl- and Polyvinylsilsesquioxanes as a Facile Route to Mixed Functional Phenyl,Vinyl T_{10} and T_{12} Silsesquioxanes. *J. Am. Chem. Soc.* **2010**, *132*, 3723–3736.